Syracuse University

SURFACE

Earth Sciences - Dissertations   College of Arts and Sciences

5-2012

Using Emerging Methods to Investigate Stream and Groundwater Interaction at Multiple Spatial Scales

Martin Ashley Briggs
Syracuse University

Follow this and additional works at: https://surface.syr.edu/ear_etd

Part of the Biogeochemistry Commons

General Abstract

Fundamentally, streams represent physical conduits of water across gradients, yet a more holistic definition reveals stream corridors support a mosaic of living communities in a blend of surface and ground waters. The physical and biogeochemical patterns these dynamic systems support affect natural habitat and water quality, directly impacting the human experience. Our understanding of stream and groundwater interactions is at a time of rapid expansion due to an increase in environmental awareness, accountability, and emerging techniques which can be used to decipher underlying controls and develop predictive relationships. Water temperature has been used as a qualitative environmental tracer during the forging of this country from Lewis and Clarks pioneering spatial explorations to Thoreau's revolutionary scientific investigations; yet only very recent modeling and technological advancements have allowed us to apply these principles in a more distributed quantitative fashion. The resulting description of physical flow dynamics can be combined with innovative biogeochemical assessments to determine the fundamental linkages between inert and living processes along the stream corridor.

The magnitude and spatial distribution of groundwater inflows to streams is a known control on stream water quality. These inflows can be recognized and evaluated through a variety of methods, each with its own sensitivity and basic requirements. One such method is using the temperature differential between surface and groundwaters to both locate and quantify groundwater inputs. The emerging method of fiber-optic distributed temperature sensing (DTS) uses the temperature dependent backscatter of light along fiber-optic cables to determine temperature at high spatial and temporal resolution, essential creating continuous thermometers that may be applied to aquatic systems over a broad range of spatial scales. My initial investigations involved a quantitative comparison of heat tracing with DTS to existing methods

of evaluating groundwater inflows (dye dilution gauging, differential gauging, and geochemical end-member mixing) along Nine Mile Creek in Syracuse, New York, USA. I found that DTS heat tracing generated comparable quantitative estimates of groundwater discharge to the stream, and provided the finest spatial characterization of these inflows of all methods tested.

The "hyporheic zone" describes where stream water temporarily enters the sub-surface, which is known to be biogeochemically reactive, before potentially mixing with shallow groundwaters and returning to the stream. This flux across the streambed interface has driven much recent research, but the intrinsic spatial and temporal variability have proven a challenge to define. I modified DTS optical fibers to improve spatial resolution from 1.0 to 0.014 meter so the propagation of diurnal temperature patterns into the steambed could be recorded and applied to one-dimensional conduction-advection-dispersion models to determine the vertical component of hyporheic flux. I installed these custom high-resolution fiber-optic temperature sensors within the streambed above two beaver dams in Lander, Wyoming, USA for five weeks as stream discharge dropped by 45%. The resulting rich datasets revealed flux was organized by streambed morphology with strong, deep flux at glides and near-dam bars, and weak, shallow flux at pools and bars set farther upstream. Additionally, these morphologic units showed contrasting temporal trends in flux penetration and magnitude.

One benefit of such refined descriptions of the physical hyporheic system is that they can be directly compared to ambient biogeochemical data collected in coincident vertical profiles to evaluate the physical controls on streambed chemistry and nutrient cycling. I collected pore water at multiple depths, once a week, and analyzed these samples for several conservative and redox-sensitive solutes. The results revealed strong correlation between vertical flux magnitude and the degree to which hyporheic water was "oxic-stream-like" or "anoxic-reduced".

Residence time along hyporheic flowpaths was found to be a dominant control on redox condition, a relationship that held for both spatial and temporal flux patterns. This data set was augmented by an injection of the new biologically sensitive resazurin environmental tracer which showed that hyporheic flowpaths had much greater rates of aerobic reactivity compared to the net streamflow, but this signal was indistinguishable at the reach scale.

The cumulative result of the past three years of stream research using emerging ideas and methods is an improved understanding of these intricate and fascinating biomes. I hope this knowledge will serve to improve the management of, and appreciation for, the veins of our shared landscape.

Using Emerging Methods to Investigate Stream and Groundwater Interaction at Multiple Spatial Scales

by

Martin Ashley Briggs

B.S. Geology University of Massachusetts, 2002
M.S. Hydrology Colorado School of Mines, 2009

DISSERTATION

Submitted in partial fulfillment of the requirements for the degree of
Doctor of Philosophy in Earth Sciences

Syracuse University
May 2012

Acknowledgements

I would like to thank everybody who has had a positive influence on my life thus far, in some way you have contributed to this work. My PhD advisor Dr. Laura Lautz, MS advisor Dr. Michael Gooseff, and hydrology intern supervisor Dr. Andrew Fisher have been instrumental in my professional development. In particular, thank you to Dr. Lautz for providing me the guidance, freedom and budget to pursue an amazing multifaceted project, and to Danielle Hare for making sure it actually got done. The hydro group here at Syracuse, specifically Tim and Gordon, have proved amazing colleagues and friends. Of course I could have not accomplished any of this without the support of my family, the up-the-hill down-the-hill crew.

Table of Contents

List of Figures

Chapter 1

Chapter 2

Chapter 3

List of Tables

"Have you also learned that secret from the river; that there is no such thing as time? That the river is everywhere at the same time, at the source and at the mouth, at the waterfall, at the ferry, at the current, in the ocean and in the mountains, everywhere and that the present only exists for it, not the shadow of the past nor the shadow of the future."

Herman Hesse

Chapter 1: A comparison of fiber-optic distributed temperature sensing to traditional methods of evaluating groundwater inflow to streams

Abstract

There are several methods for determining the spatial distribution and magnitude of groundwater inputs to streams. I compared results of conventional methods (dye dilution gauging, acoustic Doppler velocimeter (ADV) differential gauging, and geochemical end-member mixing) to Distributed Temperature Sensing (DTS) using a fiber-optic cable installed along 900 m of Nine Mile Creek in Syracuse, New York, USA during low-flow conditions (discharge = 1.4 m^3s^{-1}). With the exception of differential gauging, all methods identified a focused, contaminated groundwater inflow and produced similar groundwater discharge estimates for that point, with a mean of 66.8 Ls^{-1} between all methods although the precision of these estimates varied. ADV discharge measurement accuracy was reduced by non-ideal conditions and failed to identify, much less quantify, the modest groundwater input, which was only 5% of total stream flow. These results indicate ambient tracers, such as heat and geochemical mixing, can yield spatially and quantitatively refined estimates of relatively modest groundwater inflow even in large rivers. DTS heat tracing, in particular, provided the finest spatial characterization of groundwater inflow, and may be more universally applicable than geochemical methods, for which a distinct and consistent groundwater end member may be more difficult to identify.

Introduction

      Groundwater enters streams as baseflow by passing across the streambed interface, a process that is governed by a complex combination of geomorphologic variables and hydraulic head gradients. Depending on the site specific dissolved gasses, dissolved load, and temperature of groundwater inflow, these inputs often serve as a vital control on the water quality and stream ecology of gaining systems. During dry periods baseflow often maintains habitat and is the principle component of total stream discharge [*Brunke and Gonser*, 1997]. Therefore accurate evaluations of the spatial distribution and magnitudes of groundwater inflows to streams are of primary interest to researchers and water resource managers. This is particularly significant when determining dissolved mass inputs from groundwater influenced by point source contamination [*Kalbus et al.*, 2006]. Many potential groundwater contaminants of interest are toxic in very low concentrations, yet inputs to large streams may be difficult to locate and quantify as they generally contribute only a small fraction of overall streamflow. There are several well known field techniques available with which to evaluate groundwater inflows to streams, each with particular strengths and scale applicability. Other researchers have compared and contrasted many of these traditional techniques [*Fulford*, 2001; *Kalbus et al.*, 2006; *Soupir et al.*, 2009; *Zellweger*, 1994]; but I compare three of the most widely used with the new distributed temperature sensing heat tracing method in a large stream influenced by contaminated groundwater to assess the repeatability, practicality, and spatial resolution of discharge estimates. One of the most common methods of measuring groundwater inflows to streams is differential gauging, where the net change in stream flow between incremental stream cross-sections is determined. Discharge through a cross-section is estimated by the velocity gauging method [*Carter and Davidian*, 1968] for which total discharge is determined by multiplying

representative velocity estimates by corresponding areas and summing over the section.

Velocity point measurements are often made at representative depths (e.g. 6/10 of the total

depth) with current meters consisting of rotating propellers or electromagnetic sensors. More

recently, acoustic doppler devices have become available that measure flow in multiple

dimensions [*Soupir et al.*, 2009] and may include integrated software packages to calculate

discharge and assess error (e.g. SonTek/YSI 2009). Another variant on this popular method of

determining discharge at successive points is dilution gauging, for which an introduced

conservative tracer, such as a salt or dye, is mixed with stream water and discharge is determined

from successive tracer breakthrough curves [*Kilpatrick and Cobb*, 1985; *Zellweger*, 1994]. A

combination of the velocity gauging and dilution gauging methods can be used to estimate

simultaneous water gains and losses over a stream reach by comparing the tracer mass balance to

net stream flow change determined through differential velocity gauging [*Harvey and Wagner*,

2000; *Payn et al.*, 2009].

Ambient water tracers, such as heat and geochemical constituents, may also be utilized to

evaluate groundwater inflows to streams. The ratios between various chemical constituents in

solution can be used to determine if the solution is a mixture of two well-defined end-members

[*Langmuir et al.*, 1978], which can be incorporated into mixing models to determine

groundwater contributions to streams [*Land et al.*, 2000; *Robson and Neal*, 1990]. In particular,

dissolved solutes derived from the dissolution of inorganic salts (e.g. Na, Ca, Cl, Br) may be

used to source waters influenced by leachate contamination [*Christensen et al.*, 2001; *Panno et*

al., 2006; *Whittemore*, 2007]. Therefore in cases of groundwater contamination, geochemical

mixing models may be particularly useful as the surface water and discharging groundwater

likely have distinct chemical signatures resulting in well-defined end members. Quantitative

estimates of the magnitude and spatial distribution of groundwater inflows to streams can be made under these circumstances at relatively high resolution when stream waters are well mixed. Heat has been used formally as a groundwater tracer for over 50 years [*Anderson*, 2005] and was recognized as a qualitative indicator of groundwater flow to surface waters over 150 years ago [*Thoreau*, 1854]. Many of these methods have been limited by spatially disperse point measurements of temperature, a factor that has recently been resolved by development of fiber-optic distributed temperature sensing (DTS) technologies for environmental applications. DTS systems function by initiating a laser pulse down an optical fiber and determining temperature along the fiber by measuring the ratio of temperature independent Raman backscatter (Stokes) to temperature dependent backscatter (anti-Stokes) of the laser pulse [*Dakin et al.*, 1985; *Grattan and Sun*, 2000; *Selker et al.*, 2006b; *Tyler et al.*, 2009]. Timing of this backscatter yields a measure of location, which can be resolved to approximately 1 m resolution at the scale of several kilometers. This yields a spatially continuous temperature sensor which can be installed along the stream channel bed to identify groundwater seepage [*Lowry et al.*, 2007; *Moffett et al.*, 2008; *Selker et al.*, 2006a] and provide data for both simple surface water- groundwater mixing models [*Selker et al.*, 2006a] and more complicated total stream heat budget models [*Westhoff et al.*, 2007]. I compare emerging DTS technology to differential gauging, dilution gauging and geochemical mixing methods to evaluate the application of DTS to measuring modest (~5% total stream flow) contaminated groundwater inflow to a large stream in Syracuse, New York, USA. Additionally I explore the sensitivity of groundwater inflow estimates made with DTS data to integration times, time of day when temperature measurements are taken, and the rate of change in stream temperatures over time.

Study Site

Nine Mile Creek is a natural tributary to Onondaga Lake, a 12 km^2 water body located adjacent to the northwest corner of Syracuse, New York, USA (Figure 1). The creek drains ~298 km^2 land area, and although the stream is rated 2nd order it has a large average stream discharge of 5.05 m^{3}s^{-1}, which ranges from an average snow melt flow of 9.57 m^{3}s^{-1} in April to an average base flow of 2.41 m^{3}s^{-1} in August (U.S. Geologic Survey (USGS) 04240300 Ninemile Creek at Lakeland, NY; stream flow statistics for 1971 – 2008). The lower 5.5 km of the creek are of particular interest because they flow between several large settling basins that were filled with the byproducts of soda ash (Na$_2$CO$_3$) production from 1944 to the 1980's by Allied Chemical Company, which is now Honeywell Incorporated (Effler and Whitehead, 1996) (Figure 1). Inorganic salts, largely CaCl$_2$, CaCO$_3$, CaO and NaCl, dominate the waste material and leach from the settling basins into Nine Mile Creek. The creek contributed approximately 1 million metric tons of Cl$^-$ to Onondaga Lake between 1987 and 2000 [*Matthews and Effler*, 2003]. One likely consequence of salt loading to Nine Mile Creek is a degradation of the local recreational fishery. The lower section of the stream has low fish diversity relative to upstream sites, and the dominant fish species are less desirable (Whitesucker, Carp, White Perch) in comparison to upstream sites that are dominated by Brown Trout [*Matthews and Effler*, 2003]. Work has been done by Honeywell Incorporated to remediate some sediments of Nine Mile Creek, but there is also interest in identifying the spatial distribution and magnitudes of saline groundwater fluxes to the stream. The 900 m reach of Nine Mile Creek selected for this investigation ends approximately 1.5 km upstream of the USGS 04240300 gauge (Figure 1). This reach coincides with a previously identified region of increased stream water salinity [*Effler and Whitehead*, 1996], which was assumed to reflect the influence of settling basin leachate,

6

although the absolute location and magnitude of groundwater flux had yet to be rigorously quantified. The channelized reach was bound by clays, sands, and coarse cobbles and had extensive macrophyte growth at the time of the experiments.

Methods

Differential and Dilution Gauging

Differential gauging was performed with a top-setting wading rod equipped with a handheld acoustic doppler velocimeter (SonTek/YSI FlowTracker ADV) that has a velocity range of 0.001 ms^{-1} to 4.0 ms^{-1}. This instrument was chosen, in part, because of the integrated software package that allows for several quality control evaluations of each velocity measurement. Additionally, there is a general discharge uncertainty evaluation based on the International Organization for Standardization (ISO) uncertainty calculation or the USGS statistical uncertainty calculation, which are explained in detail in the FlowTracker manual (SonTek/YSI, 2009). The ISO method interprets the physical characteristics of each velocity measurement to generate discharge uncertainty estimates, while the USGS statistical method uses adjacent measurements of each estimated variable. As the USGS statistical method always generated a similar or larger uncertainty estimate compared to the ISO method, and has been shown to be more universally reliable (SonTek/YSI, 2009), it was used to more conservatively estimate the uncertainty of each discharge measurement.

All measurements were made during the day on September 9th, 2009 at 6/10 the total stream depth, normal to flow direction, approximately every 100 m except where stream depth was greater than the height of the wading rod (>1.4 m), making measurements unfeasible (Figure 1). Over several transects excessive macrophyte growth was cleared from the streambed to allow a more representative velocity measurement. Repeated measurements were made in

sequence at the 900 m location and averaged to determine a "known" point of discharge for use in the tracer two-component mixing models because the cross-section was uniform, weed-free and much less turbulent than other sections.

Rhodamine water tracer (RWT) dye was used as a conservative tracer to estimate groundwater inflow and discharge by dilution gauging [*Kilpatrick and Cobb*, 1985]. RWT may not behave conservatively in some systems due to sorption [*Kasnavia et al.*, 1999], but this should not significantly affect mixing models generated at plateau concentration where sorption/de-sorption processes should be at steady state. A small bridge focused flow 530 m upstream of the reach head and served as the injection point to ensure the RWT was fully mixed with stream water before entering the experimental reach. Mixing was further enhanced by a multi-drip injection line installed perpendicular to flow. The 20% liquid stock RWT was diluted with stream water to 1640 mg RWT L^{-1} and injected at 500 mL min^{-1} from 11:55 to 13:55 on September 9th, 2009. Concentration change through time was monitored with a hand-held fluorometer (YSI 600 OMS) at the 150 m reach location until plateau concentration was reached. After that time, grab samples were collected along the thalweg in several locations and were stored on ice until transport back to the laboratory. There, they were filtered using Whatman GF/F Glass Microfiber Filters and analyzed for RWT concentration with an Opti-Sciences GFL-1 fluorometer. Dilution of the injected tracer was used to determine total stream discharge and identify and quantify groundwater influx to the stream reach between sampling locations.

Ambient Tracers

Both the stream and groundwater geochemistry and temperature were used to locate and measure groundwater inputs to the 900 m stream reach. The groundwater temperature was determined with a Traceable Digital Thermometer probe with 0.05 K accuracy. Groundwater

was pumped from 9 individual wells on both sides of the stream at various depths ranging from 3.0-36.6 m (installed by Honeywell Incorporated, Figure 1, Table 1), and from two shallow piezometers (0.45-0.50 m screen depth) installed in a diffuse North-side stream bank seep at approximately the 320 m mark on the experimental reach (Figure 1). Groundwater temperatures were also measured in free-flowing water from the same seep.

Stream temperature data were collected using an Agilent Distributed Temperature Sensor (N4386A) using a 1.5 minute sampling interval in dual-ended mode, yielding 3 minute integrated 1.5 m spatially distributed temperature estimates for 24 hours (17:00 September 8th - 17:00 September 9th) along the fiber. The instrument collected temperature traces every 10 seconds on alternating channels along the looped fiber, reversing the directionality of the incident laser to help account for differential signal loss, and these measurements were integrated over 3 minute time intervals by the onboard DTS software to yield a single temperature estimate for every 1.5 m of fiber. As suggested by *Tyler et al*. [2009], this integration time was kept short (3 minutes) to provide flexibility in post-collection data analysis, during which varying longer integration times could be explored. The fiber optics were loosely packed in hydrophobic gel and housed within stainless steel armoring and installed along the reach thalweg at the sediment/water interface. The heavy dense armoring of the cable helped keep the sensor in place along the streambed. Additionally, vegetation was cleared locally in places of thick macrophyte growth and the cable was anchored with flat river stones in regions of high velocity.

An initial 34 m of fiber was coiled in a cooler kept packed full with ice and interstitial water for calibration purposes [*Tyler et al.*, 2009]. The calibration bath temperature was independently monitored with a Thermochron iButton with 0.5 K accuracy and 0.0625 K precision. In double-ended mode the tandem fibers in the cable are fused at one end to allow a

single pulse from the instrument to measure temperature twice at every reach location, including the ice bath, aiding in calibration of the data. A slight temperature offset and systematic drift of the instrument over the 24 hr period were identified by comparing the iButton temperature record to the temperatures recorded at the coiled fibers in the bath. The entire data set was adjusted in MATLAB ™ by removing the systematic drift and offset through time from the entire stream temperature record. The cable was geo-referenced along the reach by linearly modifying (stretching or compressing) the distance measured by the DTS unit using the return speed of the laser to known points on the cable every 50 m. Known points were identified by exposing the submerged cable to warmer air at 50 m increment thalwag points determined with measuring tape, and finding those warm points within the temperature trace. This adjustment was typically on the order of a few meters or less, and differences between the "actual" and DTS distance estimates were likely due to the loose packing of the fibers within the outer cable, and slight meandering of the cable over the streambed.

The 24 hr mean stream temperature was calculated every 1.5 m along the cable to spatially identify areas of relatively low temperature, which indicate the influence of a constant, low temperature groundwater source [*Constantz*, 1998]. In the late summer, surface waters are warmer than the regional groundwater (~12 $^{\circ}$C), and therefore areas of focused groundwater inputs should be consistently colder than other stream segments and the cooling effect should persist a measurable distance downstream. In contrast, hyporheic exchange can buffer diurnal temperature changes by moderating both stream warming and cooling, which can be distinguished from constant cold groundwater inflows [*Loheide and Gorelick*, 2006]. Bed conduction may affect equilibrium stream temperatures due to cold groundwater at depth, but it was assumed that the only process of sufficient magnitude to decrease mixed stream temperature

10

in stepwise fashion in this large stream was focused groundwater inflows. The 24 hr mean temperature distinguishes consistently cold areas from the variable heating and cooling of the channel resulting from sensible, latent, and short/long wave energy fluxes over the diurnal period, influences which can have great effect on shorter duration temperature integrations. Assuming groundwater inflow is consistent over the 24-hr period a simple quantitative estimate of groundwater flux to the stream can be made using the change in mixed stream temperature from above a point where stream water temperature decreases to below that point using a two-component mixing model derived from the following relationships:

$$Q_i T_i + Q_{gw} T_{gw} = Q_o T_o \qquad [1]$$

$$Q_i + Q_{gw} = Q_o \qquad [2]$$

where Q is discharge, T is temperature; and subscripts i, o and gw refer to the stream water into the section, out of the section and groundwater inflow over the section respectively. These equations can be combined to solve for the groundwater discharge over the cold section as [*Kobayashi*, 1985]:

$$Q_{gw} = Q_i \left[\frac{T_o - T_i}{T_{gw} - T_o} \right] \qquad [3]$$

We determined Q_o with repeat FlowTracker measurement within an "ideal" cross-section at the end of the reach with low velocity, no macrophyte growth and uniform bed morphology and Q_i was derived from this using the model with the observed change in temperature. T_i and T_o were taken as the 50 m mean temperature bracketing a focused point of stream cooling, or the mean temperature over a distance of 50 m above and 50 m below such a point respectively.

If the cable passes directly over an area of groundwater inflow at the streambed interface, the groundwater at that point is likely not completely mixed with the water column. The result is

11

"anomalous" cold temperature measurements that may result in local overestimation of groundwater flux. Such cold points were identified by fitting a line to the mixed stream temperature data below the cold water input to identify outliers (Figure 2), and these points were removed from the 50 m downstream mean. In addition to Q_{gw} determined from the 24 hr mean temperature record, an estimate of Q_{gw} was made for every individual time-step of the double-ended measurement (i.e. every 3.0 minute integration) and for several different two-hour time intervals over the 24 hr record. These varied time interval estimates were used to evaluate method sensitivity to system noise, temporally varying differences between the stream and groundwater temperature, and rates of overall stream temperature change with time.

In-channel stream water chemistry samples were taken along the thalwag at 50 m increments along the 900 m reach, and groundwater samples were collected from the same well locations where temperature was measured (Figure 1). Samples were kept cooled (temperature < 4 °C) and filtered upon return to the lab where they were analyzed for Ca^{2+}, Na^+ and Cl^- using Ion Chromatography (Dionex ICS-2000). These three ions are known to be present naturally in regional surface waters and concentrated in local groundwater due to settling basin leachate. Bi-variate ratio-ratio plots of stream water Cl:Na and Ca:Na were used to evaluate whether stream water was a simple mixture of two consistent and distinct end members. A linear trend on a plot of two ratios with common denominators indicates two end-member mixing (Langmuir et al. 1978). The groundwater concentrations from various sources (e.g. wells at various depths/locations and piezometers) were also depicted on this plot to help identify the appropriate end member for the mass balance mixing analysis. The magnitude of Q_{gw} for focused inflows was determined using mixing models in the same manner as Equation 3, with T replaced by

either [Ca^{2+}] or [Cl^-]. Transport of Ca^{2+} and Cl^- was assumed to be conservative on the timescales of local surface water/groundwater exchange in this system.

We determined the expected error range for each groundwater inflow estimate generated using heat, dye and geochemical methods from the precision of the temperature, Rhodamine WT and solute observations used in the mixing models, respectively. We estimated the precision of temperature, dye and solute observations using the standard deviation of repeat measurements of each parameter. Assuming the groundwater end-member is known, the absolute error of the groundwater inflow estimate is a function of both the data precision and the relative difference between the surface water and groundwater temperatures or concentrations. Because the groundwater inflow estimates are generated from the difference between measurements that bracket the inflow, the error of these respective measurements must be taken into account when using the mixing model (Equation 3). The inflow must modify mixed stream temperature or concentration by more than twice the data precision for such a change to be considered significantly different from zero. We approximated the range of error of each individual groundwater inflow estimate by modifying the upstream and downstream temperature or concentration observations used in the heat or geochemical mixing models by the estimated precision of the values. The error for each method also theoretically corresponds to the smallest measureable groundwater inflow using each method. These numbers are specific to this experiment as the estimates of error (or sensitivity) are reflective of both intrinsic instrument error, and the range and difference in observed surface water/groundwater temperatures or chemical concentrations at this site at the time of the experiment. Additionally, as this error method is based on only on instrument sensitivity, other possible errors based on factors such as mixing are not included [*Schmadel et al.*, 2010].

Results

Differential and Dilution Gauging

Flow at the USGS gauge (04240300) downstream of the study site indicated net discharge from lower Nine Mile Creek remained constant for the 24 hr study period. Repeat discharge estimates generated at the 900 m "ideal" cross section with the ADV were identical (1399.8 Ls^{-1}) providing a known point for the mixing model analysis. Stream discharge estimates made at eight other locations along the reach with the ADV were highly variable in magnitude (Figure 3) with a standard deviation of 130 Ls^{-1}, while mean velocities for the cross sections ranged from 0.08-0.53 m s^{-1}. Variations in discharge displayed no clear pattern based on physical processes, and there was virtually no net change in discharge from the head to end of the reach (Figure 3). There was an apparent increase in stream discharge around the 335 m reach location, but this is followed by apparent loss to the 600 m location and a return to the upper reach boundary discharge by the 900 m location. This variability was significant according to the USGS statistical uncertainty analysis, which determined a mean flow uncertainty of 5.6%. The conditions for making velocity measurements were poor in many locations due to high turbulence, high and variable velocity, variable bedform, depth and excessive macrophyte growth. This resulted in several measurements with high signal to noise ratio, high angle to flow, and although at least 14 measurements were taken for each cross section, representative sections of many cross sections exceeded 10% of overall flow.

The RWT injection identified a groundwater inflow around the 335 m location, as stream concentrations dropped from an average plateau of 10.5 ppb RWT above to 10.0 ppb RWT below the inflow (Figure 3). The standard deviation of repeated RWT concentration measurements within this concentration range was determined to be 0.07 ppb. The relative

14

precision of the RWT concentration measurements yielded the largest estimated error range (lowest sensitivity) for any of the mixing model methods of +/- 20 Ls^{-1}. The injection was also used to estimate total stream discharge below the input based on dilution of the tracer, which was 1360.0 +/- 10 Ls^{-1} and comparable to the repeat differential gauging measurement of 1399.8 Ls^{-1}.

Ambient Tracers

A plot of stream temperature against time and distance clearly showed a short stretch of thalweg from 325-340 m that was consistently colder than the rest of the reach (Figure 4). Also evident was the persistent cooling effect of this input on downstream water temperatures for several hundred meters. The exact location of this colder zone was determined by exposing the submerged cable to warmer air at the location of the cold signal in the temperature trace, analogous to how the cable was geo-referenced. There were two much smaller areas of persistently colder stream temperatures at approximately 112 m and 430 m, but these had no measurable downstream temperature influence. Further inspection of the field site revealed that the 430 m location was likely a very small localized groundwater spring, but the 112 m "cold" spot may have been an artifact of a damaged fiber as no cold input was found there using an independent temperature probe.

When the 24 hr mean temperatures from the DTS dataset were plotted with distance, the inflow around 335 m was even more apparent (Figure 2). The mean temperature for 50 meters above the input was 0.24 ^{o}C higher compared to the 50 meter mean from directly below the input. This change is much larger than the estimated precision of the measurements, which were +/- 0.01 ^{o}C, based on the standard deviation of the 2-hr mean temperature over a 30 m distance for the ice bath calibration coil. The standard deviation of the 2-hr mean ice bath temperatures generated an error estimate of +/- 6 Ls^{-1} for this temperature range. This value corresponds to a

conservative estimate of error for the 24 hr mean temperature which likely had higher precision, but this could not be directly determined by repeat measurement as there was only one 24 hr period recorded. The 24-hr mean stream temperature was used to quantify the groundwater inflow at 58.6 +/- 6 Ls^{-1}, which was similar to that determined with 2-hr means taken during the coldest (63.7 +/- 6 Ls^{-1}), warmest (69.9 +/- 6 Ls^{-1}) and fastest cooling (58.6 +/- 6 Ls^{-1}) portions of the diurnal temperature cycle (Figure 5, Table 1). The inflow calculated as the stream was warming at the highest overall rate was found to be significantly less than these values (40.7 +/- 6 Ls^{-1}). Inflow estimates made with the original 3-minute time-step were variable with a larger range error of +/- 31 Ls^{-1} (Figure 6), which generally encompassed the inflow values determined using the 24-hr and 2-hr means, with the consistent exception of values during the mid-day. Stream chemistry changed abruptly around 335 m, and after initial mixing, a stable chemical composition was sustained for the remainder of the reach (Figure 7). Stream samples from 50 m above the 335 m input were compared to the 400-900 m reach chemistry and showed a total increase in Cl^- of 324.3 +/- 0.1 ppm, and of Ca^{2+} of 95.3 +/- 0.2 ppm, both of which represented similar proportional increases from their respective upstream values. The ratio-ratio plot of Cl:Na and Ca:Na in mixed stream water yielded a linear relationship as the stream water evolved toward groundwater concentrations with downstream transport. This confirmed the use of two end-member geochemical mixing models of Cl^- and Ca^{2+} using stream and groundwater concentrations (Figure 8). Both the Cl^- and Ca^{2+} mixing models produced similar precise focused groundwater inflow estimates around the 335 m reach location of 72.8 +/- 0.1 Ls^{-1} and 68.8 +/- 0.2 Ls^{-1}, respectively. Additionally, the chemical mixing models indicated there was a net total diffuse groundwater inflow of ~ 12 Ls^{-1} over the 75 m stream reach leading up to the more focused input which was not apparent from the other temperature and dye data.

Discussion

Spatial Distribution of Groundwater Inflow

The 900 m experimental reach had a focused groundwater inflow centered at the 335 m

reach location, as was identified most clearly from the ambient heat and geochemical tracing.

Heat tracing, in particular, provided the highest spatial resolution, allowing the inflow to be

pinpointed at the 1.5 m scale. The groundwater input had a persistent cooling effect on stream

temperatures until the 730 m location. This distance was calculated by fitting a line to the linear

re-warming of stream temperature and determining where this line reached the mean observed

upstream of the input (16.5 ^{o}C). A two sample t-test (p=0.69) indicated that the mean stream

temperature was not statistically different between the region upstream of the input and stream

temperatures after 730 m, but did vary significantly before this point downstream of the input

(p<0.001). The fitted line was also used to identify outliers from the mixed stream temperature

[*Selker et al.*, 2006a], which were very cold areas recorded as the cable passed directly over

springs through the streambed. These values were generally localized to the 325-340 m location

and were not included in the mixing model as they did not reflect mixed stream water

temperatures. This result illustrates the strength of the DTS method as a reconnaissance tool for

precisely locating groundwater inflows. Cold areas can also result from stratification of stream

waters [*Neilson et al.*, 2010], especially in deep pools, but the flow velocities, mixing and

morphology of this reach indicated stratification was likely not an important factor.

The cold section identified by the DTS at 335 m coincided with a sharp change in stream water

chemistry longitudinally along the creek. The chemistry data is more sensitive to small

groundwater inputs (minimum groundwater input estimate precision of ~+/- 0.2 Ls^{-1}) than

temperature at this site (minimum groundwater input estimate precision of ~+/- 6 Ls^{-1}), given the

high precision of the solute concentration data and very large geochemical gradient between stream water and groundwater, and therefore can allow the identification of diffuse inputs. The geochemical method identified diffuse inputs over the ~75 m above the focused input, which was not detected with the heat tracing (Figure 7). Despite this advantage of geochemical mixing at this site, large geochemical gradients are unique to this location and the grab samples are spatially limited compared to the continuous DTS sensor. Further, the instantaneous nature of point grab-sampling renders them susceptible to mixing issues which can be influential in a large, fast flowing stream and may explain the noisy data directly below the 335 m input. In contrast, the DTS data is integrated through space and time which reduces noise for this experiment. Similar to previous research [e.g. *Lowry et al.*, 2007; *Moffett et al.*, 2008; *Selker et al.*, 2006a] I found that installation of the cable directly on the streambed over springs can lead to measurement of groundwater inflow unmixed with surface water. As discussed, this may actually be viewed as a benefit in terms of identifying the exact locations of groundwater inflows, and these points can be easily isolated from the mixed stream temperature by fitting a curve to the mixed data, and can therefore be excluded from mixing model analysis.

Dye tracing identified an apparent focused groundwater inflow around 335 m which agreed with the other methods as the mixed stream RWT concentration dropped by a mean of 0.5 ppb. Introduced tracers may be problematic because it can be difficult to determine when the stream is truly at a plateau concentration, particularly if flow conditions are transient. This limitation may have affected data collected further downstream within the experimental reach in this study and, consequently, that data was not included in the RWT groundwater discharge calculations. As with instantaneous chemical samples, lack of groundwater mixing may compromise RWT data as was shown by *Schmadel et al.* [2010] who found that mixing uncertainty represented the

18

majority of the +/- 8.4 % estimated error they rigorously determined when using the dilution gauging method. Without the supporting heat and chemical data it might be difficult to definitively attribute a 0.5 ppb change in RWT concentration to the physical process of groundwater gain.

Non-ideal field conditions such as large depth and turbulence, variable velocity and bedform, and an abundance of macrophyte growth adversely affected differential gauging measurements. The integrated software of the FlowTracker ADV helped to identify some of these possible sources of error, but the general discharge uncertainty measurements generated by both the USGS statistical method and the ISO method appear to have underestimated the true uncertainty. This is consistent with previous work that found current meters performed poorer than their respective manufacturers published accuracy limits [*Fulford*, 2001]. Perhaps a finer measurement spacing and further clearing of macrophyte growth would have provided more accurate discharge estimates, but both of these activities can be treacherous within a deep, fast flowing large stream. Our results were similar to that found by *Soupir et al.* [2009] who compared various gauging techniques to a control discharge in two small steams. The two ADV devices they tested (which did not include the FlowTracker ADV) had median percent relative error that ranged from 57.7% to 122.2%. Other instruments used for measuring velocity (four current meters) generally had better agreement with the control discharge, but none had a median percent relative error less than 24.0%, which is far greater than the 5% increase in flow found at Nine Mile Creek. Interestingly, one of the worst performing methods tested by *Soupir et al.* [2009] in two small streams was dilution gauging using RWT, which had a median percent relative error of 58.7%. They attributed this error in part to inadequate mixing across the reach

19

length, although the method for determining the correct length prescribed by *Kilpatrick and Cobb* [1985].

Comparison of Groundwater Inflow Estimates

All of the methods discussed above, with the exception of differential gauging, provided similar estimates of focused groundwater inflow centered around the 335 m reach location with a mean of 66.8 Ls^{-1} with the geochemical methods providing the highest precision (Table 1). The focused nature of this inflow may result from the re-routing of Nine Mile Creek during settling bed construction from its natural channel into clay and fill deposits (unpublished data provided by O'Brien and Gere 2011), forcing down-valley groundwater flow to the surface. Some dense clay material is evident along the banks and in the well logs from this area. Although in an absolute sense this inflow is large, it only represents a 4.8% increase in total stream discharge (Table 1), which is modest compared to previous studies using DTS in smaller streams [*Selker et al.*, 2006b]. Differential gauging indicated little net change in stream flow over the reach, and error estimates made with the ADV software likely underestimated true error and exceeded the inflow in question. This is consistent with previous work which found differential gauging with the same ADV unit did not capture gains from groundwater springs identified by DTS when the magnitude of these gains was within the ADV measurement accuracy [*Lowry et al.*, 2007].

The 24-hr mean heat tracing estimate of 58.6 +/- 6 Ls^{-1} was determined using Equation 3 and the change in mean mixed stream temperature of 0.26 $^{\circ}$C between the 200-250 m and 350-400m reach lengths. Although the 24-hr mean is an effective method for identifying groundwater inflow, it may not be the most appropriate for determination of flow magnitude. Estimates of groundwater inflow based on shorter time scales (i.e. 2-hr) when total stream temperature was relatively steady produced results more comparable to the other methods, and

this sensitivity effect is discussed in the following section. For this study, groundwater

temperature used for the mixing model was determined from shallow piezometers, but in systems

such as bedrock lined reaches installation of wells may not be feasible. In these settings

groundwater temperature may be determined from the mixed stream temperature when it is

found to be consistent across a region of known groundwater inflow, assuming the stream water

reaches groundwater temperature at some point over the diurnal cycle [*Selker et al.*, 2006b].

The mixed stream chemistry had a large shift in the ion ratios around the 335 m location, and

evolution of stream water toward groundwater concentrations above the 335 m inflow indicated

diffuse groundwater inflow (Figure 8). An increase in both the Cl^- and Ca^+ concentration at the

focused input yielded similar focused inflow estimates of 72.8 +/- 0.1 Ls^{-1} and 68.8 +/- 0.2 Ls^{-1},

which are somewhat larger and outside of the error bounds of the 24-hr mean temperature

estimate. The ratio-ratio plot of groundwater from wells at various depths adjacent to the stream

produced a different linear mixing line than that observed for the stream (Figure 8), likely the

result of mixing between leachate influenced groundwater and deep basin brines. Given the

large variability of the groundwater composition (e.g. Ca:Na and Cl:Na ratios) and the

groundwater Ca^{2+} and Cl^- concentrations, the groundwater end-member chosen for this analysis

was that collected from the shallow piezometers in the stream bank seep, as these samples were

in close physical proximity to the focused streambed input and generally fell along the stream

water mixing line (Figure 8, Table 2).

In point-source contaminated streams, such as Nine Mile Creek, with two well-defined

end-members, geochemical mixing models are an effective tool for estimating groundwater

inflow because chemical gradients between the surface water and groundwater are large and data

precision is high. Although even in these settings the geochemical method is limited by the need

to identify the "true" groundwater end-member, and whether this end-member is constant in space and time [*Kalbus et al.*, 2006]. Figure 8 underscores this concern, as many of the deeper groundwater wells had similar chemical ratios to the piezometers and also fell along the stream water mixing line, yet their concentrations were highly variable (Table 2), likely resulting from differential dilution from recharge. If the more concentrated groundwater end-members from the deep wells were used in the mixing models, the focused groundwater input to the creek would have been greatly under-estimated. Therefore identifying changes in mixed stream chemistry and actually quantifying rates of groundwater inflow are different, the latter being dependent on identifying a correct groundwater end-member that is constant in space. Large errors outside of those derived from concentration measurement precision may be incorporated into groundwater inflow estimates if the groundwater end-member is variable, a concern which is evident from the groundwater chemistry at this site. This, combined with the potential problems with using introduced tracers such as RWT as discussed above (e.g. sorption, mixing, plateau), may render heat tracing more reliable in stream systems where end-members are difficult to characterize. The heat, chemistry and dye mixing models all resulted in similar groundwater inflow estimates that were approximately 5% of total overall stream flow, although groundwater inflow estimated from dilution of RWT was the least precise. This modest input is likely too small to be captured with differential gauging, even in ideal conditions. In large streams such as Nine Mile Creek, a 5% inflow of contaminated groundwater can represent a significant mass input. For example, if this one focused inflow has been relatively constant in magnitude and concentration through time, it could have contributed over 13% of the approximately 1 million metric tons of Cl^- estimated to have entered Onondaga Lake from lower Nine Mile Creek over the years 1987-2000 [*Matthews and Effler*, 2003]

Sensitivity of heat tracing inflow estimates to integration time and time of day

Once the fiber-optic cables are installed in a stream, DTS can produce extensive data sets and often the challenge is to then determining the correct system parameters to best characterize the stream process in question. DTS precision is proportional to the square root of time, increasing with the number of photons collected, which better defines the Stokes to anti-Stokes backscatter ratio and subsequently improve temperature measurements [*Tyler et al.*, 2009]. Longer integration times, while more precise, may mask the complexity of stream processes, such as propagation of the diurnal signal through the bed [*Hatch et al.*, 2006; *Keery et al.*, 2007]. Previous work by *Selker et al.* [2006a] in a very small stream (1-2 Ls^{-1}) quantified groundwater inputs that made up a large fraction of total flow using the mixing model method and short DTS integration times. For my larger system, with comparatively smaller groundwater inputs (5%), I found that when the focused groundwater inflow was calculated using the specified fundamental 3-minute time-step the noisier data resulted in an expected error range of +/- 31 Ls^{-1} in contrast to the +/- 6 Ls^{-1} estimated for the 2-hr integration times (Figure 6). This variability is generally clustered around the mean inflow determined through dilution gauging and geochemical tracing (69.5 Ls^{-1}), with systematic negative deviation from this mean outside of the estimated error range during the daylight hours when solar radiation inputs were large. Many estimates of groundwater influx made during the middle of the day were extremely small or even negative, indicating the stream was warming faster downstream of the 335 m inflow location than upstream. Interestingly, the standard deviation of the 3-minute time-step inflow estimates was not significantly larger during times when stream temperature was changing rapidly, further indicating longer integration times are necessary to reduce systematic noise and to more

accurately determine modest groundwater inflow even when stream temperatures are relativity stable.

The rate of change in stream temperatures and differential heating of the channel varies over the diurnal cycle due to a combination of environmental factors that affect how the stream gains, retains and loses energy (Figure 2). Estimates of groundwater inflow may be adversely affected, as heat tracing may no longer be initially "conservative." This concern is particularly pronounced during the hours of peak solar radiation, when the stream is heated differentially due to depth, shading, streambed color, water velocity, turbidity and macrophyte growth. Recent research has shown that DTS deployments along the streambed are sensitive to heat conduction from sediments in contact with DTS cable, particularly in shallow, clear streams, and this process may impair measurement of bulk stream water temperature [*Neilson et al.*, 2010]. Therefore, in streams where the sediments are directly warmed by solar radiation, a DTS installation along the streambed interface may be influenced by sediments that are warmer than the mixed water column. In addition, *Neilson et al.* [2010] found that the cable itself may be directly warmed by short wave radiation under certain conditions. The 24-hr mean temperature incorporates time intervals when steam temperatures change quickly and incoming solar radiation is at a peak, and therefore may incorporate avoidable error in the groundwater inflow estimate. In the case of this study, the effect was to lower the overall inflow estimate by including anomalously low estimates of inflow determined during the hours of peak solar radiation.

We calculated the 2-hr mean DTS temperatures with distance as a method to dampen system noise found in the 3-minute measurements by providing a longer integration time, but still allow for greater focus on a specific time of day and rate of change in stream temperature

over time (Figure 2B). Groundwater inflow estimates generated using the 2-hr means at the coldest (63.7 Ls^{-1}) and warmest (69.9 Ls^{-1}) sections of the diurnal temperature cycle were in best agreement with those made using the chemical and dye methods (Figure 5). These times corresponded with the slowest rates of overall stream temperature change with time and when solar input to the stream was low. Conversely, groundwater inflow estimates made over the 2-hr interval when stream temperature had the highest and most uneven rate of change during peak solar radiation input provided the least comparable estimate to the other methods (40.7 +/- 6 Ls^{-1}). During this time the downstream temperature was warmer and more variable than upstream, likely due to direct differential heating of the bed in shallow, slow flowing areas. This incorporated error into the inflow calculation in addition to that determined through the sensor precision error analysis discussed above. In that case the bed surface would not be in equilibrium with the mixed water column above, and would influence temperature measurements made along the adjacent DTS cable. These influences were so pronounced that the 2-hr afternoon trace (Figure 5, panel 3) shows temperature step changes of similar magnitude to the true groundwater inflow, indicating physical hydrologic gains that do not actually exist. The estimate of groundwater inflow made when the stream was cooling quickly during late evening did not exhibit nearly as large a deviation from the other methods as the mid-day estimate, producing the same result as that made using the 24-hr mean (58.6 +/- 6 Ls^{-1}). This indicates differential heating and possible direct warming of the sediments with conduction to the cable are the major sources of error rather than the stream simply not being at some relative temperature equilibrium.

These results suggest that although the 24-hr mean stream temperature may be an effective tool to identify groundwater inflows to streams, it can be influenced by differential

heating and potentially bed conduction during peak solar radiation. Estimates of groundwater inflow integrated over several hours when the stream has the slowest rate of overall temperature change provided results most consistent with the chemical and dilution gauging methods, and had much greater precision compared to the 3-minute integrated estimates . As temperature records can be averaged over time with relative ease during post processing, it may be best to record data at a relatively fine time step, such as 3 minutes in this case, and increase those integration times after a preliminary review of the data to best characterize the process in question. Regardless, data collected during the hours of peak solar radiation should not be used to quantify groundwater inflow.

Conclusions

The longitudinal stream 24-hr mean temperature, Cl^- and Ca^{2+} chemistry, and RWT dilution methods all identified both the location and magnitude of a focused inflow of saline groundwater to Nine Mile Creek, though their spatial resolution and limitations differed. The absolute inflow magnitude estimates were all quite similar (24-hr DTS 58.6 +/- 6 Ls^{-1}; Cl^- 72.8 +/- 0.1 Ls^{-1}, Ca^{2+} 68.8 +/- 0.2 Ls^{-1}; RWT 67.0 +/- 20 Ls^{-1}) with a mean of 66.8 Ls^{-1}. Differential gauging failed to characterize this small (5%) input due to a level of uncertainty that exceeded the inflow size, and this uncertainty seemed to be underestimated using the ISO and USGS statistical uncertainty analyses. Non-ideal field conditions over most stream cross-sections caused by high turbulence, velocity, macrophyte growth and variable bedform influenced observed error and may be avoided in other systems. The RWT dilution captured the focused groundwater inflow accurately in this study, but the estimate was less precise and indicated this method would be insensitive to inflows less than 20 Ls^{-1}, although this precision could be improved with higher tracer plateau concentrations.

Changes in stream chemistry were used in two end-member mixing models for both Cl^- and Ca^{2+} because the ratio-ratio plot of Cl:Na and Ca:Na in mixed stream water yielded a linear relationship, indicating two well defined end-members. The abrupt change in stream chemistry around the focused input was easily identified and used to determine a precise estimate of groundwater inflow, but the samples taken directly below this input were variable due to mixing noise captured by the instantaneous point measurements. A more diffuse inflow of groundwater $(12.0\ Ls^{-1})$ over a 75 m reach leading up to the focused input was described by chemical analysis, but indistinguishable with the DTS and RWT data. Such small, diffuse groundwater inflows can be identified with the end-member mixing, given the high precision of the method based on the sensitivity analysis, which indicated inflows as small as $0.1\ Ls^{-1}$ could be quantified under these site-specific conditions. The chemical makeup of the local groundwater was highly variable with depth and location, and water collected from shallow piezometers within the stream bank were used for this analysis in part because they fell along the stream mixing line of the ratio-ratio plot. Some deeper wells with higher saline concentrations had the same ratios but would have greatly underestimated inflow if applied to the mixing models, suggesting caution must be used when selecting the groundwater end member from local wells. In this case the stream bank seep was an obvious place to install piezometers, but in more ambiguous settings heat tracing or very high resolution water sampling may be necessary to identify areas from which to sample groundwater reliably.

DTS data had the highest spatial resolution (1.5 m) and allowed for the direct identification of the focused groundwater seep. A curve fit to the return of stream water to ambient temperature allowed both an estimate of the spring's downstream temperature influence (~ 400 m) and identification of unmixed groundwater inputs, which corresponded with the exact

location of springs. Overall, mixing of stream and groundwater in close proximity to the inflow was best characterized by the DTS, as data were integrated over time in contrast to the instantaneous chemical and RWT samples. Absolute groundwater inflow estimates were sensitive to time of day and integration time, which likely affected the 24-hr mean method. Times of fast stream temperature change provided poorer estimates of groundwater inflow, especially when solar input was at a peak and the stream was warmed differentially and the cable may have been affected by heat conduction from the sediments. Estimates made over 2-hr periods, when direct solar input was low and overall stream temperature was changing slowly, generated groundwater inflow estimates that were most similar to the other methods (69.9 +/- 6 Ls^{-1} and 63.7 +/- 6 Ls^{-1}). Even during optimal times of day, data integration times of several hours may be necessary to reduce error introduced by systematic noise in the temperature signal. The use of ambient tracers such as heat and geochemistry for mixing models is viable in part because they provide direct information regarding groundwater inflows, and these tracers should be at relative steady state assuming stream discharge change is slow temporally. We have shown that geochemical analysis can be very effective when the chemistry of surface and groundwater differ, as may be case for groundwater contamination. Further, when the groundwater temperature differs from stream water, DTS data can provide similar estimates of focused groundwater inflow to the chemical data but provides a finer spatial characterization of inflow distribution. Even if groundwater temperatures are similar to the stream, inflows may also be identified as areas of lower diurnal stream temperature variance influenced by the constant temperature groundwater source. Although the cost of a DTS unit may be a prohibitive, they may be rented or borrowed from a variety of sources [e.g. *Tyler and Selker*, 2009], and the fiber-optic cables themselves are relatively affordable and may be viewed as a consumable of the

installation. Once the cable is installed, a spatially and temporally continuous and extensive data-set can be collected at varied flow and climate conditions, moving stream research beyond the point measurement limits and allowing focused-source contaminant loading to be better quantified. In summary, distributed temperature data can be used to estimate groundwater inflow magnitude in a comparable manner to more traditional methods, and describes inflow distribution at higher spatial resolution, even modest inputs to large streams.

Tables

Table 1. The focused groundwater inflow estimates for the 335 m reach location. Estimates were similar except those generated using temperatures collected during peak solar hours and flow calculations made with the ADV, which were too noisy to identify the small (~5%) inflow. Error was estimated by applying the standard deviations of repeat sample measurement on data specific instruments to the mixing model (Equation 3) over the observed concentration ranges. Numbers following DTS heat tracing methods refer to the time periods indicated in Figure 2B and Figure 5.

Method	Focused GW inflow (Ls^{-1})	Estimated error $(+/- Ls^{-1})$	Fraction total discharge (%)
Geochemical mixing models			
Cl mixing model	72.8	0.1	5.2
Ca mixing model	68.8	0.2	4.9
Dilution gauging			
RWT dye dilution	67.0	20	4.8
Differential gauging			
ADV flow gauging	*little net change, noisy data*		
DTS heat tracing			
mean 24-hr	58.6	6	4.2
warmest 2-hr (1)	69.9	6	5.0
coldest 2-hr (2)	63.7	6	4.5
high warming (solar) 2-hr (3)	40.7	6	2.9
high cooling (night) 2-hr (4)	58.6	6	4.2

Table 2. Chemical constituents of interest in the local groundwater in wells at varying depths and distance from the 335 m focused inflow. The mean of the similar shallow bank samples was used for the two-end member mixing model with stream water to determine groundwater inflow. Many of the deeper groundwater wells, especially the 84/85 series from the south side of the stream, had similar chemical ratios as the shallow samples but were more concentrated and would have provide an underestimate of groundwater discharge if they were used in the mixing models.

Well number	Cl (ppm)	Ca (ppm)	Na (ppm)
shallow bank samples			
piezometer 1 (0.45-0.50 m)	6295.	2071.	1472.
piezometer 2 (0.45-0.50 m)	6718.	2245.	1567.
seep (surface)	6278.	2103.	1498.
deeper groundwater samples			
WB05M (16.2-19.2 m)	12006.	3544.	3288.
WB05D (33.5-36.6 m)	70036.	20668.	21032.
MW70S (4.6-7.6 m)	9074.	3183.	1996.
MW70D (16.2-19.2 m)	45295.	15766.	10599.
MW59S (3.0-6.1 m)	11275.	3605.	2639.
85/S (4.9-7.9 m)	6829.	2157.	1728.
85/D (20.6-23.6 m)	53243.	18876.	12677.
85/I (13.4-16.5 m)	44732.	15468.	10665.
84/D (16.6-19.7 m)	51927.	17692.	12644.

Figures
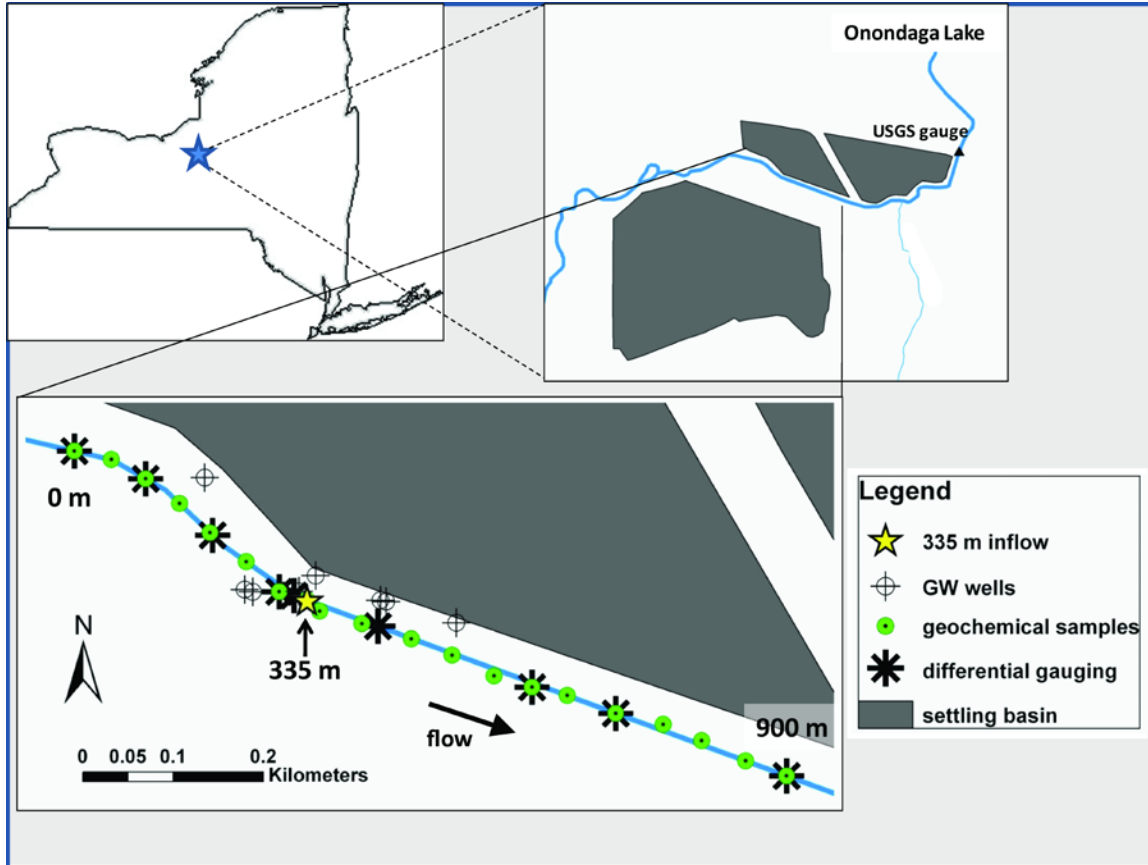
Figure 1. The Nine Mile Creek reach and adjacent inorganic salt waste settling basins in Syracuse, New York USA.
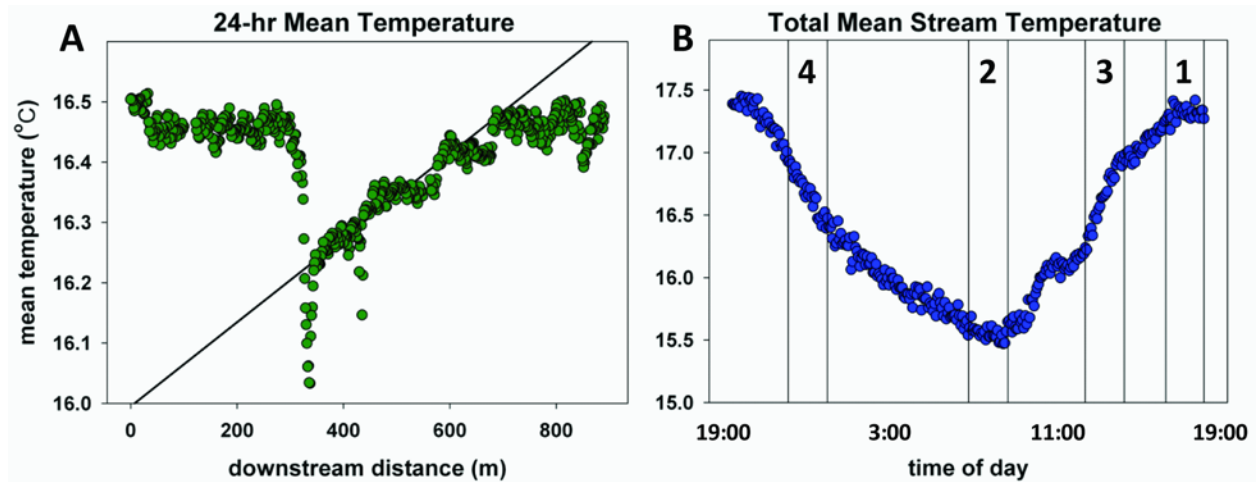
Figure 2. Panel A depicts the 24-hr mean temperature with distance, clearly showing the focused groundwater input at 335 m, which lowered stream temperature by 0.26 $^{\circ}$C, generating a focused groundwater inflow estimate of 58.6 +/- 6 Ls^{-1}. A curve fit to the return of mixed stream water to ambient temperature was used to both identify the unmixed groundwater signals and the duration of downstream affect, which was estimated to be approximately 400 m. Panel B shows total stream temperature as a function of time. High rates of change were observed in late evening (4) and mid-afternoon (3). The groundwater inflow estimate calculated during these 2-hr time periods was poorest for (3) when solar input was highest, while groundwater inflow determined when stream temperature was relatively stable (1, 2) generated estimates in closest agreement with other methods.
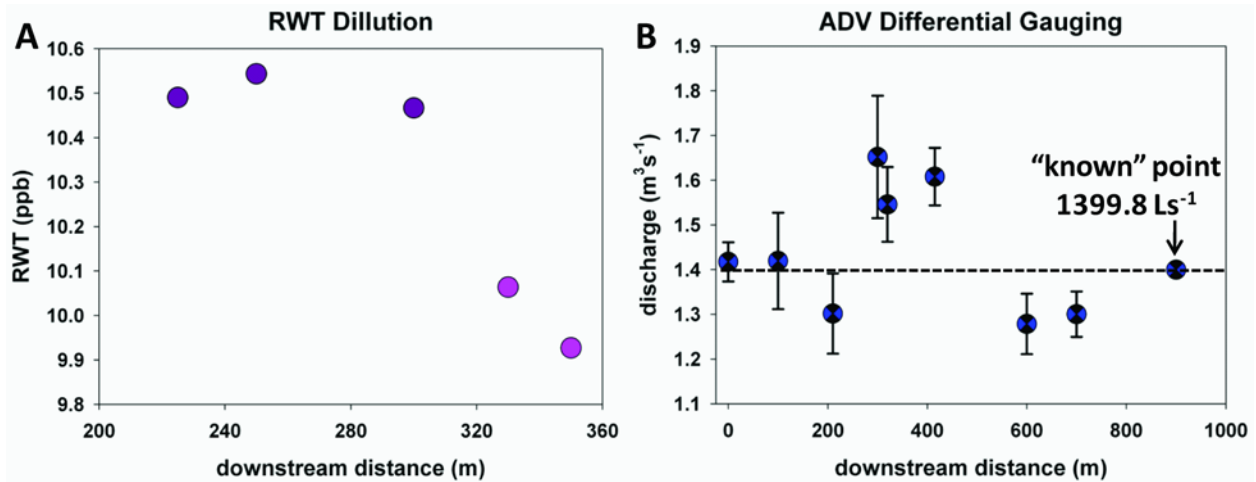
Figure 3. Plot A shows the dilution of the RWT tracer over the focused input and produced a groundwater inflow estimate of 67.0 +/- 20 Ls^{-1}. Plot B displays estimates of total stream discharge made with the ADV, which were highly variable with a standard deviation of 130 L s^{-1}, but showed no net change over the reach. Error estimates generated using the ADV software and USGS statistical uncertainty method underestimated true error, which is larger than the groundwater inflow magnitude in question. Identical repeat measurement at the 900 m cross section under ideal conditions were used as the starting point for all mixing models (1399.8 Ls^{-1}), and this value was corroborated by RWT dilution.
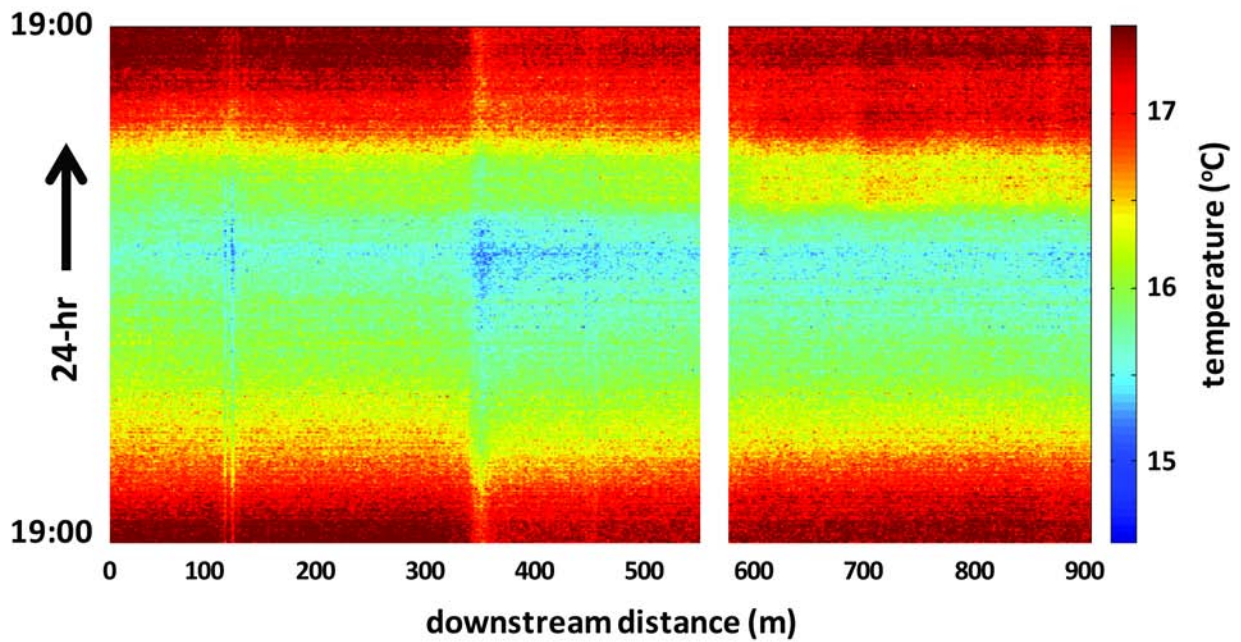
Figure 4. Stream temperature at 1.5 m spatial resolution integrated over 3.0 min sampling intervals over 24 hr starting at 19:00 on September 8th, 2009. The strong diurnal signal was consistently cooled around the 335 m reach location with persistent downstream affect. A splice in the fiber generated erroneous data at 580 m and was removed, and the "cold" spot at 112 m was likely an artifact.
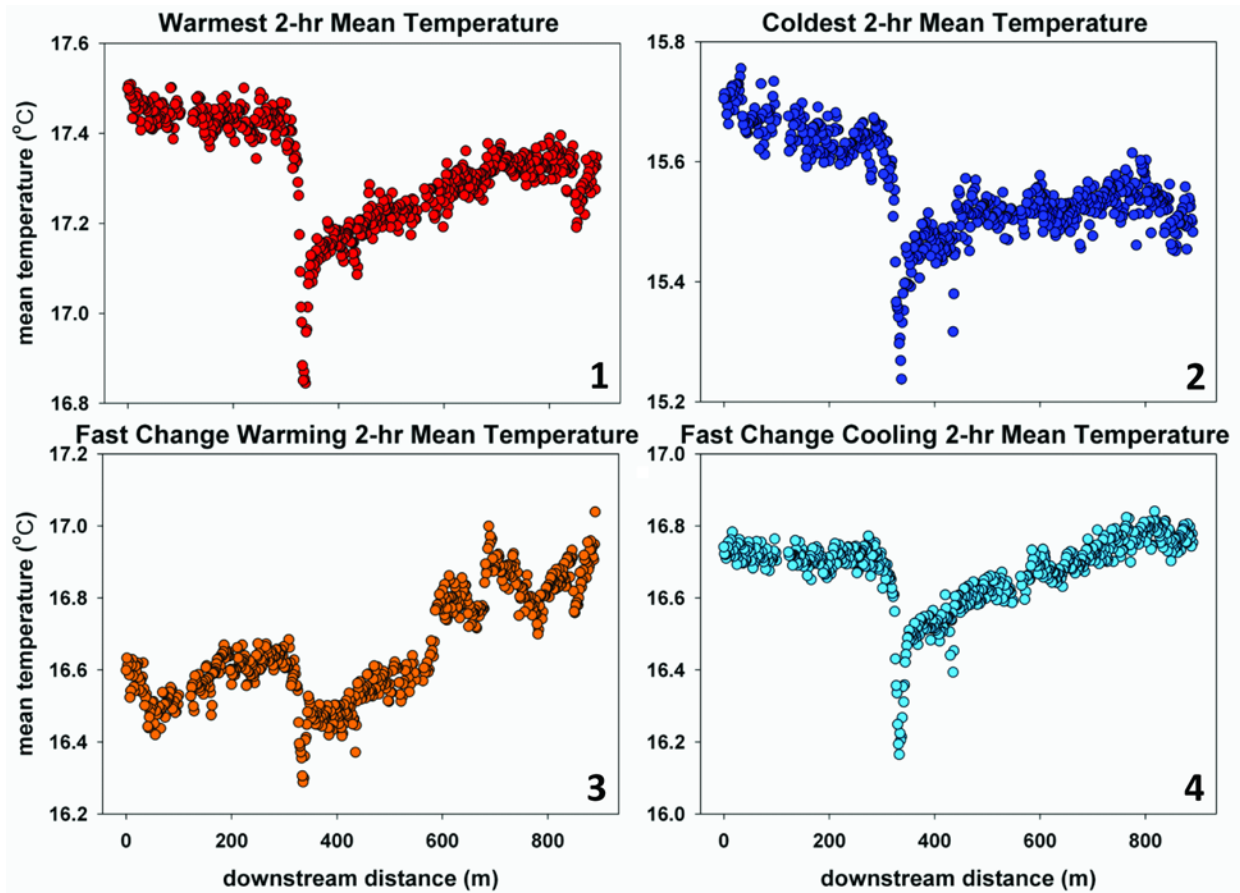
Figure 5. Various 2-hr mean stream temperatures with reach distance that all clearly show the influence of groundwater centered on the 335 m location, with the exception of plot 3, which is generated from the time of peak solar input and high temperature change. Plots 1 and 2 depict when stream temperatures were at their warmest and coldest respectively, and generated inflow estimates most similar to other methods (69.9 +/- 6 Ls^{-1}, 63.7 +/- 6 Ls^{-1}) as overall stream temperature was most stable (Figure 2). Differential heating of the stream depicted in plot 3 yielded the poorest inflow estimate (40.7 +/- 6 Ls^{-1}) while inflow calculated when the stream was cooling rapidly yielded the same value as the 24-hr mean (58.6 +/- 6 Ls^{-1})
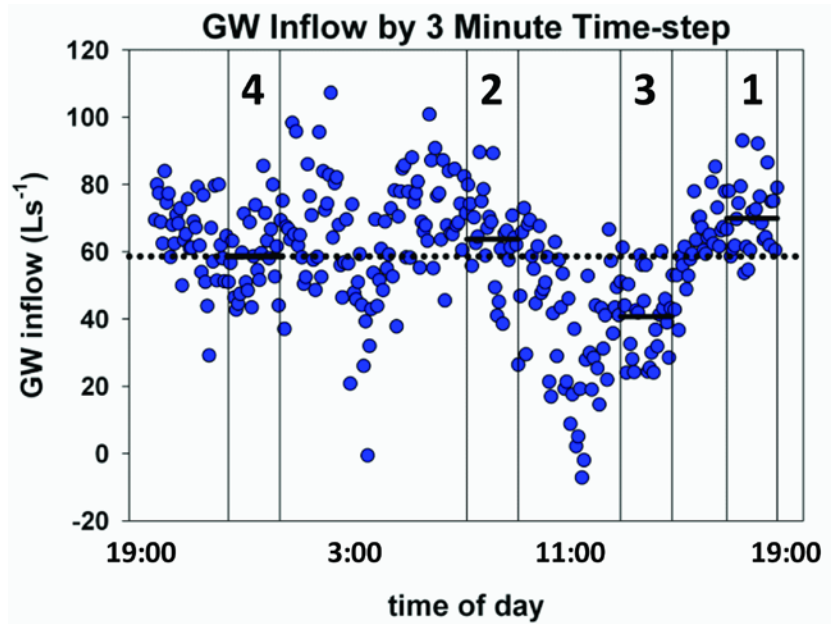
Figure 6. The variable groundwater inflow estimates made for each 3 min time-step of the double-ended DTS measurement with the 24-hr mean of 58.6 +/- 6 Ls^{-1} as the dotted line. This mean is decreased by data collected during the daylight hours of peak solar radiation. Times of slow and fast overall stream temperature change are shown (Figure 2B) with solid lines depicting their respective means.
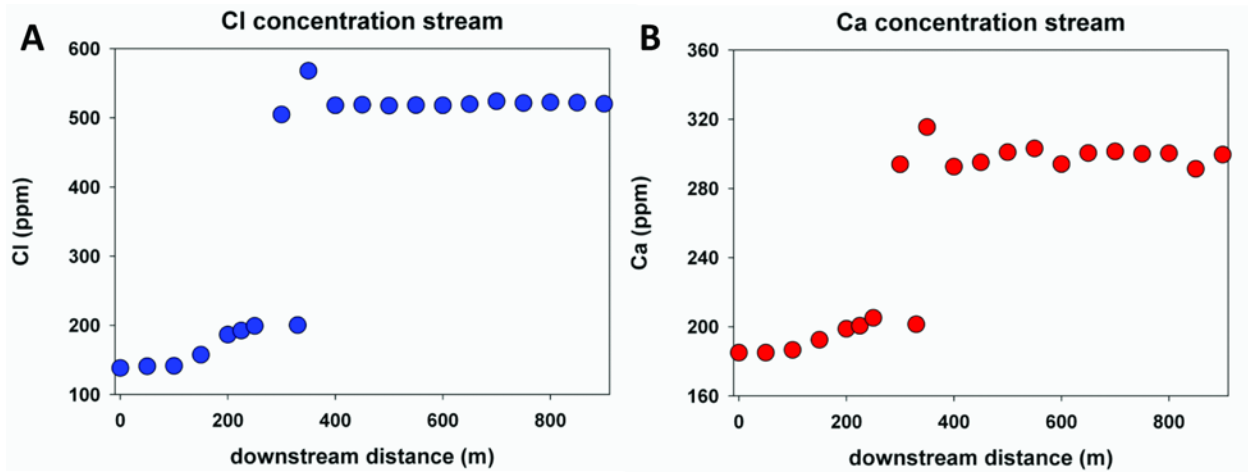
Figure 7. Plots A (Cl) and B (Ca) both show a sharp increase in concentration around the 335 m

input with some mixing noise downstream of the input. This shift in concentration was used to

calculate a focused groundwater inflow of 72.8 +/- 0.1 Ls^{-1} for Cl and 68.8 +/- 0.2 Ls^{-1} for Ca.

The slight increase in concentrations for ~ 75 m leading up to the focused input indicated diffuse

groundwater inflow of approximately 12 Ls^{-1} not captured by other methods.
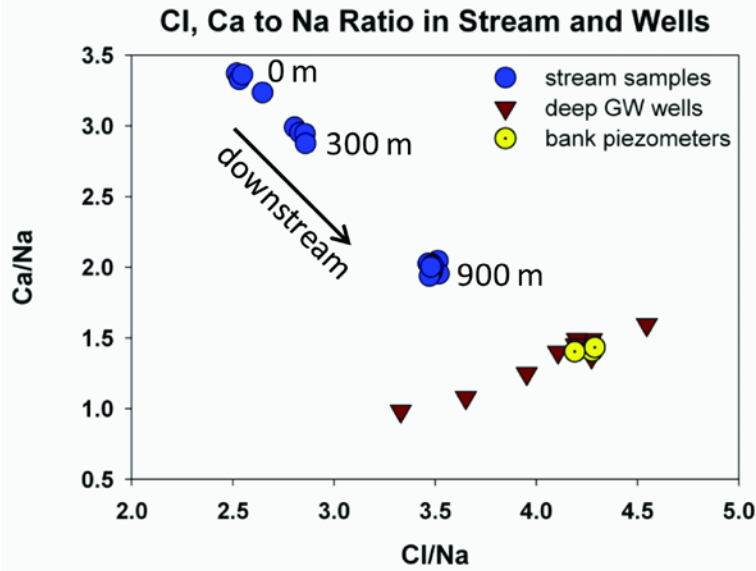
Figure 8. Stream water Cl to Na and Ca to Na ratios fall on a straight line indicating mixing of two distinct groundwater end members, with a distinct jump at the 335 m focused input. The shallow bank piezometers generally plot along this line, along with some deeper groundwater wells. The groundwater wells at various depths and locations also display another mixing pattern, likely between leachate and deep bedrock brine.

Chapter 2: Using high-resolution distributed temperature sensing to quantify spatial and temporal variability in vertical hyporheic flux

Abstract

Hyporheic flow can be extremely variable in space and time, and our understanding of complicated flow systems, such as exchange around small dams, has generally been limited to reach-averaged parameters or discrete point measurements. Emerging techniques are starting to fill the void between these disparate scales, increasing the utility of hyporheic research. When ambient diurnal temperature patterns are collected at high spatial resolution across vertical profiles in the streambed, the data can be applied to one-dimensional conduction-advection-dispersion models to quantitatively describe the vertical component of hyporheic flux at the same high spatial resolution. We have built on recent work by constructing custom fiber-optic distributed temperature sensors with 0.014 m spatial resolution that are robust enough to be installed by hand into the streambed, maintain high signal strength, and permit several sensors to be run in series off a single distributed temperature sensing unit. Data were collected continuously for one month above two beaver dams in a Wyoming stream to determine the spatial and temporal nature of vertical flux induced by the dams. Flux was organized by streambed morphology with strong, variable gradients with depth indicating a transition to horizontal flow across a spectrum of hyporheic flowpaths. Several profiles showed contrasting temporal trends as discharge decreased by 45 percent. The high resolution thermal sensors, combined with powerful analytical techniques, allowed a distributed quantitative description of the morphology-driven hyporheic system not before possible.

Introduction

There have been many studies of hyporheic exchange, from pore space to watershed scale, but it remains a challenge to quantitatively describe the structure and magnitude of hyporheic flow vectors at high resolution in the field. Conceptual diagrams of hyporheic flowpaths through bedforms based on hydraulic head differentials are present throughout the literature, yet the magnitude of these flow vectors are generally either modeled or inferred from relatively sparse point measurements. *Harvey and Wagner* [2000] note that traditional point measurements were likely inadequate to describe the heterogeneous hyporheic zone in a useful way, so higher resolution methods that move beyond the point scale are necessary. Hyporheic flux rates not only describe both the quantity of water moving from the stream into the subsurface, but also govern the residence time of hyporheic flowpaths, which is a first-order control on the biogeochemical processing of dissolved nutrients [*Vroblesky and Chapelle*, 1994; *Zarnetske et al.*, 2011]. Because hyporheic flow occurs over a spectrum of flow vector magnitudes and residence times [*Ward et al.*, 2010], a spatially distributed method for measuring hyporheic exchange in-situ must be flexible enough to yield accurate results under a wide range of flow conditions. Such a method would be especially useful in streams with complicated morphology and hyporheic exchange patterns, such as those affected by beaver impoundment [e.g. *Lautz et al.*, 2010].

Recently there have been advances in the quantitative application of novel geophysical and analytical tools that move beyond point estimates of surface water seepage [*Cirpka et al.*, 2007; *Pidlisecky and Knight*, 2011; *Ward et al.*, 2010]. When temperature data is collected through time at high resolution within the streambed, the diurnal signal generated by colder nights and warmer days can be used to determine spatially distributed hyporheic flux dynamics.

The diurnal, quasi-sinusoidal stream temperature signal propagates into the subsurface via conduction and advection. With increasing depth in the subsurface, the amplitude of the diurnal signal originating at the surface is attenuated and its phase is shifted forward in time. Disparities in the signal propagation from that predicted by pure conduction are attributed to the advection of heat by hyporheic water [*Anderson*, 2005; *Constantz and Thomas*, 1996; *Goto et al.*, 2005; *Hatch et al.*, 2006; *Keery et al.*, 2007; *Stallman*, 1965]. Several studies have exploited differences in the diurnal signal between two depths in the vertical to estimate hyporheic flux using one-dimensional analytical heat transport models [*Constantz*, 2008; *Hatch et al.*, 2006; *Keery et al.*, 2007], and data for these models are commonly collected with discrete thermal loggers deployed in the field at relatively low spatial resolution [*Hatch et al.*, 2006; *Keery et al.*, 2007; *Lautz et al.*, 2010; *Rau et al.*, 2010; *Schmidt et al.*, 2011]. Although this application can provide valuable information regarding the average vertical flux condition between individual temperature sensors, spatial resolution is sacrificed, which can compromise the interpretation of complex oblique flow systems. Additionally, the ideal temperature sensor spacing varies with flux magnitude, which in turn may vary with both depth and time, so the ultimate temperature data set contains a high-resolution of temperature observations in both dimensions to provide flexibility for 1-D modeling and analysis [*Hatch et al.*, 2006].

Environmental applications of fiber-optic distributed temperature sensing (DTS) permit high-resolution, continuous temperature data collection through space and time in aquatic environments. DTS systems function by initiating a light pulse down an optical fiber and determining temperature along the fiber by measuring the ratio of temperature independent Raman backscatter (Stokes) to temperature dependent backscatter (anti-Stokes) of the light pulse [*Dakin et al.*, 1985; *Selker et al.*, 2006b; *Tyler et al.*, 2009]. The timing of these backscatter

43

returns yields a measure of location, which for most systems can be resolved to approximately 0.25 to 1.0 m resolution over distances of several kilometers. Fiber-optic DTS has generally been applied to lotic systems to identify longitudinal temperature anomalies, which are used to locate and quantify groundwater discharge and hyporheic exchange [*Briggs et al.*, 2012a; *Lowry et al.*, 2007; *Moffett et al.*, 2008; *Selker et al.*, 2006a; *Westhoff et al.*, 2007]. Modified DTS configurations include wrapping the fiber around a mandrel to increase spatial resolution dramatically [*Selker et al.*, 2006a; *Suárez and Tyler*, 2011; *Vogt et al.*, 2010]. These high-resolution sensors can be installed vertically in the streambed to capture the propagation of the diurnal signal with depth. The only previously published high-resolution DTS hyporheic application used one vertical profile and found that this method was especially useful for identifying heterogeneities in flux with depth [*Vogt et al.*, 2010].

When stream velocities are reduced by beaver impoundment, their capacity to transport sediment is also significantly reduced; this results in large quantities of sediment being retained behind dams and the formation of complex bedforms [*Naiman et al.*, 1986], such as those known to enhance hyporheic exchange [*Gooseff et al.*, 2007; *Harvey and Bencala*, 1993; *Kasahara and Wondzell*, 2003]. Further, small dams drive water through the subsurface by creating punctuated head differentials along streams [*Hester and Doyle*, 2008; *Lautz et al.*, 2006]. Therefore beaver dams may generate a network of hyporheic flux "hot spots" governed by heterogeneity around individual dam complexes, enhancing microbial processing of dissolved nutrients.

Our primary research interest for this study was to describe the complicated dynamics of vertical hyporheic flux in varied streambed morphology over time, while simultaneously introducing a powerful tool for investigating streambed fluxes. To do this research using ambient temperature, custom fiber-optic high-resolution temperature sensors (HRTS) were

designed, constructed and deployed within the streambed. These specialized sensors were

designed to minimize signal loss, allow in-series configuration, and be durable enough to permit

installation by hand into the streambed. Data were collected continuously for one month along

vertical streambed profiles upstream of two beaver dams in the western United States. We then

applied a one-dimensional conduction-advection-dispersion model to the high-resolution diurnal

temperature data to quantitatively estimate the vertical component of hyporheic flux. This

allowed us to determine the penetration depth and structure of shallow hyporheic flow, which is

likely most relevant to biogeochemical processing of stream carbon and nutrients, and to

evaluate the viability and benefits of using multiple simultaneous fiber-optic HRTS over an

extended period of time in the stream environment. The observed spatial patterns in flux

determined with 1-D temperature modeling were supported with a conservative tracer injection.

Additionally, as hyporheic exchange may be variable over summer flow recession as head

gradients change, I investigated the temporal nature and correlation to potential forcing

mechanisms of high-resolution vertical flux patterns.

Methods

Site Description

Cherry Creek in Central Wyoming is a second-order stream that drains a 30 km^2 semi-

arid watershed on the east flank of the Wind River Range, and is managed by The Nature

Conservancy of Wyoming [*Jin et al.*, 2009] (Figure 1). The creek supplies approximately half of

the flow to Red Canyon Creek, a stream that has been extensively studied for surface

water/groundwater interaction [e.g. *Fanelli and Lautz*, 2008; *Lautz and Siegel*, 2006; *Lautz et al.*,

2006; *Lautz et al.*, 2010]. After emerging from a narrow canyon, the lower approximately 3 km

of Cherry Creek flows along a relatively unconstrained valley floor with an approximately 1

percent grade and is lined mainly with glacial till and alluvial deposits of sand and gravel. The annual stream hydrograph is characterized by high spring flows during snowmelt and subsequent transition to baseflow.

During the summer of 2010 there were 13 beaver dams of varied size along the lower 1.3 km of Cherry Creek that had trapped large quantities of primarily fine sediments, generating large longitudinal steps in streambed morphology. The two dams specifically chosen for this study were located 75 m apart, approximately 1160 m upstream of the confluence with Red Canyon Creek (Figures 1, 2). The larger Dam 1 caused a 0.75 m drop in water surface elevation while Dam 2 had a more modest 0.35 m drop at the beginning of the study period. Because of the high flow conditions at the time of this study and recent flood damage and scouring around both dams, water did not stagnate upstream of the dams and had velocities comparable to other broad un-impounded sections of the channel. The sediments surficial trapped behind both dams had a D_{50} of less than 2 mm, and consisted of fine gravel, sand, coarse clay and silt with abundant organic particles and the sediment-stream interface was not armored. The streambed morphology immediately above the two dams was similar, consisting of one dominant pool adjacent to a longitudinal bar structure. The bar at Dam #1 was located several meters upstream of the dam step (Figure 2A), while the bar at Dam #2 extended to the dam structure (Figure 2B).

Reach Hydrologic, Geomorphic and Climatic Characterization

Stream discharge and mean velocity were measured daily over the study period at the reach outlet with a top-setting wading rod equipped with a handheld acoustic doppler velocimeter (SonTek/YSI FlowTracker ADV) that had a velocity range of 0.001 ms^{-1} to 4.0 ms^{-1}. The channel was modified to a rectangular shape and cleared of large cobbles to provide optimal conditions for velocity-area measurements, and each velocity measurement was integrated for 40

seconds. Stream stage was monitored at lower temporal resolution above each dam by measuring changes in water surface elevation relative to a known datum. Sediment core collection was attempted at the time of HRTS installation but core integrity was poor and this data was not used. A spatial survey of the dams, banks, streambed morphology and HRTS locations was collected using a Nikon Nivo 5.M total station. At the research site, high temporal resolution stream and air temperature were recorded using loops of the in-line fiber optic cable located within the water column or on the shaded bank, respectively. Groundwater was periodically monitored for temperature in riparian piezometers adjacent to each dam, which were screened between 0.75 and 1.0 m below the land surface, and at deeper downstream water table wells located outside of the riparian zone.

High-Resolution Temperature Sensing

To investigate spatial patterns in vertical hyporheic flux, custom fiber-optic HRTS were constructed and installed within the subsurface upstream of two dams to determine the vertical component of hyporheic seepage flux. The DTS unit used for this application (Agilent Distributed Temperature Sensor N4386A) had a minimum spatial resolution of 1 m along optical fiber. Bend-insensitive fiber-optic cable was wrapped around a standard 4.8 cm PVC core, 1 m in length, to create a HRTS with 0.014 m vertical resolution. The fiber optic cable used for this application, Corning ClearCurve™, is designed to minimize light loss in wrapped configurations and had never been used for environmental DTS before. Our laboratory tests indicated signal loss along the wrapped fiber was only slightly higher than for unwrapped fibers (~ 1.4 dBkm⁻¹) and the strength of signal transmission permitted several HRTS to be run in series in dual ended mode. The ClearCurve fibers were packed in hydrophobic gel and installed within a 1.65-mm diameter stainless steel tube by AFL Telecommunications. These cables were wrapped tightly

by hand around each PVC core, which was pre-threaded at a specific pitch to allow a consistent wrap of the fiber optic cable without physical contact between consecutive coils, and yield the desired 0.014 m vertical spatial resolution. The steel tube protected the fragile glass fiber and allowed for a physically robust design that could be installed within the compacted streambed sediments. The threaded PVC rods were wrapped from top to bottom and the fiber was brought back to the top along the outside of each HRTS. At least 15 m of fiber were left at the top of the rod to facilitate connection to the next HRTS in series (Figure 3).

A total of nine HRTS were installed vertically within the streambed sediments to at least 0.75 m depth, five upstream of Dam 1 (B_1, B_2, P_1, G_1, G_2) (Figure 2A) and four upstream of Dam 2 (B_3, B_4, P_2, G_3) (Figure 2B). Installation locations were chosen to best reflect the observed heterogeneities in streambed morphology, which as discussed above consisted of one dominant pool and bar above each dam, so the naming scheme has been reduced to: B=bar, P=pool and G=glide locations. The HRTS were also installed at varied distance upstream from the dam structure (Figure 2, Table 1). Specifically G_2, B_3, G_3 and P_2 were all installed 1 m upstream from their respective dams to control for longitudinal elevation head change and isolate the effects of morphology and associated disparities in streambed hydraulic conductivity. To facilitate installation, a steel pipe with drive point of similar size to the HRTS was driven by sledge into the bed and withdrawn to create a guide hole. The HRTS were then immediately inserted into the hole and pounded gently into the sediments to the desired depth. They were connected in series using a Fujikura FSM-18S Fusion Splicer to create one continuous length of fiber that ran out and back through all of the HRTS consecutively, and was attached at each end to respective channels of the Agilent DTS unit (Figure 3).

The advantage of this looped configuration was to allow the instrument to operate in "double-ended" mode, in which bi-directional laser pulses along the fiber greatly simplify the calibration processes. Calibration is necessary due the inherent attenuation of the laser pulse as it travels down the optical fiber and passes through spliced connections [*Tyler et al.*, 2009]. By running the Agilent Sensing DTS unit in double-ended mode, signals generated in both directions were integrated, and the optical fiber properties were determined over the measurement by the onboard DTS software. The instrument was programmed to update temperature traces at 1.0 m increments every 10 seconds on alternating channels which were integrated at 10 minute time intervals by the DTS software to yield a single temperature estimate every 20 minutes for each location along the HRTS array. The DTS system was used to collected temperature measurements from June 13th - August 10th.

The precision of the DTS system in this specific configuration was 0.2 $^{\circ}$C (standard deviation) according to software provided by the instrument manufacturer. The accuracy of a DTS system is dependent on calibration at known points, and it was necessary to perform this calibration continuously over time due to variable instrument drift which can change the offset between the measured and true temperatures. The system was kept thermally calibrated using an ambient temperature water bath, which was mixed by a 950+ Lhr^{-1} bilge pump run continuously over the period of data collection. Following the recommendation of *Tyler et al*. [2009], 40 m of cable was coiled through the bath and three Thermochron iButton temperature sensors with 0.5 $^{\circ}$C accuracy and 0.0625 $^{\circ}$C precision were used to independently monitor bath temperature. We selected a subset of iButtons that most closely measured the central temperature distribution of a batch of 80 and compared well to a high precision thermistor, although for this application, where I compare temperature records at varied depth, absolute accuracy is much less important

than data precision. During data post-processing, the entire data set was adjusted for offset

between the 40-m reference coil and the mean of the independent iButton records. Spatial

calibration of the DTS fiber was accomplished by applying distinct temperature signals to the

cable at known reference points. The sediment-stream interface was identified for each

temperature profile and periodically monitored for possible changes based on scour and

deposition using a waterproof chemical heat source. No significant change in this datum was

observed over the period of data collection. During data post-processing, the temperature record

for each individual HRTS was isolated and scaled to the true vertical distance using the known

scale factor of 1.0 m to 0.014 m.

High-Resolution Vertical Flux Determination

Once the calibrated temperature records for each HRTS were identified and scaled,

vertical flux estimates were made at high spatial and temporal resolution using changes in the

diurnal temperature signal with depth along each HRTS profile. *Hatch et al.* [2006] and *Keery et*

al. [2007] presented two similar methods to calculate vertical water flux, based on the one-

dimensional conduction-advection-dispersion equation of *Stallman* [1965]:

$$\frac{\partial T}{\partial t} = k_e \frac{\partial^2 T}{\partial z^2} - q \frac{C_w}{C} \frac{\partial T}{\partial z} \qquad\qquad 1.$$

where T is temperature (°C), t is time (s), k_e is the effective thermal diffusivity of the saturated

sediment ($m^2\ s^{-1}$), z is depth (m), C_w is the volumetric heat capacity of the water, C is the

volumetric heat capacity of the saturated sediment ($J\ m^{-3}\ °C^{-1}$) (a volume weighted average

derived from C_w, porosity (n) and C_s, the volumetric heat capacity of sediment), and q is fluid

flux ($m\ s^{-1}$), for which a positive value indicates downward flow. This equation is solved

analytically using the *Hatch et al.* [2006] amplitude method as:

$$q = \frac{C}{C_w} \left(\frac{2\kappa_e}{\Delta z} \ln A_r + \sqrt{\frac{\alpha + v^2}{2}} \right)$$ 2.

where A_r is the ratio of amplitudes between a lower and an upper temperature signal (unitless),

Δz is the vertical distance between the lower and an upper temperature signal in the streambed

(m), v is the velocity of the thermal front (m s^{-1}) and κ_e (m^{2}d^{-1}) is the effective thermal diffusivity

defined as:

$$\kappa_e = \left(\frac{\lambda_o}{C} \right) + \beta |v_f|$$ 3.

where λ_o is the baseline thermal conductivity of the saturated sediment (J s^{-1}m^{-1} $^{\circ}$C^{-1}), β is thermal

dispersivity (m), and v_f is the linear particle velocity (m s^{-1}); finally, α is determined by:

$$\alpha = \sqrt{v^4 + \left(\frac{8\pi\kappa_e}{P} \right)^2}$$ 4.

Because the Hatch model is predicated on a sinusoidal temperature signal with a period

of 24 hours, it is desirable to filter non-ideal field temperature records to better isolate the

sinusoidal diurnal signal, which can be complicated by both local environmental factors and

intrinsic system noise [*Hatch et al.*, 2006; *Keery et al.*, 2007; *Vogt et al.*, 2010]. This is

particularly apparent when using the DTS in this configuration, as the relatively low HRTS

precision (0.2 $^{\circ}$C) introduces noise that can complicate analysis of the non-stationary amplitude

and phase information of the diurnal signal. We used the new MATLAB program VFLUX

[*Gordon et al.*, 2012] as an integrated way to both extract the 24-hr signal from the data and

calculate flux at high temporal and spatial resolution. Specifically VFLUX was used to: 1. low

pass filter the raw temperature record, 2. isolate the diurnal component of the temperature signal

using Dynamic Harmonic Regression (DHR) and extract its amplitude (one-half the maximum

minus the minimum of the wave) and phase information, 3. calculate flux every 2 hr at a range of

depths using multiple "sliding analysis windows" to detect changing flux magnitude with depth,

and 4. use the Monte Carlo method to incorporate uncertainty in streambed thermal parameters to assess potential for error of fluxes around zero ms^{-1}.

First, the original sampling rate of 20 min was reduced to 2 hr through an anti-aliasing decimation technique that preserved the diurnal signal information gained by using the original 20-min sampling rate. This low-pass filtering removed any components of the temperature record with a period of less than 4 hr, effectively eliminating much of the high-frequency noise introduced by the low HRTS precision and short-term weather fluctuations. DHR is a method of non-stationary time series signal processing that is used to extract periodic signal(s) of interest [*Young et al.*, 1999], and VFLUX runs the MATLAB Captain Toolbox program [*Young et al.*, 2010] to perform the DHR analysis. The Captain Toolbox DHR software has also been used by previous researchers [*Keery et al.*, 2007; *Vogt et al.*, 2010], and *Keery et al.* [2007] specifically notes that the extracted 24-hr temperature signal is not an approximation or smoothed copy, but a real component of the measured temperature series.

Subsequently two days of the diurnal signal were removed from each end of the temperature record to remove possible adverse edge effects of the filtering process [*Keery et al.*, 2007]. VFLUX was then used to determine vertical hyporheic flux at a range of depths through the difference in diurnal signal amplitude between any measured depth and a location deeper in the bed along the same vertical profile of temperature (Equation 2). These two temperature records bound a "window", or distance over which the vertical component of flux is determined (Figure 3). VFLUX uses the phase information generated from the DHR program to align analogous points in the temperature signals at each edge of the window (upper and lower) and calculate a flux for *every* 2-hr timestep using the amplitude ratio between the two signals [*Gordon et al.*, 2012].

Because any point estimate of vertical flux is essentially an integration of the vertical

component over the length of the window, I interpret each flux estimate as representative of the

midpoint between the two depths. The window size is held constant, and incrementally shifted

down the vertical profile as flux is calculated at the same spatial resolution as the original dataset

(0.014 m) at every timestep. Therefore the sliding analysis window is used to create a high-

resolution map of vertical flux along the HRTS profile. It should be noted that although window

size may vary, the spatial resolution of the resultant vertical flux profile is determined by the

HRTS spatial resolution (0.014 m), and is therefore constant for all windows.

It was desirable to use the smallest window possible between temperature observations to

distinctly identify abrupt changes in flux with depth which would be blurred when averaging

over too large an interval. Additionally, a smaller window between temperature observations

allows more flux information to be preserved very close to the streambed boundary, where we

can expect flow to be truly vertical and which can be used to estimate total flux into the

streambed. Although a small sliding analysis window is desirable for optimizing spatial

resolution, higher flux rates must be resolved using a relatively large window, so that a decrease

in amplitude can be adequately detected (e.g. window large enough to generate an $A_r < 1$).

Therefore the optimal (minimal) size sliding analysis window increases with vertical flux

magnitude (as illustrated in the Figure 3 insert). Because we may expect the patterns of shallow

hyporheic flux to vary both with stream morphology and depth, multiple window sizes are

necessary to optimize my interpretation of complicated flow systems. To address this need, I

used six consecutively sized analysis window sizes along each HRTS profile at increments of

0.014 m. For example, window sizes of 0.069, 0.083, 0.097, 0.110, 0.124 and 0.138 m were

used for the HRTS G_2 analysis. We then generated a composite flux matrix from those six

sliding analysis windows by averaging flux estimates at analogous depths between the vertical

profiles determined using each window size. This maximized results in high flux zones, while

still being able to resolve transitions to low flux at depth with high spatial resolution. The

optimal six window range was determined through trial and error for each HRTS, as that which

generated the most complete composite matrix with the fewest number of incalculable values of

flux through time and space (e.g., windows for which A_r is 1 or greater) yet preserve information

close to the sediment/water interface.

It was advantageous to perform these flux calculations automatically using VFLUX, as

six windows integrated over my HRTS lengths and temporal period resulted in over 100,000

individual 2-hr flux calculations per profile. Additionally, the peak amplitude information

generated during the DHR procedure was used to determine the depth at which the mean

amplitude of the diurnal signal was less than the 0.2 $^\circ$C precision of the DTS system, which is the

point at which the signal cannot be distinguished from noise [*Vogt et al.*, 2010]. This provided

an objective measure of the depth at which to stop calculating flux due to lack of signal, and this

extinction depth varied significantly with the magnitude of downward flux observed at each

HRTS location. Streambed thermal parameter inputs to the model and their uncertainty range

(Table 2) were estimated through field observation and the relationships presented by *Lapham*

[1989], and are consistent with the range of previous investigations of downstream reaches in the

same drainage [*Fanelli and Lautz*, 2008; *Lautz et al.*, 2010]. Monte Carlo analysis was

performed using the VFLUX software, which randomly varied all thermal parameters

simultaneously within a standard normal distribution defined by the corresponding estimated

parameter uncertainty [*Gordon et al.*, 2012] (Table 2). The results from 500 realizations were

integrated to determine 95 percent confidence intervals around flux values that ranged from

54

positive to negative through time at the 0.15 m HRTS B3 location using a 0.07 m analysis window. This allowed the estimation of bounds for determining whether flux was significantly different than zero ms^{-1} under these site specific conditions.

Vertical flux rates determined with heat tracing were compared to nominal travel times [*Harvey et al.*, 2005; *Triska et al.*, 1989] estimated during a 9-hr constant rate Cl$^-$ injection on August 8-9th. Profiles of pore water were collected in the streambed three times (3.7 hr, 5.3 hr, 8.3 hr into the injection) within 0.2 m of each HRTS using piezometer nests screened at 0.05-0.10, 0.15-0.20 and 0.30-0.35 m depth intervals. Nominal vertical velocities were multiplied by the general porosity determined for the site (0.35), which was assumed to equal effective porosity, to calculate vertical hyporheic flux which is directly comparable to that derived from the temperature records.

Temporal Evaluation of Flux Patterns

A linear trend analysis was performed for every depth along each HRTS profile to identify any general patterns in flux through time. Hyporheic flux patterns may be expected to change as the streambed pressure head boundary changes through time due to changing stream discharge and associated velocity and stage. Therefore, changes in vertical hyporheic flux over time were compared to changes in stream discharge over time, as a proxy for total pressure head change. The strength and significance of correlation between discharge and vertical flux were explored for every depth along each HRTS profile.

Results

Reach Hydrologic and Climatic Characterization

Over the period of HRTS data collection (July 13 to August 10, 2010) stream flow at the outlet of Cherry Creek dropped by 45 percent, from 383.4 Ls^{-1} to 210.7 Ls^{-1} (Figure 4). This corresponded to a generally steady drop in mean stream velocity at the outlet from 0.72 ms^{-1} to 0.55 ms^{-1}, while stage decreased by approximately 10 percent above both Dams 1 and 2. The ambient air temperature showed no significant trend over the month but fluctuated between 5.4 and 36.3 $^{\circ}$C, with notably warmer and colder stretches (Figure 4). These short-duration temperature changes were strongly dampened in the stream where temperature varied only between 10.0 and 17.7 $^{\circ}$C due to relatively high flow conditions and velocities which maintained the cold baseflow/snow-melt signal after the stream emerged from a deep, shaded canyon 2 km upstream. The diurnal signal in the stream, which is the input signal to the streambed, had a small amplitude that varied between 0.6 and 1.9 $^{\circ}$C with ambient weather conditions (Figure 4). Repeat differential gauging at the head (264.6 Ls^{-1}) and tail (256.6 Ls^{-1}) of a 650 m reach encompassing both dams on July 29th yielded mean values that varied less than 3 percent over the reach, or the mean error estimated with the FlowTracker instrument (SonTek/YSI FlowTracker ADV).

High-Resolution Temperature Sensing

For all HRTS, the diurnal signal was evident at shallow depths and was most pronounced during the continuous period of warm weather from approximately July 27th to August 2nd. Additionally, there was a time lag (or phase shift) and reduction in amplitude of the diurnal signal with depth; these effects varied strongly by location, indicating varied magnitudes of heat transport into the subsurface (Figures 5A, 6). The nearly vertical patterns of amplitude with

depth depicted in Figure 6 for the G_1, G_2, G_3 and B_4 locations indicate conservative transport of the diurnal signal (high flux). Temperature was plotted by depth through time along each profile to explore patterns in the propagation of heat (Figure 7). Similar patterns of thermal transport were observed within analogous morphological units, with the most variability among the four HRTS installed within bars. The bar profiles farthest from the dam, B_1 and B_2, had the shallowest propagation of the diurnal signal, while profiles B_3 and B_4, located closer to their respective dams, showed a more pronounced propagation of the diurnal signal (Figures 6, 7, Table 3) and greater transport of heat to depth.

The temperature patterns for the two HRTS installed within the bottoms of pools, P_1 and P_2, were very similar, having the coldest temperatures at depth of any of the HRTS locations (Figures 6, 7). Temperatures from deeper than 0.7 m ranged between 10.0 and 12.0 $^{\circ}$C over the first half of the month, which was comparable to the temperature of groundwater sampled in the deep hillslope water table wells (10.6-12.6 $^{\circ}$C), but lower than the temperature of adjacent riparian wells (approximately 14.0 $^{\circ}$C). The HRTS located along glides close to the dams, G_1, G_2, and G_3, had consistently strong penetration of the diurnal signal, as indicated by the vertical banding of the temperature signal with little apparent phase shift shallower than the 0.2 m depth (Figure 7). As with the B_3 and B_4 bar locations, there was notable propagation of heat to the deepest locations of HRTS profiles (greater than 0.7 m), although the diurnal signal was generally indistinguishable there due to attenuation below the HRTS precision.

High-Resolution Vertical Flux

Attenuation of the diurnal signal to less than 0.2 °C was used to determine the depth to which the true diurnal oscillation of temperature could be distinguished from measurement noise and therefore the maximum depth at which flux could be reasonably determined. This depth

varied greatly by HRTS location but was greatest at the glides and location B_4 (Table 3). Sliding analysis windows of optimal size for the 1-D model were applied to the data from each HRTS, as described in Methods, and results using those analysis windows were integrated to produce quantitative vertical flux matrices by depth through time (Table 3, Figure 8). The flux profiles had distinct boundary transitions from positive (downward) flux near the streambed interface to no vertical component at specific depths, though this depth varied strongly by morphologic unit. The median flux value at each depth was determined over the entire period of record to facilitate inter-HRTS comparison and more clearly depict spatial patterns (Figure 9).

Similar to the patterns of amplitude with depth described in Section 3.2 (Figure 6), patterns of vertical flux with depth at the bar locations were the most heterogeneous morphologic units. At the two most upstream bar locations (B_1 and B_2) vertical flux was modest at the bed interface (less than 0.4 md^{-1}) and both had a very shallow penetration depth of 0.12 m, above which vertical flux had a positive vertical component (Table 3, Figures 8, 9). These patterns also showed a transition to negative flux below the 0.12 m depth, at which the diurnal signal was still relatively strong (greater than 0.5 $^{\circ}$C). The other bar locations, B_3 and B_4, were located closer to their respective dam step and had much higher vertical flux at the bed interface (approximately 0.9 md^{-1}), although flux at B_3 was again very shallow and had no detectable vertical component below 0.18 m. In contrast, the vertical flux at B_4 was strong (greater than 0.7 md^{-1}) above 0.35 m, and below it transitioned to no vertical flow at a depth of 0.5 m, which was the deepest penetration of downward flux along any profile. The temporal flux patterns at B_4 were the most variable, and no flux could be determine for several discrete time periods and depths because of amplitude ratios above 1.0.

58

The flux patterns observed at the pool locations (P_1 and P_2) were very similar, although P_2 was much closer to the respective dam step (1.0 vs. 2.7 m) (Figures 2, 8, 9). Vertical flux was determined to a depth of 0.16 m in both locations, and produced negative values by 0.12 m (Table 3). Flux at the bed interface at P_2 was slightly greater than at P_1 (0.4 vs. 0.3 md^{-1}, respectively), although these values were quite modest and similar to those observed at the two upstream bar locations. Both profiles showed a change to negative flux with depth, and this effect was most noticeable at P_1. The depth of transition to negative flux varied by approximately 0.05 m and showed similar temporal patterns between profiles.

The glide locations (G_1, G_2, and G_3) had consistently strong vertical flux which extended deep into the sub-surface (Table 3, Figures 8, 9). At the streambed interface of G_1 vertical flux was 1.3 md^{-1} and attenuated quickly at shallow depths, then in a slow linear fashion until there was no vertical component by 0.34 m. G_2 was located in the same glide, 0.7 m downstream of G_1, and 1.0 m from the dam step (Figure 2A). The shallowest median vertical flux at this location was 1.6 md^{-1}, which was the largest value determined for any HRTS. Flux could not be estimated for the zone 0.0 to 0.06 m below the sediment water interface because amplitude ratios were so high that the largest HRTS spacings (0.097-0.166 m) of any profile had to be used. The vertical flux component was greater than 1.5 md^{-1} above 0.12 m, then dropped off rapidly before leveling off and dropping off again until being extinguished at 0.45 m (Figures 5, 8, 9). G_3 was located at the glide of the downstream dam, also 1.0 m back from the respective dam. Initial vertical flux here was greater than 1.4 md^{-1} above 0.08 m, below which it quickly fell off to 0.6 md^{-1} and reduced at a slower rate until reaching 0 md^{-1} at 0.41 m.

The Monte Carlo uncertainty analysis based on a plausible range of streambed thermal parameters (Table 2) indicated that flux estimates were most precise at approximately 0.4 md^{-1},

while uncertainty increased as flux transitioned to negative through time at the 0.15 m B_3 location (Figure 10). The 95 percent confidence interval was used to determine when flux estimates may be considered significantly different from zero md^{-1} under these system-specific conditions. This range was found to be ± 0.1 md^{-1}, and these bounds were applied to the median flux estimates as a guide for flux pattern interpretation (Figures 9, 10).

Hyporheic pore water was collected three times during a 9-hr constant rate Cl^{-} injection on August 8-9th to estimate flux rates and hyporheic connectivity in support of the 1-D vertical flux modeling. All sampling locations and depths had elevated levels of Cl^{-} 8.3 hrs into the injection, indicating all locations were connected to the stream. Locations G_2, G_3 and B_4 were comprised of over 80% stream water at 0.3 m depth by the end of the tracer injection. These locations corresponded to the highest modeled vertical flux rates of greater or equal to 0.69 md^{-1}. Locations comprised of less than 50% stream water at a shallower depth of 0.15 m at the end of the tracer injection corresponded to locations with modeled vertical flux rates of less than 0.4 md^{-1}. In general the Cl^{-1} tracer arrival times were inversely correlated with flux rates determined with the 1-D model, but there was some significant variability especially along the bar profiles.

Temporal Evaluation of Flux Patterns

The linear trend analysis revealed that B_1 and B_2 had increasing flux through time while B_3 and B_4 had decreasing flux at shallow depths. Correlations between flux at every depth and stream discharge, with $p \leq 0.01$, were plotted by depth for each HRTS, and several consistent patterns were evident (Figure 11). As expressed in the linear trends, the two most upstream bar locations had similar, strong negative correlations with discharge (more negative than -0.5) within the upper 0.1 m of the bed, indicating increased seepage as flow decreased. There was a brief transition to weaker positive correlation at depth corresponding to the change to negative

60

flux. The downstream bar locations had generally strong (B_3) or moderate (B_4) positive

correlations to discharge over the upper 0.2 m, indicating different mechanisms controlling flux

between the upstream and downstream bar locations (Figures 11, 12). Correlations at the pool

locations were variable; P_1 had the only other consistently negative correlation to discharge

(apart from the upstream bars) within the upper 0.1 m, and the downstream P_2 had little

correlation in this range. At depth, both pool locations showed moderate, positive correlations

between flux and discharge, at the same depth as the transition to negative flux. Finally, glide

locations G_1 and G_3 had positive correlation between flux and discharge at most depths, while G_2

had positive correlation over only a narrow range of depths. In summary, where amplitudes

were relatively high and flux estimates more reliable, most locations showed positive correlation

to discharge. The exception was the most upstream bar and pool locations (B_1, B_2, P_1), which

had a consistently strong negative correlation to discharge at shallow depths.

Discussion

High-Resolution Temperature Data and Vertical Flux Method

The raw high-resolution temperature data revealed many interesting and valuable

attributes of the subsurface condition upstream of beaver dams, even before the 1-D flux

calculation was applied. Attenuation of the diurnal signal amplitude showed significant variation

between the various HRTS locations. The upstream bar (B_1, B_2) and pool (P_1, P_2) profiles had

heat transport that was dominated by conduction as seen by the strong dampening of the signal

amplitude with depth. Conversely, the glides (G_1, G_2, G_3) and downstream bar locations (B_3, B_4)

had strong initial signal transmission due to high advective hyporheic transport. In addition to

the inter-HRTS location variability, the amplitude of the diurnal temperature signal did not

decline uniformly with depth at any profile (Figure 6), indicating that advection of heat and

associated vertical hyporheic flux was not uniform with depth. Without prior knowledge of the flow system at each profile location, traditional deployment of fewer fixed-depth temperature sensors [e.g. *Anibas et al.*, 2009; *Fanelli and Lautz*, 2008; *Hatch et al.*, 2006; *Keery et al.*, 2007] would have been inadequate to resolve the change in temperature amplitude and associated changes in vertical flux. Additionally, the ideal analysis window spacing at my profiles was not uniform, so deployment of fixed-depth sensors would have likely resulted in poor resolution of flux at some locations. The Figure 3 insert shows how using a large vertical sensor window in a variable oblique flow system would obscure the transition to horizontal flux with depth, and the necessity for multiple window sizes. Fundamentally, using the high spatial resolution temperature data, combined with flexible analysis window spacing, is beneficial when estimating flux patterns that are variable in space and time, because of the sensitivity of flux resolution to Δz [*Hatch et al.*, 2006]. By combining six analysis window spacings, optimized to the range in flux observed along each profile, locations of high flux were quantified while still resolving transitions to low flux at depth with high spatial resolution. The resulting flux matrices effectively integrate the benefits of a range of analysis window spacings (Figure 8).

Before any reasonable discussion of variable vertical flux can be made, it is crucial to understand how flux could vary along a vertical profile, particularly when using a 1-D flux model. Flux is a volume, so although in true 1-D flow pore water velocities can vary with effective porosity, the volume of water passing through a medium in 1-D at one time cannot. This may appear to create a mass balance problem when vertical flux patterns vary along a vertical profile; however, in shallow hyporheic flow cells, as we may expect around both bedforms and steps in the water surface profile, a vertical profile will ultimately cut across a series of different of flow paths each with their own flux mass balance (Figure 3). These types

of flow cells have been predicted and documented by a multitude of hyporheic research [*Buffington and Tonina*, 2009; *Cardenas et al.*, 2004; *Gooseff et al.*, 2006; *Harvey and Bencala*, 1993; *Kasahara and Wondzell*, 2003; *Lautz and Siegel*, 2006]. The variability in hyporheic flowpath magnitude, length and residence time has been considered as an explanation for why hyporheic exchange has power-law behavior [*Bayani Cardenas et al.*, 2008; *Gooseff et al.*, 2003; *Haggerty et al.*, 2002]. The shallow hyporheic flow patterns conceptualized by *Buffington and Tonina* [2009] show that in step pool sequences, analogous to beaver dams, flow paths upstream of the step are initially vertical but transition to the horizontal with depth, while deeper, long flow paths are almost completely horizontal. This transition is caused by head pressures along a flowpath equalizing with depth to the downstream discharge point, or the presence of a horizontal layer of low permeability. This concept is likely valid for the Cherry Creek reach which showed no change in net stream flow over the beaver dams, and therefore no diverging flow at depth as may be expected in the groundwater mounding below losing streams. Additionally, the presence of cold water at depth at the pool locations indicated the shallow hyporheic flow cells are underlain by deeper down-valley flow paths.   This type of strong shallow vertical hyporheic flux which diminishes with depth has recently been observed in streams using various heat tracing methods [*Jensen and Engesgaard*, 2011; *Vogt et al.*, 2010], and likely results from the transition to oblique then horizontal flowpaths down the profile.

For this setting a spectrum of hyporheic flowpaths along a vertical profile will likely transition to the horizontal plane with depth, therefore the assumption must be made that the 1-D flux model used for this analysis is valid for determining the vertical component of oblique flow. For example, *Lautz* [2010] showed this assumption to be theoretically true through a numerical modeling exercise using VS2DH [*Healy and Ronan*, 1996]. The author's results indicate that the

vertical component of the flow vector at any point within a two-dimensional flow field is well described by the 1-D model. Absolute errors of vertical flux estimates are greater than 50 percent when flow is dominated by the horizontal component (v_z:v_x < 0.31), in part because the values of v_z are so small. Despite this difference, the 1-D model estimates of flux are much more representative of the vertical velocity vector, rather than the total or horizontal velocity vectors. Consequently, the high-resolution temperature data gives us both a method to quantify the vertical component of hyporheic flux across a spectrum of flowpaths, and to determine the depth to which shallow hyporheic flow has any vertical component. In this way the high-resolution data set is novel, as it allows us to move beyond the purely conceptual and model domains, and quantitatively evaluate a spectrum of vertical hyporheic flow vectors measured in the field. It should also be noted that the A_r analytical method was chosen for this investigation because it is least affected by non-ideal field conditions [*Hatch et al.*, 2006; *Lautz*, 2010]. Models based on the phase shift of the diurnal signal with depth presented by both *Hatch et al.* [2006] and *Keery et al.* [2007] were also used for this dataset and erratically produced unreasonably high results (e.g. many estimates of flux greater than 10 md^{-1} for all profiles).

High-Resolution Vertical Flux Patterns Above Beaver Dams

The median flux with depth showed patterns that indicated both streambed morphology and proximity to the dam exerted strong controls on hyporheic exchange upstream of the beaver dams. The bar locations farthest away from the dam (B_1 and B_2) were likely dominated by "pumping model" type exchange [e.g. *Elliott and Brooks*, 1997] and showed shallow (less than 0.12 m) and modest (less than 0.4 md^{-1}) vertical flux along hyporheic flowpaths. The pools (P_1 and P_2) had a similar flux condition to that of the upstream bar sites (B_1 and B_2), even though the pools were much closer to their respective dams, and in close proximity to glide profiles that

64

showed significant flux. The collection of fine particles in the pools may have reduced hydraulic

conductivity and subsequent flux into the subsurface.

Despite this, vertical flux through pool bottoms measured in this study was significantly

higher than in previous investigations, which found very modest seepage (approximately 0.05

md^{-1}) of streamwater through pools, despite large negative hydraulic head gradients [*Fanelli and*

Lautz, 2008; *Lautz et al.*, 2010]. The combination of low flux and high gradients in these studies

was attributed to the collection of fines within the pools that may have greatly reduced hydraulic

conductivity and impaired hyporheic flux. This condition likely played a lesser role at the

Cherry Creek pools, as only a surficial layer of silt and clay was observed at those locations, and

much of this fine grained material had been scoured out during the extremely high snowmelt

flows that occurred in late spring, immediately preceding this work. Another reason why pool

locations had a reduced vertical flux component compared to the neighboring glide locations at

Cherry Creek is that the bottom of the pools were at a lower elevation than the surrounding bed

(Figure 2), and even below the downstream water surface at Dam 2. In such a configuration,

pressure head would change rapidly with depth into the streambed and we may expect any

hyporheic flux through the pool bottom to be dominated by the horizontal component, which I

cannot distinguish from low total flux using this method.

We found much higher flux in the upper bed at the glides (G$_1$, G$_2$, and G$_3$) and lower two

bar locations (B$_3$ and B$_4$) of 1.6 to 0.9 md^{-1}, exceeding fluxes determined for similar depths at

small downstream beaver and anthropogenic dams evaluated in previous investigations using

lower resolution temperature modeling (less than 0.5 md^{-1}) [*Fanelli and Lautz*, 2008; *Lautz et al.*,

2010] (Figures 8, 9). Our vertical flux values are more similar to the lower end of flux rates

found using high-resolution temperature methods in a losing section of a large gravel bed river

[*Vogt et al.*, 2010]. These results indicate that a significant volume of stream water is moving into the subsurface above beaver dams at Cherry Creek, but this infiltration is patchy and found generally at glides and sediment bars close to dams. Both of these morphological units were observed to have coarser-grained sediments than the bottoms of pools, and the pressure head along glides should also contain a significant velocity component that would add to the elevation head gradient caused by the dam alone. The B_4 profile was located very close to the estimated edge of a glide and had particularly high flux and the most temporal anomalies, often showing increasing flux with depth. Stream bar deposits are known to have heterogeneous layers [*Weissmann and Fogg*, 1999], potentially creating highly oblique flux conduits at depth. This could produce zones of incalculable flux, yielding noisy or bare zones in the flux matrix as seen along this profile.

As a common characteristic, similar magnitude fluxes were found at these locations for both sized dams, suggesting that once a threshold in water surface step is exceed, flux rates into the bed are limited by the general hydraulic conductivity of the sediments. High vertical flux zones at both dams also had similar transitions to horizontal flux with depth by approximately 0.5 m caused by head equilibration with depth and potentially the presence of confining layers. *Lautz and Siegel* [2006] predicted similar shallow flow cells (less than 1 m in depth) using numerical models, and concluded they likely dominate the biogeochemical processing capability of the hyporheic flow observed around beaver dams.

For several of the low-flux sites there was an apparent shift to upwelling at depth (Figure 9). This scenario was unlikely based on any reasonable physical process, so a Monte Carlo uncertainty analysis was performed over a reasonable range of sediment thermal properties to determine if the estimated negative flux was significantly different from zero (Table 2). The

results of the analysis indicated uncertainty was at a minimum when vertical flux values were approximately 0.4 md^{-1} (Figure 10), and increased as flux diminished and switched to negative through time at the 0.15 m HRTS B$_3$ location. This yielded an uncertainty range of ±0.1 md^{-1} around a zero flux estimate, indicating that the reversal to negative flux values at depth determined for the bar and pool locations were significant based on streambed thermal property uncertainty alone. This is interesting because for many of these depths the diurnal temperature amplitude was still discernable from instrument noise (0.3-0.7 $^{\circ}$C), although at these depths there were higher signal to noise ratios and presumably lower confidence in flux estimates as a result. We cannot rule out that the observed upwelling at depth was valid, potentially caused by horizontal flow encountering clay lenses and being forced upward. More likely the stronger thermal gradients observed with depth at the pool and bar locations may have contributed to error using the 1-D model at depth there, as the presence of a thermal gradient, which violates model assumptions, has been found to affect flux calculations especially under low vertical flow conditions [*Lautz*, 2010].

The Cl$^-$ tracer served to support the interpretation that the streambed profiles in Cherry Creek had hydraulic connection to the stream and showed varied rates of hyporheic flux, and is in concordance with earlier work that has shown good agreement between solute and thermal tracers [*Constantz et al.*, 2003]. The relatively high flux rates at glides, as determined through heat transport modeling, were supported by the high percentage of surface water at these locations, based on Cl$^-$ enrichment, and the minimum median flux estimates based on the tracer arrival time, which were 0.81 md^{-1} for the 0.15 m depth at all glide locations. The tracer-derived flux estimates are a minimum because of low temporal sampling resolution, and because the Cl$^-$ flux estimates were made assuming pure vertical connection of all points to the surface; any

longer, oblique flowpath would result in a higher flux estimate using the tracer data. The low-flux temperature profiles were also generally well supported by the Cl$^-$ data.

Temporal Evaluation of Flux Patterns

Significant positive correlations were found between falling stream discharge and temporal changes in flux at the glides and downstream bar locations (B_3 and B_4) at intermediate-to-deep profile depths (Figure 11). As discharge decreased over the period of observation, so did stage and velocity, all of which may serve to reduce pressure head along the bed, and in turn reduce vertical flux with depth at these locations. In contrast, however, the upstream bar and pool locations (B_1, B_2 and P_1) unexpectedly showed significant increase in shallow vertical flux with decreasing discharge. A comparison can be made between the downstream bars close to the dam (B_3, B_4) and the upstream bars farther back from the dam (B_1, B_2) at similar depths, which show opposite correlations with stream discharge (Figure 12). The shallow hyporheic exchange at the bar locations far from the dam were likely driven though hydraulic pumping over the bar [*Elliott and Brooks*, 1997]. Flow over the upstream bars became noticeably more turbulent as stage dropped and the dam exerted less control over the stream profile there, a condition that did not occur over the downstream bar which was closer to the dam and where the stream was much wider (Figure 2A). The pressure which forces hyporheic interstitial flow may be increased by a transition from laminar to turbulent flow, enhancing exchange between the stream and subsurface through time. *Cao et al.* [2003], who investigated the "pool-riffle reversal hypothesis" with a two-dimensional numerical model, showed that as stage falls, bed shear stress and the Froude number may peak at the riffle (bar) tail, with a secondary peak at the adjacent pool head. As the only HRTS profiles which showed significant increase in shallow hyporheic flux were found at these morphologic locations, the bar tail (B_1, B_2) showing the largest increase

68

and the pool head (P_1) showing modest increase, my field data may support these modeled dynamics. These patterns offer more evidence of the complicated spatial and temporal nature of hyporheic exchange, and could only have been captured at high data resolution in both regards.

Benefits of Fiber-Optic High-Resolution Temperature Sensors

We have shown that the high-resolution temperature records that were collected with these custom sensors provided the necessary versatility to optimize quantitative flux analysis. As vertical hyporheic flux was shown to vary by morphology, distance from the dams, and through time, it would have been very difficult to *a priori* predict appropriate analysis window spacings using individual temperature loggers. The resulting data set would be inherently less precise, and the complexity of vertical flux patterns shown across a spectrum of hyporheic flowpaths would not be well described. Precision in flux estimates may be particularly important when scaling up, such as determining total hyporheic flux at the reach scale using bed temperature as a proxy to flux rating curves [e.g. *Conant*, 2004]. If the initial vertical flux across the sediment water interface is not well quantified due to inappropriate analysis window spacing, these errors will be propagated throughout the interpolation process.

Fiber-optic systems do have significant overhead in terms of monetary cost and logistical set-up. Vertical "stacks" of many individual loggers could theoretically be used to provide analogous resolution to the fiber-optic HRTS, but they would all have to be individually calibrated and adjusted for differential instrument drift over the measurement period. In contrast, the entire nine profile DTS system collected synchronized temperature measurements and was kept calibrated for drift using one single record and procedure. This is extremely important when applying the 1-D flux model, as relative temperature accuracy is more important than absolute accuracy, e.g. modeled fluxes must be based on temperature record differences between

depths resulting from physical processes rather than instrument error or offset. Although many individual loggers have higher precision than the DTS system used at Cherry Creek, the system parameters could have been reasonably adjusted to yield much better HRTS precision as has recently been shown by *Suárez and Tyler* [2011]. Finally, although temperature precision was relatively coarse (0.2 $^{\circ}$C), the method still performed well despite a very modest input signal (amplitude of 0.6-1.9 $^{\circ}$C) associated with high stream discharge and cold baseflow. Many systems of interest would have larger diurnal amplitude swings during summer recession, even large rivers [e.g. *Constantz et al.*, 1994; *Vogt et al.*, 2010]. Moving forward, the spatially distributed temperature data collected with HRTS may be particularly useful to inform 2-D and 3-D numerical models (e.g. SUTRA, FLOW 3-D) which can be used to describe the total vector of oblique hyporheic flow.

Managing the shear amount of data produced by high-resolution temperature monitoring systems can be challenging. Fortunately, programs are available for software such as MATLAB which can automate and streamline these processes significantly. We utilized the program VFLUX [*Gordon et al.*, 2012] to seamlessly integrate many existing data manipulation and signal processing tools to perform many complex processes on large data sets quickly and cleanly. Over 100,000 individual flux measurements were generated from pure diurnal signals (Figure 5A) extracted from the original temperature records for each profile above Cherry Creek beaver dams. This kind of computational efficiency allowed us the flexibility to use the high-resolution records to their greatest potential. This flexibility included integration of multiple-sized sliding analysis windows that allowed us to optimize the evaluation of vertical flux which was highly variable with depth along vertical profiles.

Conclusions

The purpose of this project was to use high resolution temperature data to investigate the complicated hyporheic exchange dynamics observed around beaver dams, and to evaluate the feasibility and benefits of using multiple simultaneous fiber-optic HRTS over an extended period of time in the stream environment. The high-resolution temperature records provided a rich picture of flux through the streambed with depth through time, and similar patterns of diurnal signal transport were observed by general morphologic unit above two dams of varied size. The attenuation of the diurnal signal was used to quantitatively describe the vertical component of hyporheic flux from the stream into the subsurface using a 1-D flux model. This flux was patchy with evident "hot-spots" of seepage near the dams though glides and bars, and more modest shallow flux through pools and bar locations farther upstream from the dams. Because hyporheic flux is fundamentally driven by streambed pressure and resisted by streambed hydraulic conductivity and competing groundwater inflow, the different observed flux patterns resulted both from the proximity to the dam step and from bedform heterogeneity. Specifically, shallow vertical flux at the glides and two close bar locations was 1.6 to 0.9 md^{-1}, while shallow vertical flux at the upstream bars and pools was generally less than 0.3 md^{-1}. These general patterns of flux were supported with conservative transport of Cl^{-} injected into the stream. All profiles showed a transition to horizontal flow with depth across a spectrum of hyporheic flowpaths, with a penetration of vertical flux to approximately 0.45 m at glides and close bars and only approximately 0.12 m at pools and upstream bars. Finally, the upstream bars showed increasing flux with falling discharge over the month, which may be due to pumping model type exchange, while the other bar locations showed reduced flux with time, which may be due to decreasing head gradients over the beaver dams with decreasing stage.

The HRTS design and installation was successful, with strong signal transmission allowing the system to be run in double-ended mode which aided in calibration. As all HRTS were run inline off the same unit, all data were on the same timestep, and could all be adjusted simultaneously for instrument drift over the extended data collection period. The high-resolution temperature records allowed us to optimize the analysis window spacings to flux magnitude, which was highly variable in space. The fiber-optic HRTS is a valuable emerging tool, which can be used to describe hyporheic flow dynamics at high-resolution across a spectrum of flowpaths. These sensors are an important addition to emerging geophysical and analytical methods which are moving my descriptions of the heterogeneous hyporheic zone beyond the point scale, to a more useful understanding integrated through space and time.

Acknowledgments

Tables

Table 1. The morphology and longitudinal HRTS distances above beaver dams 1 and 2.

HRTS	Distance from beaver dam (m)	Morphology at HRTS location
B_1	4.3	edge of bar, fine gravel/silt
B_2	3.1	middle of bar, fine gravel/silt
B_3	1.0	middle of bar, fine gravel/silt
B_4	1.7	middle of bar, fine gravel/silt
P_1	2.7	bottom of pool, fine silt/clay/organics
P_2	1.0	bottom of pool, fine silt/clay/organics
G_1	1.7	mid-glide, fine silt/sand
G_2	1.0	end of glide, silt/sand/gravel
G_3	1.0	mid-glide (lateral), fine gravel/silt/sand

Table 2. The estimated thermal properties of the saturated streambed used for 1-D modeling of vertical hyporheic flux with the estimated uncertainty (standard deviation) of each parameter used for the Monte Carlo analysis in italics.

Thermal Parameter	Estimated Value
porosity (n)	0.35 (*0.05*)
volumetric heat capacity of the sediment (C_s)	2.09×10^6 (*8.4×10^4*) $\text{Jm}^{-3}{}^{\circ}\text{C}^{-1}$
volumetric heat capacity of the water (C_w)	4.18×10^6 (*1.3×10^4*) $\text{Jm}^{-3}{}^{\circ}\text{C}^{-1}$
thermal dispersivity (β)	0.001(*0.0001*) m
thermal conductivity of the saturated sediment (λ_o)	1.4 J $\text{s}^{-1}\text{m}^{-1}$ (*0.21*) $^{\circ}\text{C}^{-1}$

Table 3. The optimized sliding analysis window range and vertical flux calculation depth along each profile.

HRTS	range of (6) analysis window spacings, every 0.014 (m)	maximum depth at which flux could be resolved (m)	depth of transition to no positive vertical flux (m)
B_1	0.014-0.083	0.17	0.12
B_2	0.014-0.083	0.16	0.12
B_3	0.055-0.124	0.28	0.18
B_4	0.083-0.152	0.57	0.50
P_1	0.014-0.083	0.21	0.13
P_2	0.014-0.083	0.20	0.14
G_1	0.069-0.138	0.41	0.34
G_2	0.097-0.166	0.52	0.45
G_3	0.083-0.152	0.50	0.41

Figures
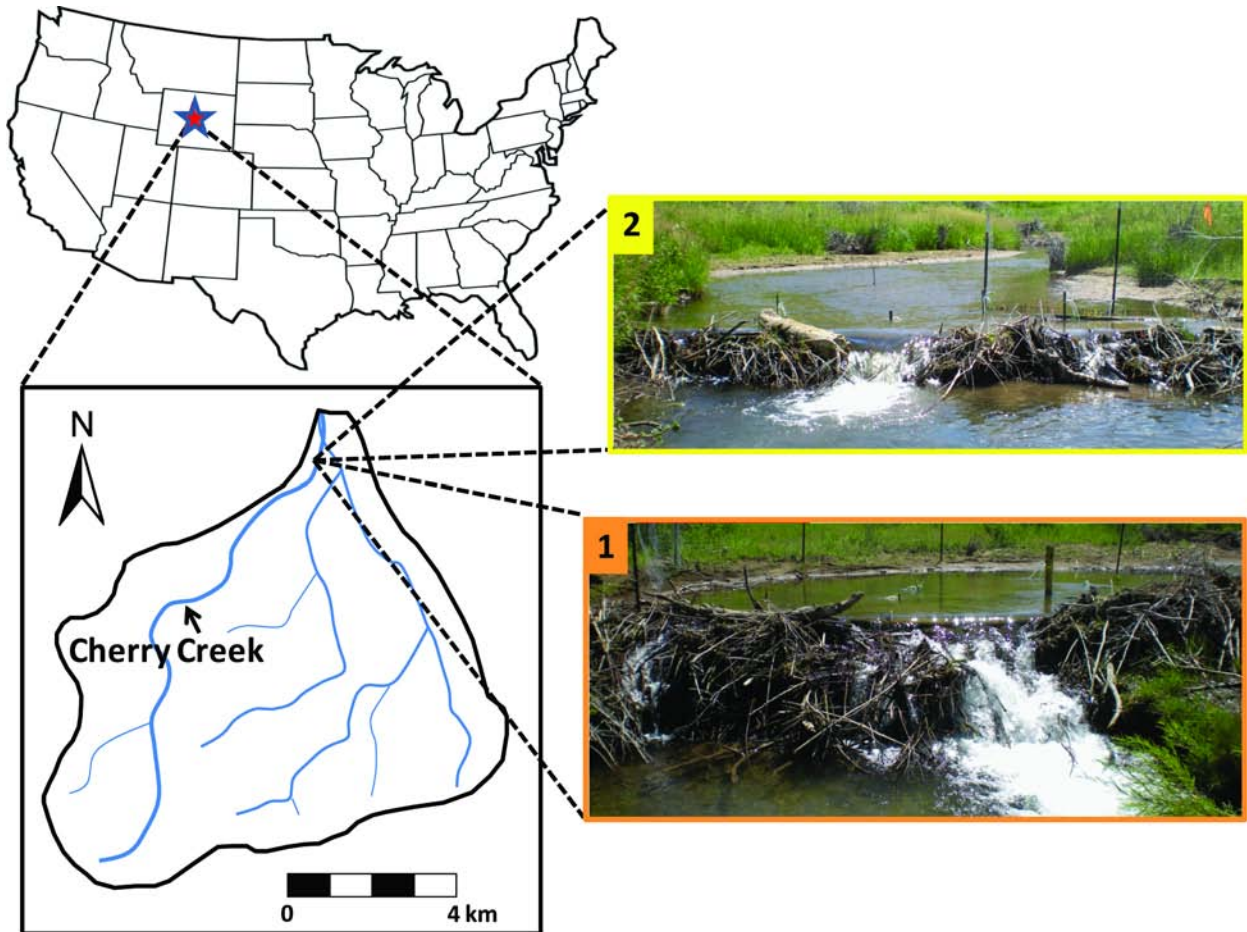
Figure 1. The Upper Red Canyon Creek drainage where Cherry Creek emerges from a deep, narrow canyon into the unconstrained valley floor along which many small beaver dams were located in the summer of 2010, including Dam 1 (0.75 m) and Dam 2 (0.35 m).
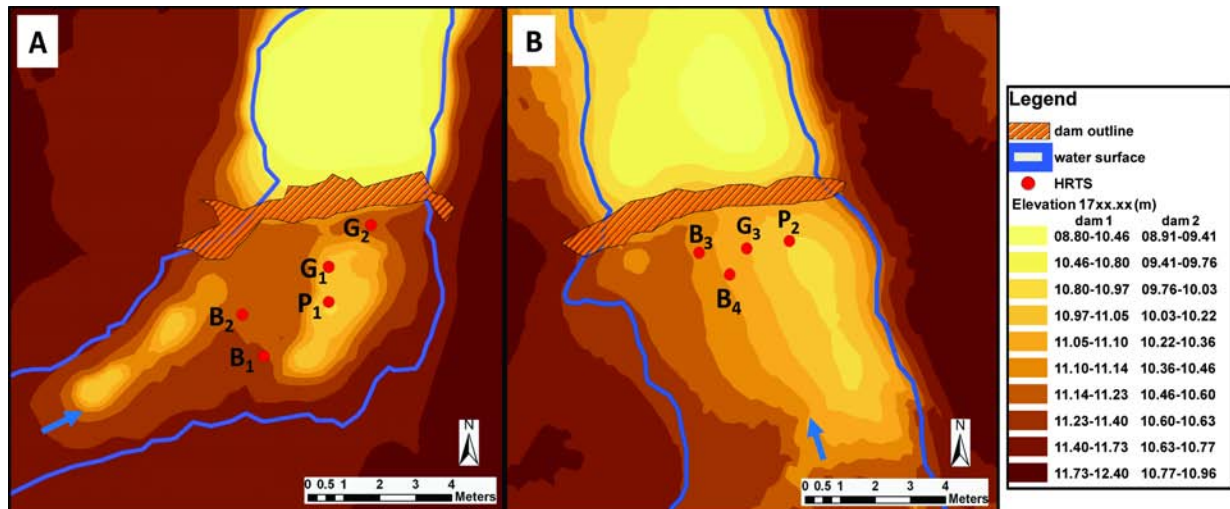
Figure 2. The streambed morphology around A) Dam 1, and B) Dam 2, the HRTS locations were classified as bar (B), pool (P) or glide (G). The water surface profile reflects the conditions on July 14th, 2010 near the beginning of the study period.
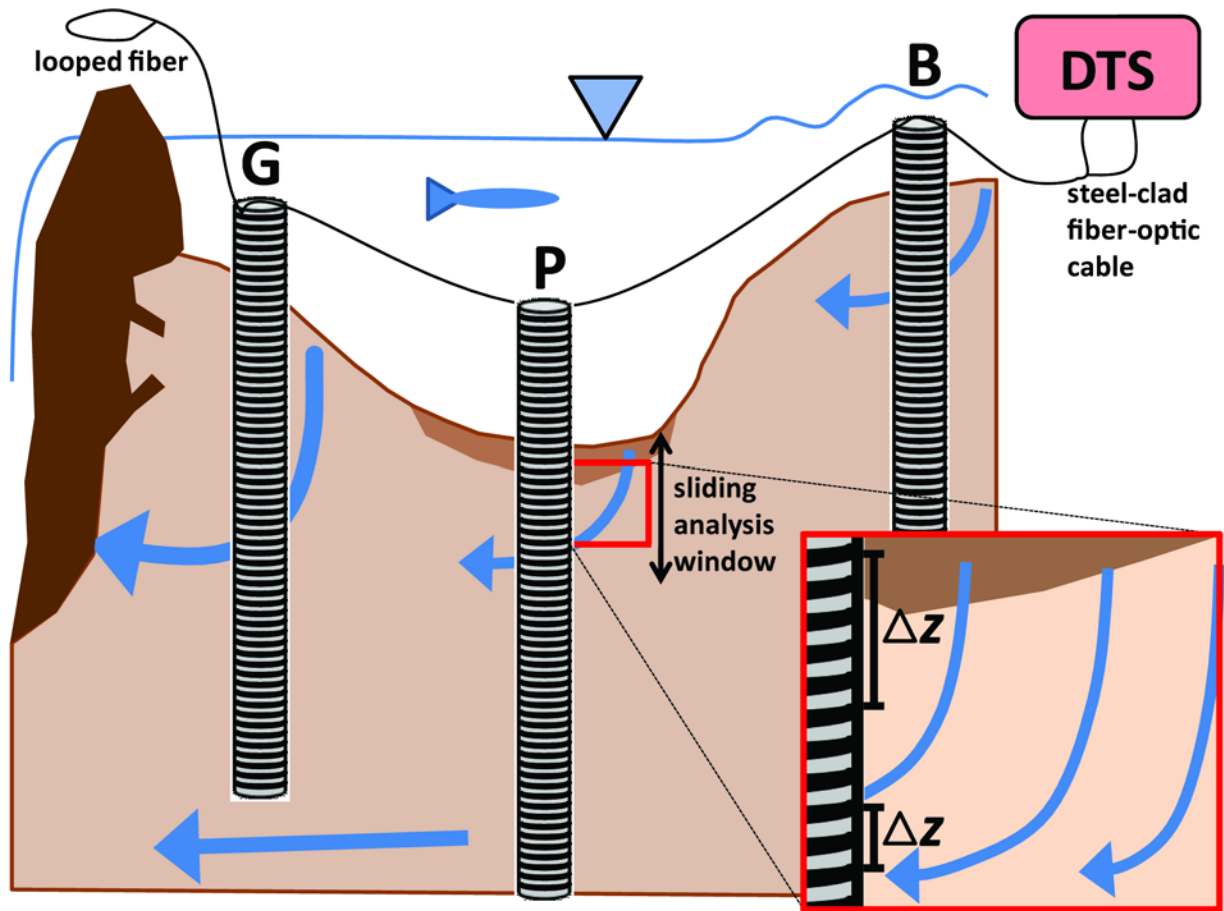
Figure 3. A longitudinal cross-section view of a bar-pool-dam sequence and the wrapped configuration of the high-resolution temperature sensors (HRTS), which provided 0.014 m spatial temperature resolution in the vertical. Two fibers ran through the stainless-steel housing and were connected through several HRTS in series, the end of which was spliced and looped to allow bi-directional laser pulses from the DTS to improve calibration. The rods were installed in streambed bars (B), pools (P) and glides (G), and the inset shows how they were found to cut across a spectrum of oblique hyporheic flow paths which transitioned from vertical to horizontal with depth, patterns that were described using the integrated "sliding analysis windows". The optimal window size (Δz) decreases with vertical flux magnitude.

77
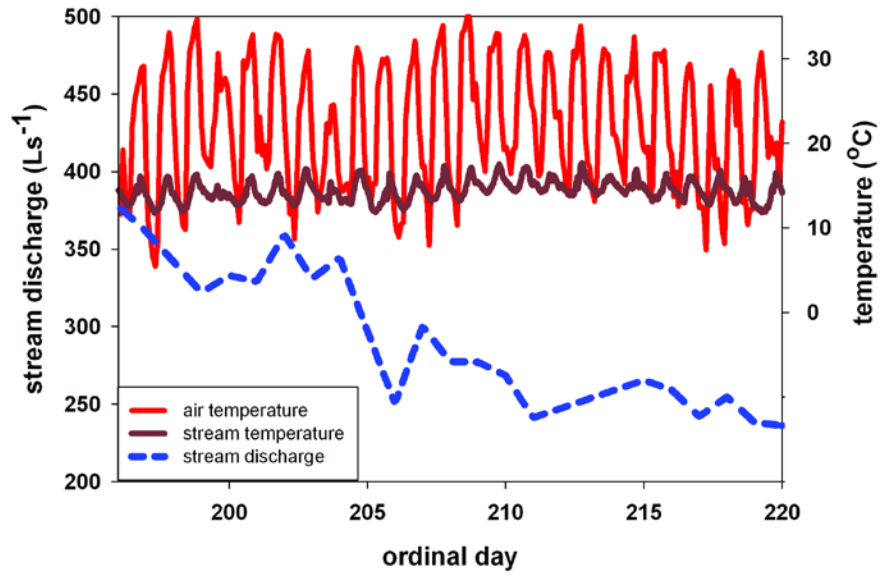
Figure 4. Daily discharge and both air and stream temperatures at Cherry Creek over the period of record. The ambient air and stream temperatures had no consistent trend over the period, and the stream strongly muted the ambient air temperature and diurnal oscillations.
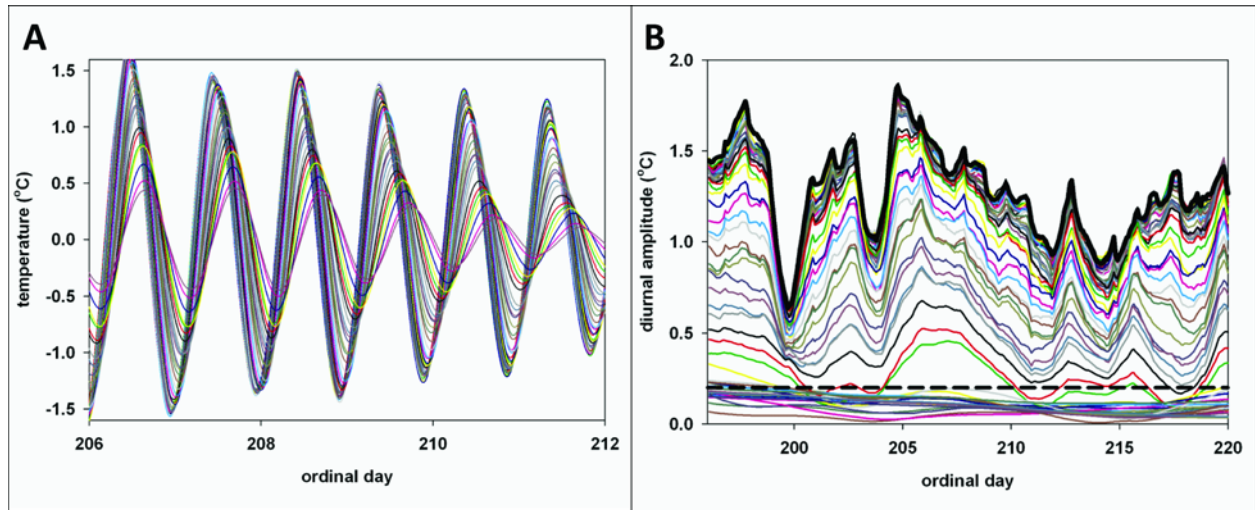
Figure 5. Panel 5A) depicts the extracted diurnal signals over several days in late July, 2010 for all depths which had signal amplitude greater than HRTS precision (0.2 $^\circ$C) along the G_2 profile. Increasing depth into the streambed was characterized by the reduction of signal amplitude and phase shift forward in time. Panel 5B) displays the changes in the amplitude of the stream diurnal signal (thick black line) through time, and subsequent reduction with propagation into the streambed along G_2 until the HRTS precision was reached (dashed line).
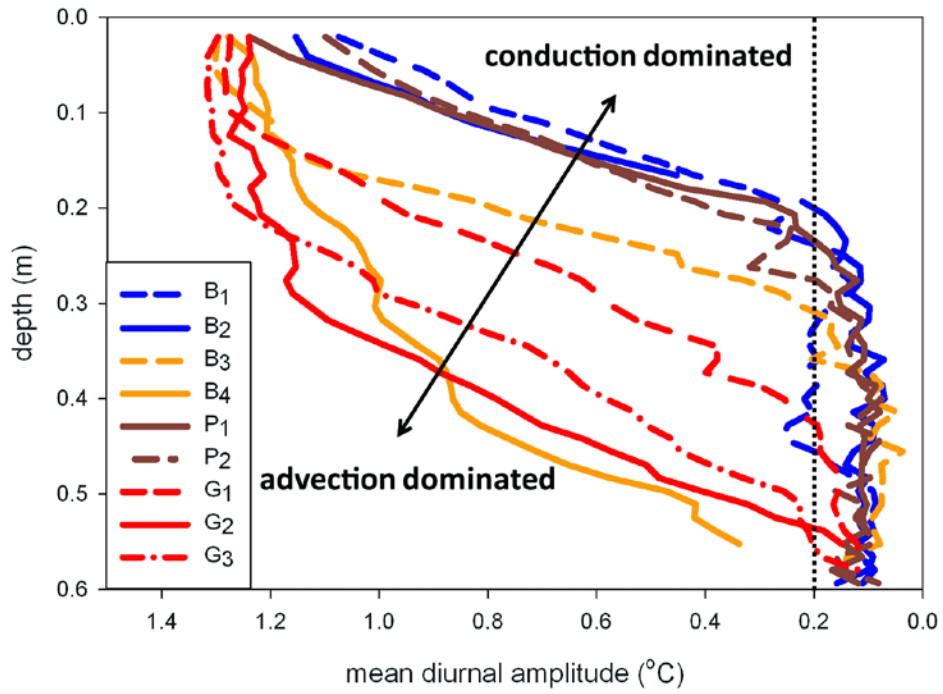
Figure 6. The variable attenuation of the diurnal signal with propagation into the streambed along each HRTS profile, the sensor precision is marked by the vertical dotted line.
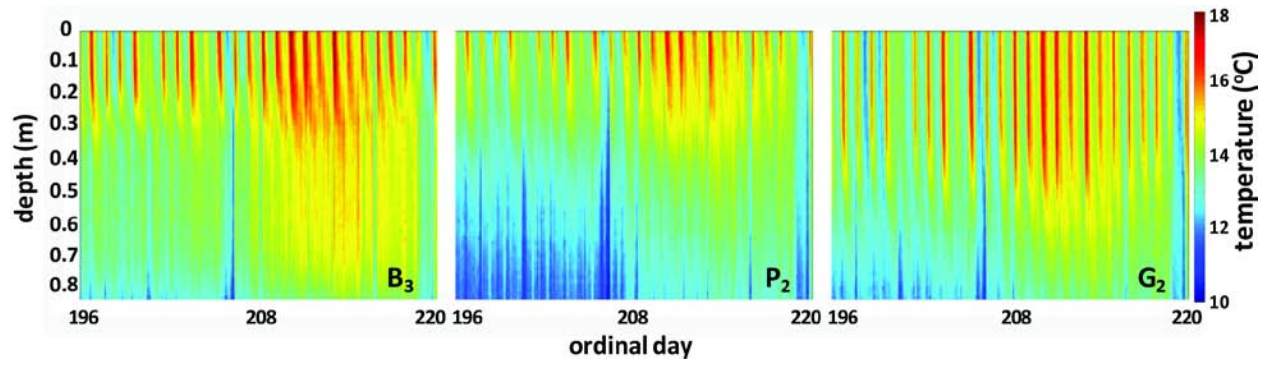
Figure 7. The temperature records at 0.014 m spatial and 2-hr temporal resolution for representative bar (B$_3$), pool (P$_2$), and the glide (G$_2$) profiles. Each "pulse" of hot color indicates the propagation of the warm daytime signal from the sediment/water interface into the streambed.
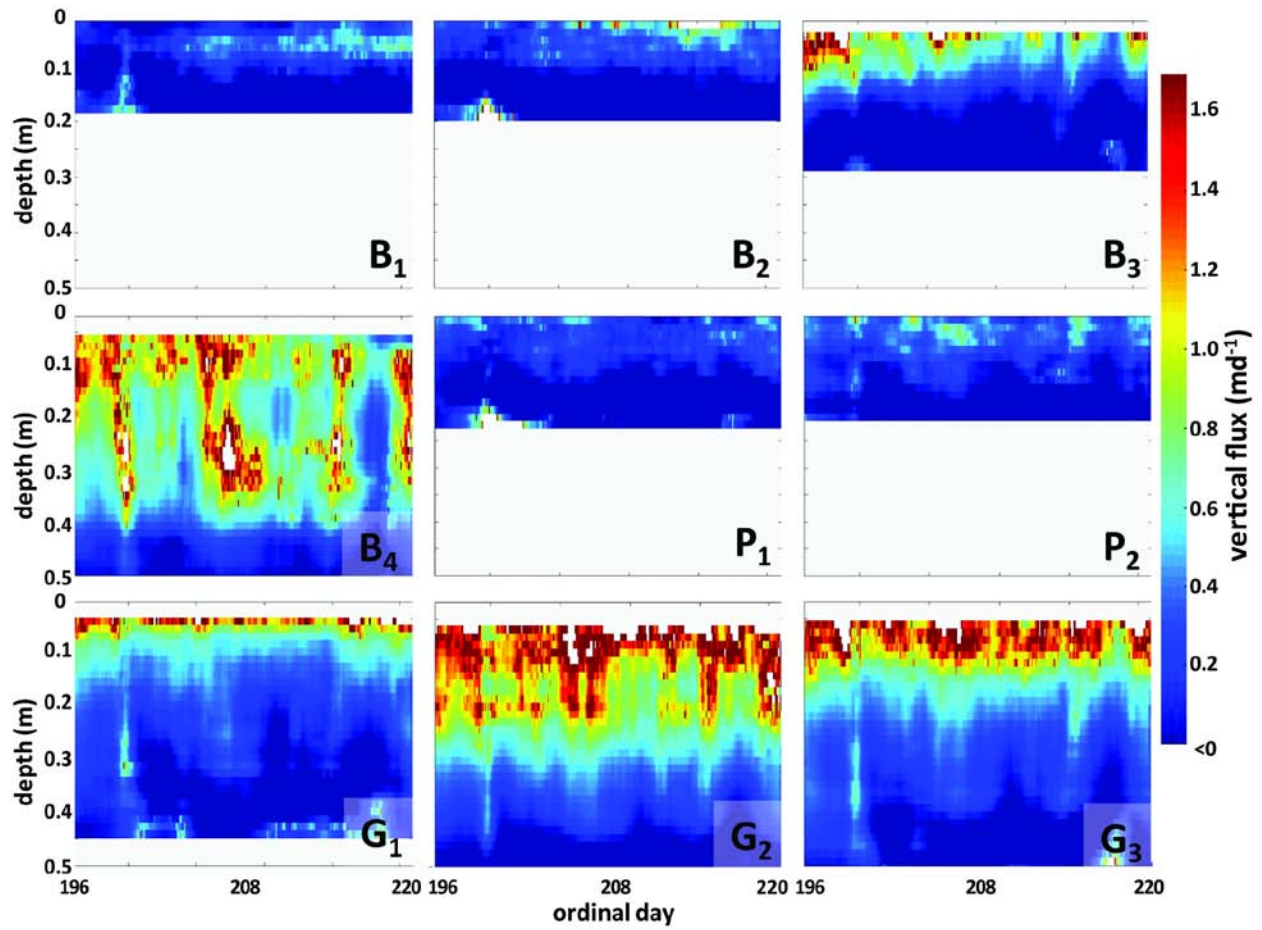
Figure 8. Vertical flux through time along each profile to the 0.5 m depth, with notable similarities by the general streambed morphology classification: B (bar), P (pool), G (glide). The white area on the graphs indicates the depths at which the vertical component of flux could not be resolved due to minimal diurnal signal propagation.
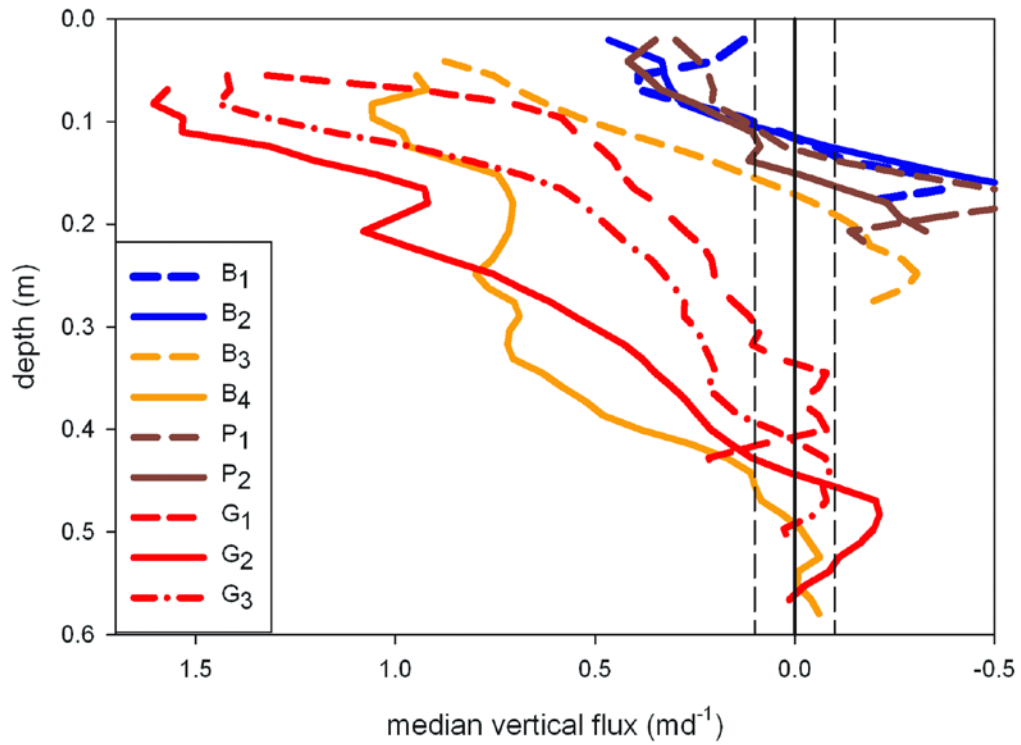
Figure 9. The median vertical flux for the study period with depth for each HRTS profile; the dashed lines show the region flux which may not be considered significantly different than 0 (± 0.1 md^{-1}) based on a reasonable range of thermal parameter uncertainty.
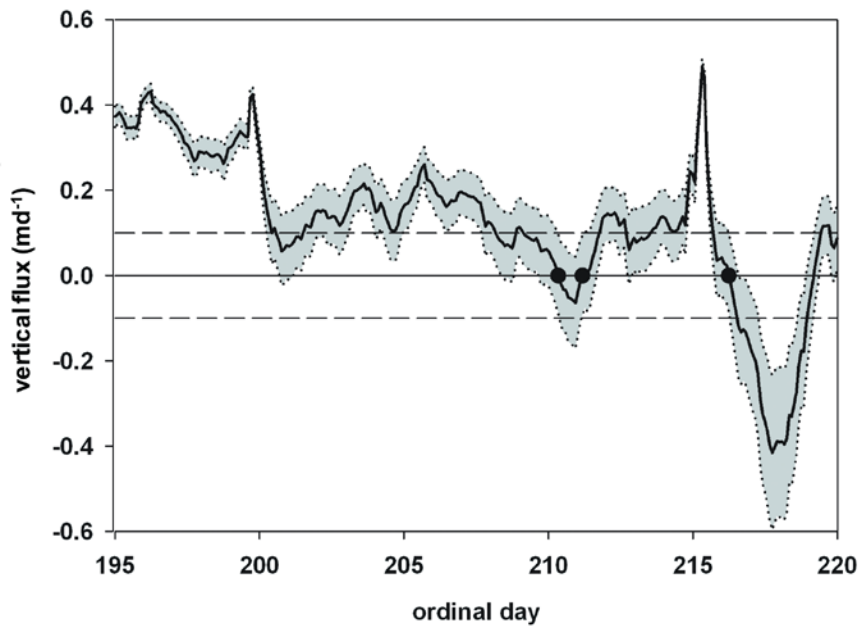
Figure 10. The 95 percent confidence interval around flux through time at the 0.15 m depth

along HRTS B$_3$. The locations where flux was zero (circles) were used to determine the ±0.1

md^{-1} where flux estimates could not be considered significantly different from zero (dashed

lines) based on thermal parameter uncertainty.
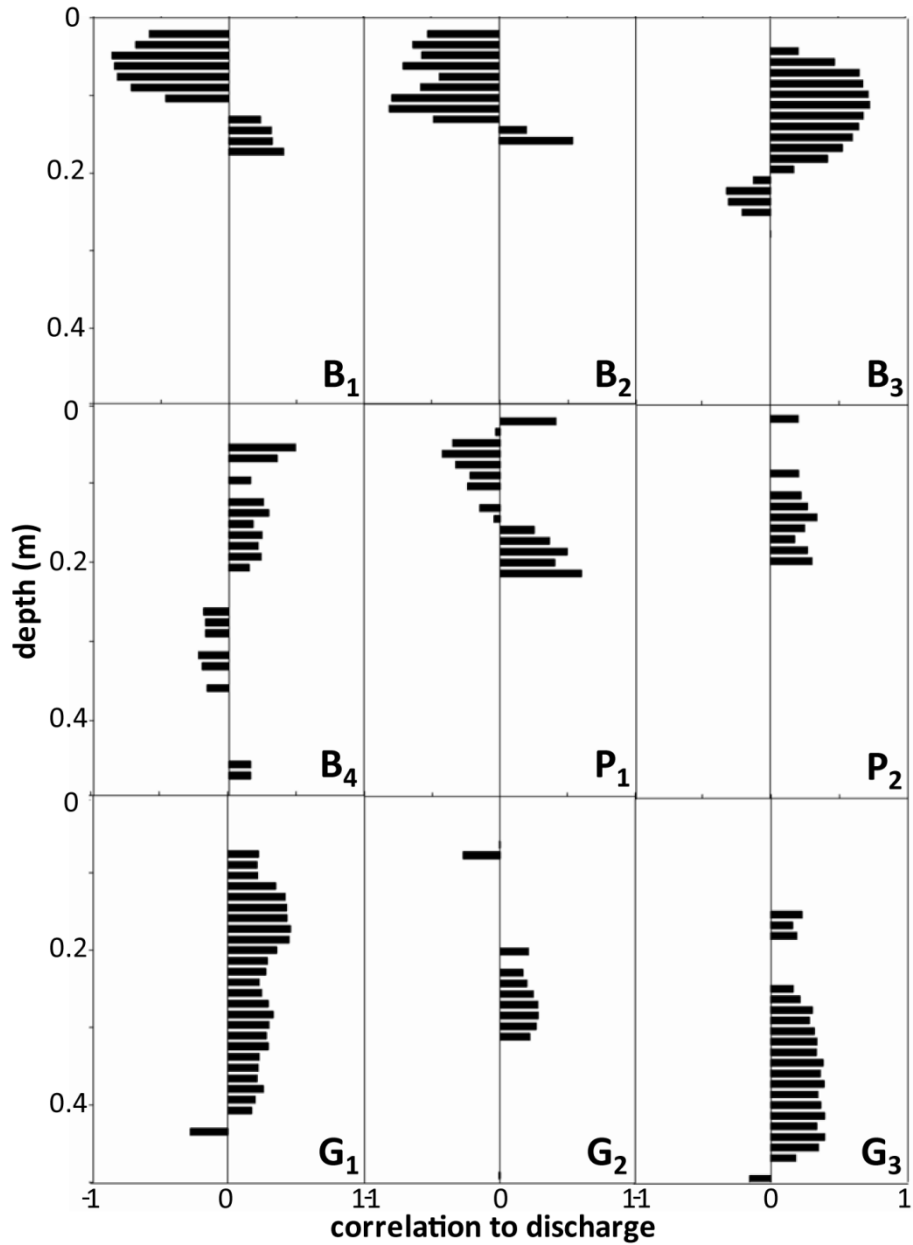
Figure 11. The correlations between vertical flux over the study period (every two hours) and discharge with significance greater than p=0.01, plotted by depth for each HRTS. Significant positive correlation was generally observed at the glides (G_1, G_2, G_3) and lower bar sites (B_3, B_4) while the upstream bar locations (B_1, B_2) had strong negative correlations within the upper 0.1 m of the bed, indicating increased seepage as flow decreased.
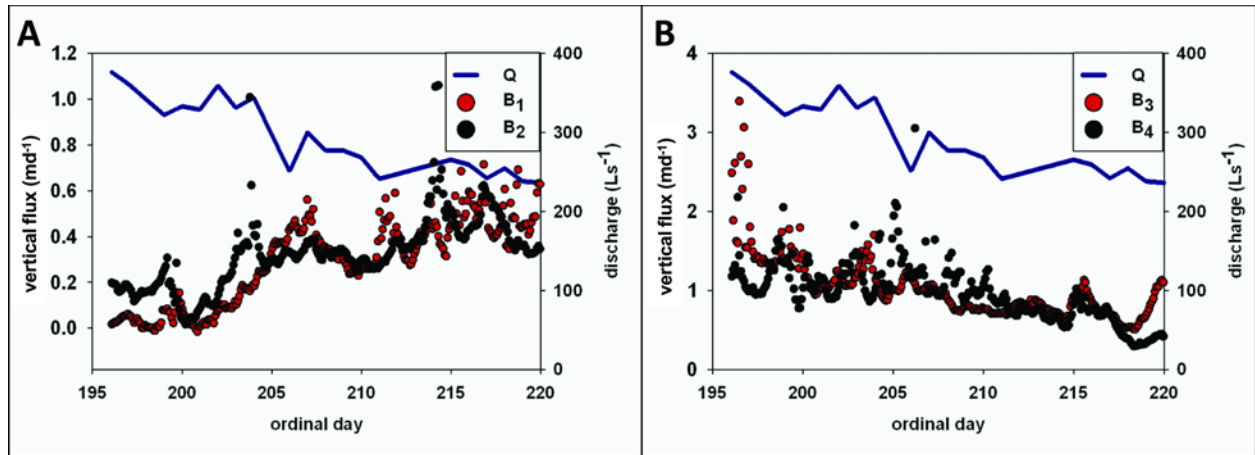
Figure 12. The patterns of vertical flux at similar shallow depths (0.05-0.1 m) at the bar locations which showed A) strong positive correlation (B_3 of -0.72, B_4 of -0.49) or B) strong negative correlation (B_1 of -0.86, B_2 of -0.57) to stream discharge through time. The flux at B_3 and B_4 was of much higher magnitude initially, but by the end of the period all locations had similar values. The shallow hyporheic exchange at the bar locations farther from the dam (B_1, B_2) was likely driven by hydraulic pumping, which may have been enhanced as stage dropped and flow became more turbulent. Conversely, B_3 and B_4 were close to their respective dam where the channel was wide; therefore flux was probably influenced by the reduction in stream stage and velocity which would have reduced pressure head on the streambed.

Chapter 3: The influence of spatial and temporal hyporheic flux patterns on streambed biogeochemistry

Submitted For Publication As:

Briggs, M.A., L.K. Lautz, D.H. Hare, R. Gonzalez (*in-review*), The influence of spatial and temporal hyporheic flux patterns on streambed biogeochemistry, *Journal of Geophysical Research Biogeosciences.*

Abstract

Small dams enhance the development of patchy micro-environments along stream corridors by trapping sediment and creating complex streambed morphologies. This drives intricate hyporheic flux patterns that govern the exchange of oxygen and redox sensitive solutes between the water column and the streambed. We used multiple tracer techniques, natural and injected, to evaluate hyporheic flow dynamics and associated biogeochemical cycling and microbial reactivity around two beaver dams in Wyoming (USA). High resolution fiber-optic distributed temperature sensing (DTS) was used to collect temperature data over nine vertical streambed profiles and generate comprehensive vertical flux maps using 1-D heat transport modeling. Coincident with these locations, vertical profiles of pore water were collected every week and analyzed for dissolved oxygen, pH, dissolved organic carbon and several conservative and redox sensitive solutes. Additionally, hyporheic and net stream aerobic microbial reactivity was analyzed with a constant rate injection of the biologically-sensitive resazurin tracer. The combined results revealed a heterogeneous system with rates of downwelling hyporheic flow organized by morphologic unit and tightly coupled to the redox condition of the subsurface. Principal component analysis was used to summarize the variability of all redox sensitive species, and results indicated hyporheic pore water varied from "oxic-stream-like" to "anoxic-reduced" in direct response to the physical hydrology and associated residence time. Temporal flux variability in low-flux morphologies generated a much greater range in hyporheic redox condition compared to high-flux zones, and these chemical changes were consistent with the empirical relationship of redox condition as a function of residence time.

Introduction

Exchange of water between streams and the subsurface may be a critical control on surface water chemistry and temperature, yet this transient process has proven to be remarkably difficult to quantify, and occurs along a spectrum of flowpath lengths and residence times [*Gooseff et al.*, 2006; *Harvey and Bencala*, 1993; *Harvey et al.*, 1996; *Kasahara and Wondzell*, 2003]. The magnitude of physical flux of stream water into the hyporheic zone governs the supply of dissolved carbon and terminal electron acceptors required to fuel biogeochemical reactions, as well as the residence time along subsurface flowpaths. Residence time controls the net effect of biogeochemical reactions on pore water chemistry by determining the degree to which the end products of these reactions can accumulate in pore water [*Lautz and Fanelli*, 2008; *Morrice et al.*, 2000; *Valett et al.*, 1996; *Zarnetske et al.*, 2011]. Because hyporheic vertical flux has fine scale variability through time [*Briggs et al.*, 2012; *Jensen and Engesgaard*, 2011; *G Rau et al.*, 2010], there may be temporal shifts in the spatial arrangement of redox horizons within the streambed [*Argerich et al.*, 2011a; *Schmidt et al.*, 2011; *Vroblesky and Chapelle*, 1994], relocating hotspots and creating hot moments of biogeochemical cycling [*McClain et al.*, 2003]. There is likely to be a strong correlation between fine scale spatial and temporal physical flux patterns, associated residence times, and streambed pore water chemistry, but compelling relationships have proven difficult to define [*Schmidt et al.*, 2011]. This is likely due in part to the difficulty in refining characterizations of hyporheic flux at a scale comparable to measured variability in pore water chemistry.

Functional units of streambed morphology (e.g., bars, pools, riffles/glides) have been suggested as controls that spatially organize paired physical and biogeochemical patterns [*Claret and Boulton*, 2009; *Marzadri et al.*, 2011; *Valett et al.*, 1996]. The streambed morphology

surrounding small dams can affect hyporheic exchange and generate predictable spatial arrangements in pore water chemistry that are highly variable over short distances [*Fanelli and Lautz*, 2008]. Beaver dams in particular trap large quantities of sediment and organic material [*Naiman et al.*, 1986], generating streambed morphologies that both enhance and diversify local hyporheic exchange [*Briggs et al.*, 2012b]. Patches of downwelling water from the stream, induced by bedform and pressure changes over dam structures, may correspond with hotspots of biogeochemical transformation and uptake, as water rich in dissolved oxygen (DO) and organic carbon is transported into the subsurface [*Lautz and Fanelli*, 2008]. Such downwelling flowpaths through fine sediment may also serve to trap particulate organic matter which further fuels biogeochemical reactions [*Boulton et al.*, 1998].

Net oxygen removal from hyporheic pore water by aerobic respiration will primarily depend on residence time [*Morrice et al.*, 2000; *Valett et al.*, 1996; *Zarnetske et al.*, 2011], temperature, microbial density/contact with biofilms, and the availability of organic carbon [*Baker et al.*, 2000; *Vroblesky and Chapelle*, 1994]. As DO is consumed, microbial communities make use of other available terminal electron acceptors in a predictable sequence based primarily on redox thermodynamics which maximize free energy change [*Baker et al.*, 2000; *Hedin et al.*, 1998]. This sequence should proceed from aerobic respiration to denitrification, followed by manganese (Mn IV), iron (Fe III), and sulfate (SO_4^{2-}) reduction [*Champ et al.*, 1979]. Phosphorus (P) may also be "redox sensitive", as it can be released during metal reduction and desorbed from sediments under anoxic conditions [*Boulton et al.*, 1998; *Mortimer*, 1941]. Nitrification may occur in aerobic streambed zones where ammonia has been produced by the mineralization of organic nitrogen [*Jones et al.*, 1995]; but, as nitrification can only take place

90

under oxic conditions [*Duff and Triska*, 2000; *Jones et al.*, 1995], ammonium (NH_4^+) may accumulate along anoxic flowpaths when not assimilated [*Pretty et al.*, 2006].

For this study I combined some of the latest sensing and analytical methods to explore the link between fine scale hyporheic flux patterns and the assemblage of bioreactive zones in the streambed. Fiber optic high-resolution distributed temperature sensors (HRTS) were used to determine vertical advective flux at high spatial (0.014 m) and temporal (2 hr) resolution, as described by *Briggs et al*. [2012b] and summarized below. In conjunction with the vertical flux data, profiles of pore water were collected weekly and analyzed for a suite of solute concentrations, including seven redox sensitive species (DO, NO_3^-, Mn, Fe, SO_4^{2-}, P, NH_4^+). This solute geochemical data was augmented with a hyporheic and reach scale resazurin injection. Resazurin (Raz) is a fluorescent dye that undergoes irreversible conversion to resorufin (Rru) in the presence of functioning aerobic microbial communities (*González-Pinzón et al*., submitted to *J. Geophys. Res.,* 2012), and has recently been applied in streams as a field tool to identify aerobically reactive flowpaths [*Argerich et al.*, 2011b; *Haggerty et al.*, 2009]. The Raz/Rru conversion rate is approximately three orders of magnitude higher in the hyporheic zone than in the stream water column [*Haggerty et al.*, 2009], so Raz provides an extremely targeted tool for identifying subsurface reactive flowpaths. The rates of conversion are much higher in the hyporheic zone because there is greater contact between water molecules and bioreactive surfaces as they pass through interstitial pores, a similar mechanism that creates hotspots of nutrient cycling. During constant rate in-stream injections, Raz samples can be collected in the subsurface to quantify aerobic reactivity along specific flowpaths, or within the stream channel to evaluate net reach reactivity. Therefore, Raz provides a quantitative technique to link local and reach scale processes, which is vital to evaluate the degree to which microbial

reactivity in the hyporheic zone at beaver dams influences reach-scale reactive exchange and nutrient spiraling in streams. The detailed flux data generated by the HRTS technique allowed a spatially refined description of the physical hydrology of the system that was directly compared to biogeochemical patterns to develop definitive relationships between hyporheic flux, residence time and streambed biogeochemical cycling. The objectives of this work were to: 1) characterize spatial variability of biogeochemical conditions in the hyporheic zone with depth and between morphological units, and analyze how those spatial patterns correlate with spatial patterns of hyporheic flux; 2) correlate temporal changes in streambed biogeochemical profiles with temporal changes in vertical hyporheic flux; and 3) develop a predictive relationship between biogeochemical conditions in the hyporheic zone and hyporheic zone residence time.

Methods

Site Description and Geomorphic Characterization

This study was conducted from July 13th to August 10th, 2010, at Cherry Creek, a tributary to Red Canyon Creek and the Little Popo Agie River, which drains the south-eastern flank of the Wind River Range south of Lander, Wyoming (USA) [*Lautz et al.*, 2006]. The creek is located on a large parcel of land owned by The Nature Conservancy of Wyoming, which practices sustainable cattle management in the watershed. Although the contributing area for Cherry Creek is a modest 30 km^2, the system is characterized by large snow-melt flows which transition to baseflow over the summer. Cherry Creek originates in a high alpine area at about 2650 m.a.s.l., then passes through a narrow canyon before emerging onto an open plain of unconsolidated deposits of glacial till and alluvial sands and gravel at about 1750 m.a.s.l. [*Jin et al.*, 2009]. The lower 3 km of creek is generally incised, and impeded by multiple beaver dams that trap large quantities of sediment and organic matter, creating a stepped streambed

morphology and reducing the overall 1% grade. Although numerous beaver dams have been present on the creek since at least 2007 [*Jin et al.*, 2009], many of the dams were damaged or destroyed by an exceptionally large melt event during the spring of 2010. These anomalously high flows also scoured much of the fine sediments above the dam structures, creating complex bedforms. Discharge in Cherry Creek, just above the confluence with Red Canyon Creek, dropped from 383 Ls^{-1} to 211 Ls^{-1} (45 percent) over the study period, as recorded with a handheld acoustic doppler velocimeter (SonTek/YSI FlowTracker ADV) [*Briggs et al.*, 2012b].

The two dams selected for this investigation were located 75 m apart and 1160 m upstream of the confluence with Red Canyon Creek (Figure 1). Dam 1 created a 0.75 m step in the water surface profile at the beginning of the study period, while the downstream Dam 2 had a 0.35 m step. The morphology above both dams was analogous: defined by a longitudinal bar adjacent to a scour pool. These features were mapped from a high density spatial survey collected with a Nikon Nivo 5.M total station. A modified Wolman pebble count [*Wolman*, 1954] of 100 random surficial sediment grains collected above each dam was used to determine that the D_{50} above both structures was less than 2 mm, and organic particles made up 15 and 5 percent of the samples collected above Dams 1 and 2, respectively. Profiles of streambed temperature and pore water chemistry were collected at varied distances from both dams in locations chosen to represent the dominant morphologies of pools (P), bars (B) and riffles/glides (G). Bar profiles B_1 and B_2 were set back farther from their respective dam than bar profiles B_3 and B_4 (Figure 1). Profiles B_3, B_4, P_2, and the glide profiles (G_1, G_2 and G_3) were within 1.7 m of their respective dam step, while P_1 was set farther back from the dam, in closer proximity to the farthest upstream bar profiles (B_1, B_2) (Figure 1).

High-Resolution Hyporheic Flux

The vertical hyporheic flux rates presented here were originally reported by *Briggs et al.* [2012] where the associated methodology is discussed in detail, and briefly summarized here. Custom high-resolution temperature sensors (HRTS) were used to generate high-resolution profiles of vertical hyporheic flux for a period of about 6 weeks at the nine profile locations shown in Figure 1. HRTS are comprised of fiber optic cables wrapped around 0.05 m diameter rods, which are connected in series to a distributed temperature sensor (DTS) to measure temperature along the fiber continuously in time. The HRTS sensors were installed vertically within the streambed sediments to at least the 0.8 m depth and recorded integrated streambed temperatures every 20 min with 0.014 m vertical resolution and a precision of 0.2 °C.

The HRTS data were used to observe the variable propagation of the stream's diurnal temperature fluctuations to depth in the streambed. The extensive temperature data sets generated by the sensors were compiled using MATLAB (The Mathworks Inc., Natick, Massachusetts, USA), and interpreted using an analytical solution to the one-dimensional heat transport equation [*Hatch* et al., 2006], as implemented by the new VFLUX MATLAB program, which is described in detail by *Gordon et al*. [2012]. VFLUX was used to determine vertical hyporheic flux at 2-hr intervals at all depths where the amplitude of the diurnal temperature fluctuation exceeded 0.2 °C. Out of the four VFLUX analytical options to determine vertical flux I chose the amplitude method originally presented by [*Hatch et al.*, 2006]; this technique has been shown to perform best under non-ideal field conditions [*Lautz*, 2010]. The amplitude method makes use of the variable attenuation of the stream's diurnal temperature signal with depth in the streambed to determine the vertical component of advective hyporheic flux. For the HRTS profiles, temperature time series separated by varied vertical distances were compared;

observed differences between the propagation of the diurnal signal amplitude and that expected based on pure conduction were attributed to convective transport [*Hatch et al.*, 2006]. The result for each HRTS profile is a map of vertical flux through time at 0.014 m spatial resolution and 2-hr temporal resolution (Figure 2). For spatial comparison of average flux rates between morphologic units, the temporal complexity of these maps was reduced by taking the median flux value through time at each depth. For temporal analysis of the flux data, linear trends over time were computed at each depth and correlations between the flux rate and stream discharge over time were explored.

Hyporheic Water Chemistry

Profiles of pore water were collected in the streambed within 0.2 m of each HRTS using piezometer nests screened at 0.05-0.10, 0.15-0.20, 0.30-0.35 and 0.50-0.55 m depth intervals (Figure 2). For clarity in presentation, each piezometer will be identified by the center of the screened depth interval for the remainder of the manuscript (0.08, 0.18, 0.33 and 0.53 m). The piezometers were constructed of 0.32 cm inner-diameter plastic tubing and screened with 0.05 m pressed-sand air diffusers arranged along a vertical profile. Samples were collected once a week for five weeks during midday between July 13th and August 9th, 2010, or ordinal days 194, 203, 210, 216 and 221. For the final round of sampling the 0.53 m depth was not included. Prior to collecting each sample, the piezometer was cleared, then water was drawn slowly using 60 mL syringes and filtered immediately through Whatman GF/F Glass Microfiber Filters. Samples were frozen until the time of the analyses, before which they were thawed and acidified. DO and pH were measured in the field using a WTW 340i multiprobe, then analyzed upon return to the lab using ion chromatography (Dionex ICS-2000) for Na^+, K^+, Mg^+, NH_4^+, Ca^{2+}, Cl^-, NO_3^-, and SO_4^{2-} and using inductively coupled plasma optical emission spectroscopy (Perkin-Elmer

OPTIMA 3300DV) for Fe, Mn, P, Sr, K, Mg, Na, Si and Ca. Non-detections of solutes were replaced in the data matrix by the precision of the given instruments determined by the standard deviation of repeat samples at similar concentration range (Table 1). DOC was measured with a UV-Persulfate TOC analyzer (Dohrmann Phoenix 8000).

Hyporheic water may be a mixture of surface and groundwater end-members; therefore it is important to monitor both stream and groundwater chemistry through time to parse changes in pore water chemistry that are due to biogeochemical processes occurring in the hyporheic zone from changes due to variable contributions of the two end-members. Therefore, in-channel stream water samples were collected just upstream of the study site several times per week and analyzed for the same suite of constituents as the pore water samples. Local groundwater was collected once per week from piezometers constructed of 0.04 m diameter PVC screened from 0.75 to 1.0 m depth and installed within the riparian zone adjacent to both dams. Additionally, deep streambed water samples were collected from 0.75-0.80 m depth at the B_1 and P_1 profiles on day 194 and from a group of water table wells located down valley just outside of the riparian zone on day 223. Spatial and temporal mixing relationships of stream, hyporheic and groundwater were explored using ratio-ratio plots of "conservative" ions [*Langmuir et al.*, 1978].

Principal Component Analysis

Principal component analysis (PCA) was used to summarize the spatial and temporal variability in DO and the redox-sensitive solutes (NO_3^-, Mn, Fe, SO_4^-, P, NH_4^+) in stream water and pore water along each profile. When concentrations of solutes within a geochemical dataset covary due to fundamental underlying processes, PCA can summarize the variability into a set of components that is created from a linear combination of the normalized and transformed solute concentrations [*Cloutier et al.*, 2008; *Davis*, 1986]. Because DO and redox-sensitive solutes are

consumed or released via microbial activity in a predictable sequence, there should be predictable covariance among constituents of the "redox ladder", dynamics which have been successfully described using PCA [e.g. *Lautz and Fanelli*, 2008].

Prior to PCA analysis the concentrations of each solute were square-root transformed to increase normality and standardized (mean of zero and standard deviation of one) to make concentration ranges and magnitudes between species comparable. The PCA analysis was performed using MATLAB, which reports the eigenvectors (e.g., loadings), eigenvalues (e.g., explained variance) and linear scores of each principal component. The loadings indicate the relative importance of each individual species to the respective principal components [*Davis*, 1986], while the eigenvalues describe how much of the original total variance of the combined data matrix is explained by each component. When using standardized data, an eigenvalue of 1.0 indicates the principal component explains as much variance as one of the original variables; therefore, components with an explained variance less than 1.0 are often neglected [*Davis*, 1986; *Preisendorfer*, 1981].

For this analysis only the first principal component was needed to explain the majority of the data variance, and the first component scores were interpreted as a linear "redox score", indicating where a specific sample fell on the gradient from stream-like-oxic conditions to reduced-anoxic conditions. Therefore each sample had its own unique redox component score. For spatial analysis of biogeochemical conditions between sites, the redox scores were averaged through time at each depth along profiles to create mean redox profiles (Figure 2). Correlations between median vertical hyporheic flux with depth, as measured with heat tracing, and corresponding mean redox scores with depth were explored to assess linkages between rates of hyporheic flux and biogeochemical conditions. The temporal variability in redox scores along

97

each profile were also compared to temporal flux patterns at the same depths to investigate the

transient control of residence time on streambed biogeochemical cycling. Additionally, the

complete profiles upstream of Dam #1 (B_2, P_1, G_1, G_2) were plotted in two-dimensions as

distance from the dam vs. depth to create cross-sections of redox score variability. Interpolations

between measured points were made using the "nearest neighbor" analysis in GIS software

ArcMap 9.3 (ESRI, Redlands, California, USA).

Resazurin Tracer

Hyporheic water was collected from the same piezometer nests used for measuring *in situ*

pore water chemistry at 3.7, 5.3 and 8.3 hr into a 9-hr constant rate injection of paired Raz and

chloride (Cl^-) tracers on ordinal days 220-221, 2010. In addition to hyporheic water, in-channel

samples were collected from the thalweg at both dams and 1200 m downstream of Dam 1. The

tracer injectate concentration was approximately 1 gL^{-1} Raz and 270 gL^{-1} NaCl, and was kept

mixed inside a 1.0 m^3 irrigation tank using a 1900 Lh^{-1} bilge pump operated continuously. The

injection tank was located 200 m upstream of Dam 1, and the injection rate was kept constant at

1500 $mLmin^{-1}$ using a custom piston pump governed by a fluid meter (Fluid Metering, Inc.,

Syosset, New York, USA).

Pore water Cl^- concentrations observed during the injection were corrected for

background using depth specific pre-injection values. The Raz/Rru samples were analyzed at

Oregon State University with a Cary Eclipse Fluorescence Spectrophotometer (Agilent

Technologies), and Raz/Rru concentrations were corrected for dilution using the Cl^- tracer. We

investigated hotspots of aerobic respiration within the hyporheic zone around the dams by

comparing the [Rru]/[Raz] ratio in streambed pore water samples to the stream input signal along

each profile at plateau conditions. Additionally, these values were compared to the in-stream

ratios collected at the downstream location to provide a comparison between the hyporheic zone aerobic reactivity and the net stream signal after 1400 m of transport.

Results

Hyporheic Flux

As noted in the methods, the vertical hyporheic flux rates for each profile are presented in detail in *Briggs et al*. [2012b], but a summary of the relevant information is as follows. Vertical flux rates from the HRTS analysis had a vertical spatial resolution of 0.014 m and therefore three vertical flux time series fell within the depth range of each 0.05 m piezometer screen (Figure 2). The flux rates at these three depths were averaged to yield one flux time series for each piezometer screen that could be directly compared to the corresponding geochemical dataset. All vertical fluxes at the streambed interface were found to be downwelling, and flux magnitudes were organized by streambed morphologic unit. The vertical component of flux was attenuated with depth over all profiles, which was interpreted as a transition to horizontal hyporheic flow. Differences between morphological units are clear when the median flux along each profile is plotted, as in Figure 3A. The strongest and deepest hyporheic flow cells were found at the glide locations, but the downstream bar locations were similar, particularly B_4. Conversely, the upstream bar (B_1, B_2) and pool (P_1, P_2) profiles had shallow flux of much smaller magnitude that attenuated rapidly with depth (Figure 3A). The estimated transition to upwelling at depth along these profiles was considered unlikely, and may have resulted from model error (see discussion in *Briggs et al.* [2012b]).

Significant increasing temporal trends from circum-neutral flux to greater than 0.3 md^{-1} downwelling were found for the upstream bar (B_1, B_2) and adjacent pool (P_1) locations over the course of the six-week study period (Figure 4A). These trends were attributed to an increase in

99

pumping-model type exchange, where hyporheic flux is enhanced by increasing pressure differentials across the bedforms, which are caused by increasingly turbulent water flow [*Elliott and Brooks*, 1997]. As stage dropped and the depth of water overlying the bedforms decreased, turbulence and bed shear stress increased. These profiles all showed a simultaneous short-term decrease in vertical flux at shallow depths around day 200 to flux rates below (0.1 md^{-1}), which is the threshold below which fluxes cannot be considered significantly different from zero, as determined through Monte Carlo analysis by *Briggs et al*. [2012b](Figure 4A).

The downstream bar locations close to the dam (B$_3$, B$_4$) showed marked decreases in vertical flux at shallow depths, from fluxes greater than 1.2 md^{-1} at the beginning of the study period to moderate fluxes generally less than 0.8 md^{-1} by the end of the study period. This decreasing trend over time was attributed to the declining stream stage and associated hydraulic gradient across the streambed interface immediately above the dam as discharge decreased by 45%. Flux at the glide locations showed some shallow short term variation (e.g., high spikes), and modest decreases at depth, but generally remained high over time and depth.

Spatial Stream, Groundwater and Hyporheic Water Chemistry

Some solute concentrations were not significantly different between the stream and the local riparian water (Cl$^-$, K$^+$, Mg^{2+}, Si), but Na$^+$, Ca^{2+}, Sr and the redox sensitive species (NO$_3^-$, Mn, Fe, SO$_4^{2-}$, P, NH$_4^+$) all varied considerably between the two end-members. A ratio-ratio plot of Ca^{2+}:Na$^+$ and Sr:Na$^+$, which were considered generally conservative in terms of local mixing (Figure 5), indicated that temporal changes in stream water chemistry were similar to variations in hyporheic chemistry, while the riparian and deep groundwater followed a different spatial/temporal mixing pattern.

The pH of stream water and hyporheic water along all profiles through time averaged 7.9 (sigma 0.3) and there were no clear spatial trends. DOC in stream water varied between 1.8-3.7 mg-C L^{-1} over the period but showed no temporal trend, and DOC in the 0.08 m pore water was also variable, but similar to stream values (Figure 6). The pool locations had the highest mean [DOC] of 3.3 and 3.0 mg-C L^{-1} for P_1 and P_2, respectively, while the lowest value of 2.0 mg-C L^{-1} was found at B_1. Examples of changes in the mean concentrations of terminal electron acceptors for the oxidation of organic carbon (O_2, NO_3^-, Mn, Fe, SO_4^{2-}) with depth along the B_2 and G_1 profiles are shown in Table 1. Both spatial variability (by depth) and temporal variability (reflected by the standard deviation) are much greater in all species along the B_2 profile, which has lower flux and longer residence time, while the variability along the G_1 profile, which has higher flux, more closely mirrors the small temporal changes in the input stream signal.

Concentrations of SO_4^{2-} were similar to stream values or decreased with depth along all profiles, indicating conservative transport or microbial reduction given that groundwater SO_4^{2-} concentrations were higher than stream water [*Lautz and Fanelli*, 2008]. One exception was the 0.53 m depth at P_2 that showed an elevated SO_4^{2-} concentration despite strong reduction at shallower depths. The stream had a mean SO_4^{2-} concentration of 12.1 mg L^{-1}, while riparian piezometers and the deeper groundwater wells averaged 84.6 and 865.1 mg L^{-1} respectively (Table 1). Bed samples collected once at 0.78 m depth, below the B_1 and P_1 profiles, showed elevated SO_4^{2-} concentrations of 31.8 and 41.2 mg L^{-1} respectively, indicating a groundwater influence. Given that the 0.53 m depth at P_2 was the only hyporheic site with elevated SO_4^{2-} concentrations compared to shallower depths it was also assumed to have appreciable groundwater mixing; therefore samples from the 0.53 m depth at P_2 were not included in the PCA analysis, which was intended to describe microbially mediated changes in SO_4^{2-}.

The similarities between stream and hyporheic water chemistry, combined with the temperature derived flux estimates, indicated that all streambed profiles (except for P_2 0.53 m) intersected downwelling hyporheic flowpaths that originated in the stream and did not appreciably mix with groundwater. Therefore, changes in pore water chemistry along the profiles were dominated by reactive processes and consumption of DO. Variation in water chemistry among the hyporheic samples was much greater for the redox sensitive species than their more conservative counterparts, such as Sr and Cl$^-$. The PCA analysis confirmed that one underlying process was controlling the differences in concentrations of redox sensitive species in the hyporheic zone and allowed for the creation of a linear redox score based on the first principal component alone. This first component had an eigenvalue of 4.5, indicating it explained 64.2 percent of the total variance in the stream/streambed data matrix (n=164) comprised of 7 species (Table 2). The second component explained only an additional 11.5 percent of the variance, and the eigenvalue of 0.81 is below the criterion of 1.0 so it was neglected [*Davis*, 1986; *Preisendorfer*, 1981]. The loadings for each principle component indicate the importance of each species in the data matrix to the component in question [*Cloutier et al.*, 2008]. In the Cherry Creek data, the loadings (absolute value) of the first component were similar for all species, signifying that they all exerted comparable influence on the redox score, and linear correlations between all species and redox score (n=164) were strong (Table 2). The sign of the loadings and correlations were positive for DO, NO_3^- and SO_4^{2-}, and negative for Mn, Fe, P and NH_4^+, which is consistent with the predicted relationships of known biogeochemical thermodynamics [*Baker et al.*, 2000; *Boulton et al.*, 1998; *Pretty et al.*, 2006]. Therefore, given that the first component summarizes variance associated with biogeochemical transformations in the hyporheic zone, I call the first principal component score a "redox score."

The highest redox scores, which averaged 2.1 in stream water, indicated oxic, stream-like conditions of high DO, NO_3^- and SO_4^- and low or no measurable Mn, Fe, P and NH_4^+, while low redox scores, which ranged down to -6.1 at the 0.53 P_1 depth, signified anoxic or reduced conditions with the inverse species relationships. The relationship between redox score and DO indicated that a score of zero corresponded to a [DO] of approximately 4.0 mgL^{-1}, which was suggested by *Marzadri et al.* [2011] as the cutoff between aerobic/anaerobic conditions, while the lowest observed [DO] was 1.5 mgL^{-1}. The relationship between NO_3^- and hyporheic residence time is expected to be non-linear because of NO_3^- production in oxic streambed sediments [*Zarnetske et al.*, 2011], but these complexities are obscured with a linear redox score and, therefore, the reactive nitrogen dynamics will be described in detail in a subsequent manuscript.

Spatial Hyporheic Water Chemistry and Vertical Flux

The temporal dimension of raw geochemical and PCA redox score data can be collapsed by taking the mean for every variable through time by depth along each profile (Table 1, Figure 3B). Table 1 provides two examples of the relationships observed between the redox-sensitive solute concentrations and redox scores with depth at high and low flux profiles. The high flux G_1 profile had much lower levels of Mn and Fe but higher levels of DO and NO_3^- than the low flux B_2 profile, and generally had much less variability with depth. When the mean redox sensitive concentration data are compared to the mean PCA values for all depths/profiles (n=34) the correlations are quite strong, with *r* values ranging from 0.91 for NO_3^- to -0.71 for P (Table 3). When median vertical flux is compared to the mean redox sensitive concentrations at each depth, correlations are all significant, with *r* values ranging from 0.74 for DO to -0.29 for P (Table 3). These patterns can be summarized by comparing mean PCA scores and median

103

vertical flux rates for all depths at all profiles, a relationship which shows a strong positive r of 0.64, indicating the hydrologic flux was a primary driver of redox chemistry, with higher flux correlated to oxic conditions and lower flux correlated to anoxic conditions.

All profiles generally showed a gradient toward more anoxic conditions with depth, although the strength of this change varied greatly and was organized by morphology. When the mean PCA scores are plotted with depth by profile (Figure 3B) there is a clear visual relationship to the plot of median vertical flux values for corresponding locations (Figure 3A). Pool locations, which had shallow weak flux, presented the strongest redox gradients with depth showing abrupt transition to more anoxic conditions. Consequently, the 0.53 depth at P_1 had the lowest mean redox score of any profile at -6.1 (note the 0.53 depth for P_2 was not used for the PCA analysis due to assumed groundwater mixing, as discussed above). The upstream bar locations, B_1 and B_2, which had a similar median flux condition to the pools, showed the next strongest gradients toward anoxic conditions (Figure 3). Conversely, the bar locations located close to the dam (B_3 and B_4), showed stream-like oxic conditions persisting until the 0.18 m depth at B_3 and 0.33 m depth at B_4. Even these subtle differences between B_3 and B_4 could be predicted by the flux profiles, which showed that at B_3 there was no downward component of flux by the 0.33 m depth while at B_4 there was still a large vertical flux of 0.7 md^{-1} at the 0.33 m depth. Finally, all glide locations had oxic conditions at shallow depths with G_1 and G_3 being the only profiles to have positive redox scores at the 0.53 m depth. There appeared to be some disagreement between the strongest flux profile (G_2) and its corresponding redox scores, as the G_2 profile had the strongest gradient of all glide locations toward anoxic conditions, and was similar to the B_3 profile.

If purely vertical flux is assumed at all the shallowest locations (e.g., 0.08 m depth), flux can be converted to residence time along that 0.08 m flowpath using an estimated effective porosity (0.3). The assumption of pure vertical flow was shown to be generally valid for these shallow profiles based on the relatively small change in flux magnitude with depth near the sediment/water interface (Figure 3A). The relationship between mean residence time and mean redox score in the stream and at the 0.08 m depth (n=10) was fit with a quadratic polynomial with an R^2 of 0.93 (Figure 7). This non-linear relationship describes oxic conditions under short residence times up to approximately 1 hr (vertical flux of ~ 0.5 md^{-1}), after which there was a rapid transition toward more anoxic conditions. If the mean DO and NO_3^- concentrations for the 0.08 m depth are also plotted against residence time the results are similar, with DO showing little change at residence times less than 1 hr after an initial drop from stream values, and NO_3^- increasing at short residence times due to net nitrification, followed by net uptake (Figure 7). The empirical relationship between redox score and residence time was used to infer residence times for deeper oblique flowpaths along the glide locations where the flowpath length was unknown and therefore residence time could not be computed directly (Table 4). The glide profiles were chosen specifically because most of their redox scores fell within the sensitive range of the empirical relationship (-0.7 to 1.7), and the resulting estimates of residence time were reasonable and increased with depth.

Temporal Hyporheic Water Chemistry and Vertical Flux

As shown in Table 1, the temporal variability (reflected as standard deviation at each depth) in hyporheic redox score at high flux profiles (e.g., G_1) was small and similar to the limited temporal variability in stream water chemistry. At lower flux sites (e.g., P_1, B_2), which showed temporal trends in flux, redox scores had much greater temporal variability over the 5-

week period than high flux sites (Figure 4B,C,D). Both the P_1 and B_2 profiles showed a general transition toward more oxic conditions with time, especially at the shallower depths, which is consistent with the observed increase in shallow vertical flux and associated decrease in residence time (Figure 4B,D, Figure 8). If this change in flux is converted to a change in residence time at the 0.08 m depth, there was a decrease in residence time from 4.4 to 1.8 hr at B_2 and 3.0 to 1.7 hr at P_1. Interestingly, the short-term drop in flux centered around day 200 at the B_1, B_2, and P_1 profiles (Figure 4, 8) corresponded to an "anoxic event" along all three profiles. The B_2 redox profile in particular seems to track strongly with the vertical flux pattern over the shallow screened interval. In contrast, profile P_2, which did not have a significant trend of increasing vertical hyporheic exchange with time, showed little variation of redox score over the period of study and maintained a strong vertical gradient toward anoxia.

Locations B_3 and B_4 had significant decreasing flux trends over the period of study, but showed little change in the structure of their redox score profiles. Although flux decreased greatly at these locations over time, the final flux rates at the end of the study were still higher than the largest flux rates observed at B_2 and P_1. In terms of residence time at the 0.08 m depth, there was an increase from 0.4 to 1.0 hr at B_3 and 0.4 to 0.5 hr at B_4, but both profiles are still within the "insensitive" oxic residence time range of 0 to 1 hr predicted by the empirical relationship. High flux profiles that showed weaker decreasing temporal trends in hyporheic flux (i.e., G_1, G_2, G_3) also had very consistent redox score patterns, with the glide locations being generally oxic to depth.

Resazurin Tracer

Instream tracer plateau concentrations of approximately 72 μgL^{-1} Raz, 14 μgL^{-1} Rru and 17.7 mgL^{-1} Cl$^-$ (background adjusted) were established by 0.6 hr at both dams. Plateau

concentrations were reached 2.5 hr later at the 1400 m reach outlet, yielding a 1.6 hr median

reach transport time. The conservative Cl⁻ tracer indicated that all streambed profiles had

hydraulic connection to the stream to at least the 0.33 m depth, with the fastest loading generally

taking place at the glide locations. The Raz and Rru concentrations were corrected for dilution

and due to slow loading to depth, many locations did not show a measureable reactive tracer

signal, particularly the 0.18 and 0.33 m depths at the pool and bar profiles. The 0.08 m depth at

B_3 actually showed more Raz relative to Rru compared to the stream input signal, so the data

point was neglected. By the 8.3 hr sampling event significant conversion of Raz to Rru was seen

at all other hyporheic locations in comparison to both the mean stream ratio at the dams of 0.17

(Figure 9) and the mean stream ratio of 0.18 at 1400 m. The Rru:Raz ratios clustered by

geomorphic unit and generally increased with depth along profiles. The strongest conversion at

the 0.08 m depth of Raz to Rru was seen at P_1 and P_2, which had Rru:Raz ratios of 0.42 and 0.44,

respectively. With the exception of G_1 (Rru:Raz ratio=0.41) the glides all showed moderate

Rru:Raz ratios of 0.26-0.32 at the 0.08 m depth. The B_2 profile had the smallest Rru:Raz ratios of

any site until the 0.33 m depth, where the conversion was the strongest of any sample with a

Rru:Raz ratio of 1.2.

Discussion

Spatial Hyporheic Biogeochemistry and Vertical Flux

      The chemistry of the hyporheic zone can be complex due to variable mixing of stream

water and groundwater, and biogeochemical reactions which alter both of these end-members in

space and time. This study focused on two beaver dams with similar upstream morphologies,

where all streambed profiles of vertical water flux showed downwelling in the shallow sediments

and negligible mixing with local groundwater to a depth of 0.55 m. Therefore, any changes in

pore water chemistry were primarily related to the consumption of oxygen and other terminal electron acceptors through microbial respiration of organic carbon [*Baker et al.*, 2000]. The predominance of biogeochemical processes was confirmed through PCA analysis, which was used to create a "redox score" that described 64 percent of the total variability in seven redox sensitive species (DO, NO_3^-, SO_4^{2-}, Mn, Fe, P and NH_4^+), and indicated there was no other primary mechanism for chemical change. Each redox sensitive species showed directional correlation with the redox score in a manner consistent with known redox thermodynamics [*Baker et al.*, 2000](Table 2, 3). The chemical data was collected in conjunction with high vertical spatial resolution (0.014 m) temperature derived vertical flux estimates, which allowed direct comparison between physical flow properties of the hyporheic zone and biogeochemical processes along nine vertical profiles located in varied streambed morphologies of bars, pools and glides over five weeks. The result was a clear and strong relationship between vertical flux patterns and the evolution of pore water chemistry.

The temporal dimension of the physical and chemical dataset was collapsed by calculating the median flux rates through time at depths that corresponded to screened piezometer intervals and then taking the mean solute concentrations and redox scores at those depths. Mean redox scores showed strong linear correlation to all redox sensitive parameters (Table 3), specifically 0.91 to NO_3^- and 0.83 to DO. This result indicated the use of a redox score was appropriated to efficiently describe changes in the multivariate dataset, including parameters relevant to biogeochemical processing and stream water quality. Median vertical fluxes showed significant correlation to every redox sensitive species, with correlation coefficients of 0.62 to NO_3^- and 0.74 to DO. The redox score was strongly correlated to median flux ($r = 0.64$) indicating that the physical hydrology of the system, and associated residence

times, were driving the accumulated changes in pore water chemistry. Table 1 shows the relationship between the individual terminal electron acceptors and the redox score for the low flux B_2 and high flux G_1 locations by depth. Stark differences in physical hyporheic flow patterns between these profiles, spaced only 2.9 m apart in the horizontal dimension, generated very different biogeochemical conditions that were efficiently summarized with the PCA redox score.

When the median fluxes by depth for each profile are plotted alongside the mean PCA scores, the similarities are striking (Figure 3). Patterns in both flux and PCA score are organized by streambed morphology, supporting earlier work which hypothesized that alluvial features may strongly influence streambed biogeochemical patterns [*Claret and Boulton*, 2009; *Valett et al.*, 1996]. Shallow, weak fluxes observed at the pool (P_1, P_2) and upstream bar (B_1, B_2) locations resulted in the steepest gradients toward anoxic conditions with depth, particularly at the pools (Figure 3, Figure 8). The glide locations, which the heat tracing revealed to have strong, deep hyporheic flow cells, all showed "stream-like" conditions persisting along the pore water profiles (Figure 3), a result also found for glide locations upstream of a small dam in a similar system [*Lautz and Fanelli*, 2008]. Unexpectedly, the strongest flux profile (G_2) showed the most rapid transition toward reduced conditions of the glide profiles, but this difference may result from streambed heterogeneities at finer scale than the 0.2 m which separated the temperature and biogeochemical profiles.

The downstream bar profiles were particularly interesting, as they showed hydrology and chemistry analogous to the glide profiles at shallow depths, but a transition to more anoxic conditions at deeper depths indicating that the hyporheic flowcells at the downstream bars do not extend to the same depth as the glides. Specifically, the vertical flux profiles indicated that

surface water was being carried deeper and at greater rate at B_4 compared to B_3, and these

differences are clearly indicated by the corresponding redox scores with depth. Along many

profiles there was deep transport of moderately reduced water (redox score of -2 to 0) indicating

the transport of water originating in the stream to below the depth of vertical flux extinction,

which is consistent with the conceptual model of a gradient toward oblique then horizontal

flowpaths with depth [*Briggs et al.*, 2012b]. This does present an important limitation of the 1-D

heat transport model, which is that no quantitative information about flux rates along the deeper

horizontal flowpaths can be ascertained. All pore water along these profiles was shown to be of

stream origin through conservative ion chemistry and SO_4^{2-} concentrations, also supporting the

spatial interpretation of shallow hyporheic flow cells underlain by longer horizontal hyporheic

flowpaths. In summary, where vertical hyporheic flux rates were high at the glide and

downstream bar locations (G_1, G_2, G_1, B_3, B_4), stream-like conditions persisted along much of

the profiles. But, where flow rates were moderate and shallow at the pools and upstream bars

(P_1, P_2, B_1, B_2), there were strong gradients toward reduced conditions with depth.

Recently, residence time has been shown to be a principal control on the consumption of

dissolved solutes and the accumulation of products from biogeochemical reactions along

hyporheic flowpaths [*Marzadri et al.*, 2011; *Zarnetske et al.*, 2011]. If vertical flux is assumed

to the shallowest piezometer screens, an assumption shown to be generally valid for these

profiles (e.g., low rate of change in vertical flux with depth), a conversion to residence time

along the 0.08 m flowpath can be made by estimating effective porosity. The resulting strong

relationship ($r = 0.93$) between redox score and residence time is non-linear, and suggests

threshold behavior (Figure 7). At residence times less than approximately 1 hr, which

corresponds to 0.5 md^{-1} flux along the shallow flowpath, there was little change in the redox

score, after which there was a steep gradient toward anoxic conditions. These patterns suggest that temporal variability in flux values exceeding 0.5 md^{-1} would have little impact on aggregate redox chemistry (excluding NO_3^-) at shallow depths in this system as the shift would occur in the residence time "oxic zone". Additionally, the sensitivity of modeled flux rates to assumed streambed thermal parameters, as determined through Monte Carlo analysis [*Briggs et al.*, 2012b], indicated the most precise estimates of flux exist around 0.4-0.5 md^{-1}, allowing this crucial transition point for biogeochemical residence times to be well established using heat tracing.

The patterns expressed in DO and NO_3^- in response to residence time are very similar to those discussed above, illustrating that these biogeochemically important parameters are well described by the general redox score as a function of residence time (Figure 7). This is a particularly compelling result, as the redox score was generated solely from the covariance of all seven redox sensitive parameters, with no explicit physical hydrological component, and further demonstrates that residence time is driving net changes in pore water chemistry in response to biogeochemical cycling. After some initial consumption of oxygen from the stream input, due to aerobic respiration, DO was relatively insensitive to residence times less than approximately 1 hr. This did not seem to be due to DOC limitation in the high flux zones, as although the highest DOC concentration was found at the pools, the rest of the profiles showed similar values between high and low flux zones. The NO_3^- data shows a clear net nitrification signal up to residence times of 1 hr, followed by net uptake, a pattern that has recently been shown as a function of residence time in a lateral hyporheic zone [*Zarnetske et al.*, 2011]. This nitrification, which can only take place in the oxic zone [*Duff and Triska*, 2000], drives the slight increase

seen in the linear redox score at short residence times, and indicates that NO_3^- is sensitive to short residence times.

The strong relationship between residence time and redox score was determined over the same flowpath length at different profiles in varied morphology above two different beaver dams. Therefore, variability in reaction rates and labile DOC availability may be relatively minor compared to differences in the hyporheic exchange rates, which control the extent to which byproducts of biogeochemical cycling accumulate. This suggests that once the residence time-redox score relationship is established, redox scores may be used as a predictive measure of residence times at this site (Table 4). This is especially useful for the oblique and horizontal flowpaths, for which no previous residence times could be estimated, as the flowpath length and total flux vector were unknown. The sensitive and well-defined range in the empirical relationship limited the prediction of residence times to a window of greater than 1 hr but less than 2.7 hr, which covered the majority of depths at the glide locations, and generated reasonable, increasing residence time estimates with depth based on the mean redox scores (Table 4).

To establish a relationship between residence time and redox chemistry for specific points in the streambed an assumption of purely vertical flux and associated vertical flowpath length is required. These assumptions could be critically evaluated by determining vertical hyporheic flux patterns at high resolution. The conclusive link between physical hydrology and biogeochemical patterns, beyond larger transitions from streambed downwelling to upwelling, may have been difficult to make in previous studies because the physical hydrology was not suitably refined by lower resolution vertical flux data and/or VHGs alones [*Hedin et al.*, 1998; *Schmidt et al.*, 2011]. This study shows that there can be a rapid transition to oblique flow with

112

depth in some streambed morphologies, which can cause residence times to be greatly underestimated when assuming true vertical flow. Although the directionality of VHGs may be consistent with the true directionality of hyporheic flux [*Lautz et al.*, 2010; *Pretty et al.*, 2006], the magnitude of VHGs may say more about the distribution of hydraulic conductivity (K) in the streambed rather than being useful in predicting flux without very constrained estimates of K over the profile in question. It has been shown that large hydraulic gradients may be associated with reduced streambed conditions, indicating low exchange and conductivity [*Lautz and Fanelli*, 2008; *Schmidt et al.*, 2011]. For morphologies with high K the resultant VHG will be small even at high flux [*Lautz et al.*, 2010], and this can be difficult to measure accurately and temporal changes challenging to resolve.

Another advantage of flux estimates made with temperature tracing combined with biogeochemical data is that net changes in solute mass may be assessed. There have been several references to "hot spots" of biogeochemical transformation in recent literature [e.g. *Lautz and Fanelli*, 2008; *McClain et al.*, 2003]. Specifically, *McClain et al.* [2003] defines biogeochemical hot spots as patches in the system which have relatively high reaction rates in comparison to the surrounding matrix. This term is often used to describe upwelling zones rich in nutrients that stimulate production in the surface water [*Boulton et al.*, 1998]. From a hyporheic flowpath perspective, this can be viewed as the combination of factors (e.g., residence time, substrate, temperature, grain size) that produce the greatest change in solute load. If one takes a spatial view of a biogeochemical hot spot [*Lautz and Fanelli*, 2008], patches of low flux which generate strong and shallow redox gradients, such as observed here at the pools and upstream bar locations (B_1, B_2), would qualify as hotspots because they produce the largest biogeochemical transformations over a given flowpath length. However, this definition neglects

113

the mass-flux component of the hyporheic exchange process relative to total stream flux [*Kasahara and Hill*, 2006; *Wondzell*, 2011], which is likely the most relevant to the natural remediation properties of streams. Zones of high flux, and low residence time, show little biogeochemical transformation with depth; therefore there is an inverse relationship between flux and absolute chemical alteration of pore water.

Consequently, it may be most useful to define a hotspot of hyporheic biogeochemical cycling as the zone that produces the largest change in the parameter of interest in a volume weighted sense, optimizing the combination of high flux and rapid uptake/transformation, and determining the filtration capacity of hyporheic exchange. For example if maximizing NO_3^- uptake is the goal, a hotspot would be the zone where the largest mass of NO_3^- is removed from the water column, not necessarily flowpaths where NO_3^- concentrations are brought to zero. Caution must be used when estimating total mass changes over vertical transects though, as the total flowpath transport is likely not defined, and may result in further chemical alteration.

Temporal Hyporheic Biogeochemistry and Vertical Flux

Average spatial hydrologic and chemical patterns can be very useful to describe the patchiness and morphologic organization of these variables, but the temporal component is also critical to developing a predictive understanding of the system. The physical flow patterns showed increasing trends in shallow vertical flux at the upstream bar (B_1, B_2) and adjacent pool (P_1) location. This was attributed to an increase in turbulent flow upstream of the dam as discharge and stage dropped considerably, increasing pumping-model exchange. The one other low flux profile (P_2) did not show a significant trend in flux values, although there was some temporal variability. In contrast, the downstream bar locations, situated within 1.7 m of the dam, had significantly decreasing shallow flux as the hydraulic gradient imposed across the step in the

114

water surface profile decreased as stage dropped. Shallow vertical flux at the glides was variable but without trend and remained strong.

There was correlation between temporal changes in vertical flux patterns and the geochemistry of the corresponding pore water. The low flux locations that experienced increasing hyporheic exchange had much greater variability in all redox sensitive species, as is presented by the standard deviations in Table 1, in the temporal redox score plots in Figure 4, and the cross-sections of Figure 8. As flux increased, both B_2 and P_1 developed notably more oxic redox scores, and these oxic zones extended below the extinction of vertical flux along the profiles. This evolution from reduced to more stream-like shallow hyporheic water over a relatively short period may result in the conversion of a cold spot of biogeochemical cycling into a hot spot with time. The remaining profiles all showed less temporal variability in redox score at all depths that could predominantly be explained by variation in the stream signal input. Although decreasing flux rates at depth (increasing residence times) along the G_1 and G_2 profiles clearly caused a temporal shift from predominantly stream-like conditions near the dam to a much stronger redox gradient with depth (Figure 8). This streambed cross-section quantitatively describes how disparate changes in flux based on morphology and distance from the structure can generate inverse trends in streambed biogeochemistry above the same dam simultaneously.

The differences in redox score profile variability were predicted by the threshold nature of the empirical relationship between redox score and residence time developed from the spatial analysis (Figure 7). At Cherry Creek, high flux locations showed temporal changes in rates of water exchange and associated residence time, but these residence times in the shallow sediments remained in the low redox sensitivity 0-1 hr range, and therefore showed little chemical variability as they remained oxic over the duration of the study period (Figure 4, Figure 8).

Shallow, low-flux locations that showed increasing trends (B_2, P_1) had decreasing residence times from >3.0 to 1.7 hrs, which spanned the sensitive range in redox condition as a function of residence time (Figure 7). *Schmidt et al.* [2011] have recently shown high variation in shallow streambed redox conditions when vertical flux varied within a similar range. Residence time variability in the sensitive range resulted in a wider temporal "redox envelope" that encompassed a range of profiles from more reduced to more oxic (Figure 4). This concept of a redox envelope existing along vertical hyporheic profiles is similar to the concept of temperature envelopes presented in many previous studies [*Constantz*, 2008; *Lapham*, 1989], and in this case low flux zones (with temporal variability) show large swings in streambed redox condition.

Hydrologic hot moments are defined as flowpaths that experience disproportionately high reactivity over a short duration [*McClain et al.*, 2003], the inverse definition can be applied to "cold moments". The upstream group (B_1, B_2, P_1) all showed a decrease in flux to negligible values over a several day event centered around day 200 which may have been caused by a temporary increase in stage (Figure 4A). The pore water sampling round following this decrease in flux produced the lowest redox scores along these profiles at shallow depths, indicating that the corresponding increase in residence times, resulting from a cold moment in vertical flux, also yielded a cold moment in biogeochemical cycling (Figure 4, Figure 8). This biogeochemical moment behavior was likely governed by the observed short term drop in hyporheic exchange, as the DOC in the stream water, which is a primary input to the hyporheic biogeochemical cycle, showed no trend through time and was less variable than other similar systems [*Rutherford and Hynes*, 1987] (Figure 6). Interestingly, there seems to be a lag between the rebound in flux and change in redox condition. This may result from the timing of the modeled flux changes being offset from the true temporal flux patters and/or anoxic water exchanging out of less mobile pore

space. The effects of hot/cold moments on stream ecology and water quality remain to be
quantified, but they can clearly occur over short timescales and are driven at least in part by the
physical hydrology of the hyporheic zone.

Resazurin Tracer

The conversion of Raz to Rru observed in the hyporheic zone confirmed that pore water
experienced aerobic respiration at all profile locations where there was measureable tracer,
though the magnitude of this conversion was variable (Figure 9). As one would expect from the
patterns observed in the redox sensitive species, aerobic reactivity was organized by
morphologic unit, and this measure increased with depth. As discussed above, a hotspot of
microbial reactivity results in part from maximizing residence time and flux rate in concert. Pore
water had experienced the strongest reactivity in shallow sediments at the pool locations, and this
was reflected in the greatest oxygen consumption of any 0.08 m samples, a relationship that has
previously been shown [*Haggerty et al.*, 2009]. Although, if the change in the Rru:Raz ratio is
multiplied to the flux rate at the 0.08 m depth, the strongest conversion by volume was actually
observed at the glide locations by approximately a factor of two. This suggests that the high flux
glide locations are a greater "hotspot" for aerobic microbial reactivity and cycling of organic
carbon. Interestingly, at the shallow pool and B_2 locations where flux was similar, there was
much greater conversion of Raz at the pools. These patterns were also reflected in DO, and
suggest a difference in labile substrate availability, which was supported by the higher DOC
concentrations found at the pools in shallow pore water. Significant changes in the Rru:Raz ratio
at depth along the B_2 profile confirms that aerobic respiration continues throughout streambed
horizons dominated by the reduction of less favorable terminal electron acceptors until DO is
functionally exhausted.

Although significant fluxes of stream water were found to pass through the hyporheic zone around beaver dams, and aerobic reactivity in those sediments was found to be strong, these exchanges did not result in a significant change in net in-stream Rru:Raz ratios. Therefore, after 1400 m of transport through 13 beaver dam complexes of varied size, combined with all other reactive hyporheic exchange, the flux of water through the entire system was dominated by unreactive flowpaths. This result of overlapping scales can be viewed as both a positive and negative in terms of the relevance of hyporheic exchange to surface water quality as: 1) hyporheic flowpaths around beaver dams are more reactive over 0.08 m than net stream transport over 1400 m, therefore hyporheic zones are "important", and 2) beaver dams do not have significant impact on reach-scale bioreactivity at this flow regime (very low residence time over 1400 m of 1.6 hr), therefore hyporheic zones are "not important".

Consequently, it can be postulated that although hyporheic zones may create patchy micro-environments that are relevant to specific biota, their effects on reach scale nutrient processing may be negligible at high flows as the ratio of hyporheic exchange to discharge is small [*Battin et al.*, 2008; *Kasahara and Hill*, 2006; *Wondzell*, 2011]. *Wondzell* [2011] goes further to suggest that hyporheic exchange may only be relevant to reach scale chemistry in streams with discharge less than 10 Ls^{-1} in a 5th-order alpine stream network. There may be a threshold that is crossed in Cherry Creek during more regular summer flows (~50 Ls^{-1} [*Jin et al.*, 2009]) where the hyporheic aerobic respiration signal is more relevant to net stream transport, but those flows were not reached during this study period. *Stewart et al.* [2011] have recently shown through basin scale modeling that hyporheic exchanges may be minor in comparison to discharge, and inconsequential to reach scale solute transport times; but also that a large fraction of runoff actually has a high probability of entering the hyporheic zone at least once as it drains

118

through the network. We have shown that once water enters the reactive sediments around beaver dams many biogeochemical reactions can occur over short timescales. This suggests that even my relatively long 1.4 km reach length may not have been adequate to evaluate the importance of hyporheic exchange to respiration from a watershed perspective, and future large scale modeling efforts based on innovative field data collection are imperative.

Conclusions

This study shows a conclusive link between physical hyporheic flux patterns, associated residence times, and biogeochemical cycling in downwelling hyporheic zones. Vertical flux through the subsurface was measured with fiber-optic high-resolution temperature sensors (HRTS), and the variation in seven redox sensitive species (DO, NO_3^-, Mn, Fe, SO_4^-, P, NH_4^+) was summarized with one linear redox score determined through PCA analysis. The pairing of these techniques allowed a direct comparison of fine scale spatial and temporal flux variability to corresponding streambed biogeochemical patterns. Correlation of mean redox score to median vertical flux was strong ($r = 0.64$), and redox conditions and flux rates were organized by functional morphologic unit. Glide morphologies were found to cause deep hyporheic flow cells of high magnitude and low residence time which created an oxic, stream-like pore water assemblage. Bar locations located close to the beaver dam had similar flux magnitudes but shallower flow cells resulting in greater anoxic conditions at depth, while bars set farther back had shallow, modest exchange and steep gradients toward reducing conditions. Finally pool locations were similar to the upstream bars, and showed the strongest gradients with depth toward anoxia.

Residence time was determined for all the shallow 0.08 m depths, as the necessary assumption of vertical flux was shown to be generally valid along those flowpaths. The resulting

119

non-linear relationship between mean residence time and mean redox score was strong (R^2=0.93). This relationship also indicated net pore water chemistry was relatively insensitive to biogeochemical changes when residence times were less than 1 hr, after which there was a strong gradient toward reducing conditions, as expressed by the directional variability of all seven redox sensitive species. This empirical relationship also seemed to hold for temporal changes in flux and associated biogeochemical condition. Therefore, when there was temporal variability in low flux (or high residence time) zones, redox conditions changed considerably creating a wider vertical "redox envelope" than observed at temporally variable high flux profiles (Figure 4). Even short term changes in vertical flux over several days resulted in changes in the biogeochemical conditions of hyporheic pore water, and did not seem to result from changes in stream water DOC. These results suggest that in this system, hot spots and hot moments of biogeochemical cycling in the hyporheic zone are determined in a large part by physical flux patterns.

The reactive resazurin "smart" tracer showed that although hyporheic flowpaths contained reactive aerobic microbial communities resulting in strong tracer transformation over very short flowpaths and residence times, the net stream signal revealed most flowpaths in the reach scale system were unreactive over 1.4 km of transport. This connection to the larger scale indicated that beaver activity in this system does not significantly increase reach scale reactive transport over this range of discharge (>211. Ls^{-1}), but does create patchy micro-environments which may be ecologically important. The connection between physical hyporheic and biogeochemical patterns was made possible through emerging techniques, which allowed the overlay of multiple environmental tracers to better describe these complicated systems, and may

120

facilitate the development of predictive relationships which can be applied to network scale analysis.

Tables

Table 2. Mean concentrations and standard deviations (shown in italics) of the redox sensitive terminal electron acceptors and corresponding PCA-derived redox score for the stream, wells and piezometer nests from a low flux upstream bar profile (B_2) and a high flux glide profile (G_1).

Location	concentrations										redox score	
	DO ($mgL^{-1} \pm 0.5$)		NO_3^- ($ppm \pm 0.002$)		Mn ($ppb \pm 5.3$)		Fe ($ppb \pm 0.7$)		SO_4^{2-} ($ppm \pm 0.02$)			
Stream (n=5)	7.0 (*0.5*)		0.31 (*0.08*)		1. (*1.*)		0.9 (*0.6*)		12.1 (*1.6*)		2.1(*0.4*)	
Riparian (all, n=8)	1.2 (*0.9*)		0.02 (*0.02*)		652. (*283.*)		2803.3 (*2548.3*)		84.6 (*38.0*)		n/a	
deep wells (all, n=4)	n/a		0.13 (*0.23*)		384. (*317.*)		2003.3 (*2241.9*)		865.1 (*125.2*)		n/a	
Profile (n=5)	B_2	G_1	B_2	G_1	B_2	G_1	B_2	G_1	B_2	G_1	B_2	G_1
0.08 m	5.5 (*1.7*)	6.1 (*1.2*)	0.29 (*0.19*)	0.38 (*0.08*)	64.5 (*113.*)	2.3 (*3.*)	8.9 (*12.*)	6.7 (*4.0*)	12.7 (*1.2*)	12.9 (*1.0*)	0.8 (*1.7*)	1.8 (*0.5*)
0.18 m	3.9 (*2.1*)	6.4 (*1.0*)	0.26 (*0.17*)	0.37 (*0.10*)	108. (*150.*)	2.8 (*2.*)	17.9 (*30.*)	4.2 (*2.2*)	12.3 (*1.5*)	13.0 (*1.0*)	0.1 (*2.0*)	1.9 (*0.4*)
0.33 m	2.5 (*0.8*)	5.6 (*1.3*)	0.07 (*0.07*)	0.30 (*0.08*)	196. (*160.*)	4.8 (*4.*)	169.8 (*175.*)	5.1 (*6.5*)	10.9 (*1.9*)	12.4 (*2.0*)	-2.0 (*1.4*)	1.4 (*0.6*)
0.53 m	2.3 (*0.4*)	3.9 (*1.8*)	0.04 (*0.02*)	0.28 (*0.09*)	180. (*111.*)	14.4 (*24.*)	320.0 (*263.*)	7.7 (*3.9*)	9.1 (*4.4*)	13.0 (*1.6*)	-2.7 (*1.6*)	0.9 (*0.7*)

Table 2. Explained variance and loadings for the first three principal components. The first component represents the linear redox score retained for analysis, and the linear correlation between raw species and the redox score is listed in italics.

Principle Component	Eigen value (-)	explained variance (%)	loadings by redox sensitive species						
			DO	NO_3^-	Mn	Fe	SO_4^{2-}	P	NH_4^+
1 (redox score)	**4.5**	**64.2**	**0.36** (*0.76*)	**0.41** (*0.88*)	**-0.42** (*-0.89*)	**-0.39** (*-0.83*)	**0.33** (*0.70*)	**-0.33** (*-0.70*)	**-0.40** (*-0.85*)
2	0.81	11.5	-0.5	-0.08	0.32	0.17	0.69	-0.25	-0.26
3	0.63	9.0	0.29	0.27	0.12	0.28	0.31	0.77	-0.24

Table 3. Linear correlations (*r)* between mean variables for each depth along each profile (n=33), all *p* values are less than 0.0002.

	median flux (md^{-1})	*r correlations to mean redox sensitive species*						
		DO	NO$_3^-$	Mn	Fe	SO$_4^{2-}$	P	NH$_4^+$
mean PCA score	**0.64**	0.83	0.91	-0.84	-0.86	0.78	-0.71	-0.87
median flux	n.a.	0.74	0.62	-0.57	-0.46	0.39	-0.29	-0.46

Table 4. Estimated residence times along each glide streambed profile; values in bold were determined using the vertical flux data, effective porosity (0.3), and known distance; while the values in italics were estimated using the redox score and empirical relationship to residence time presented in Figure 7.

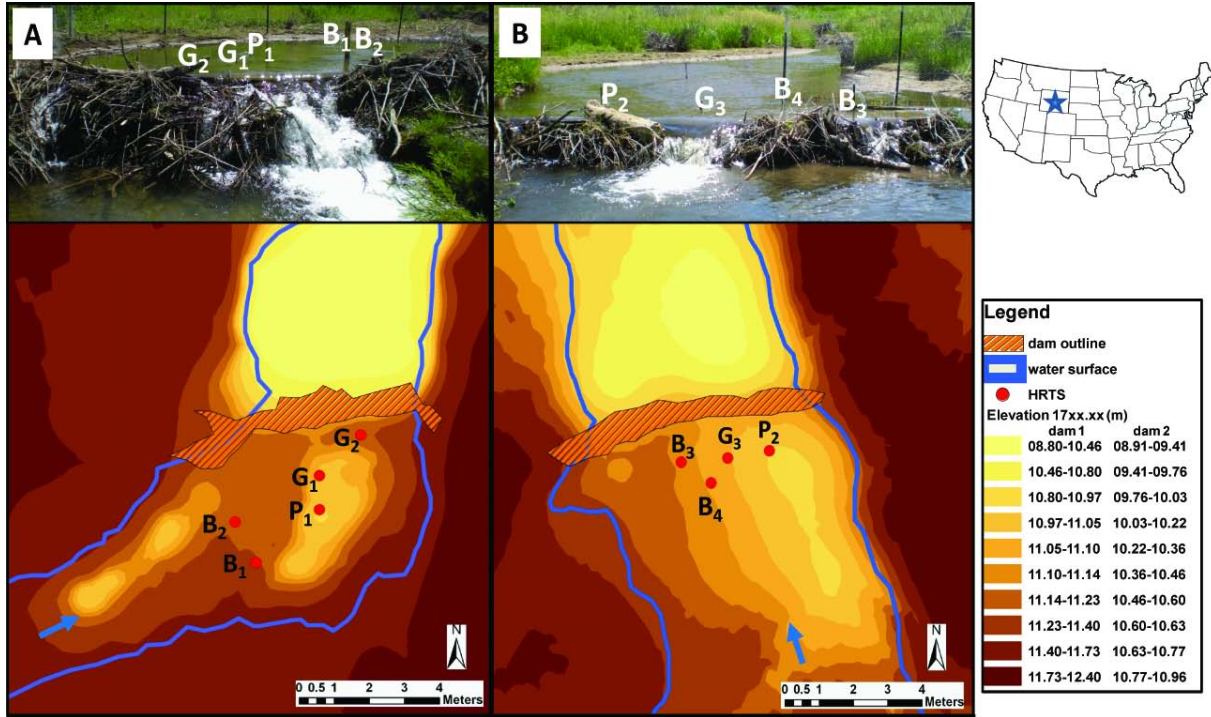| depth	*residence times (h)*		
	G$_1$	G$_2$	G$_3$
0.08	**0.6**	**0.3**	**0.4**
0.18	*<1*	*1.7*	*<1*
0.33	*1.6*	*2.6*	*1.3*
0.53	*1.9*	*>2.7*	*2.4*

Figures

Figure 1. Upstream views toward (A) Dam 1 and (B) Dam 2, with the streambed topography, as derived from a detailed spatial survey, and all profile locations, where B, G and P stand for bar, glide and pool morphologies, respectively. The wetted edge was surveyed near the beginning of the study period.
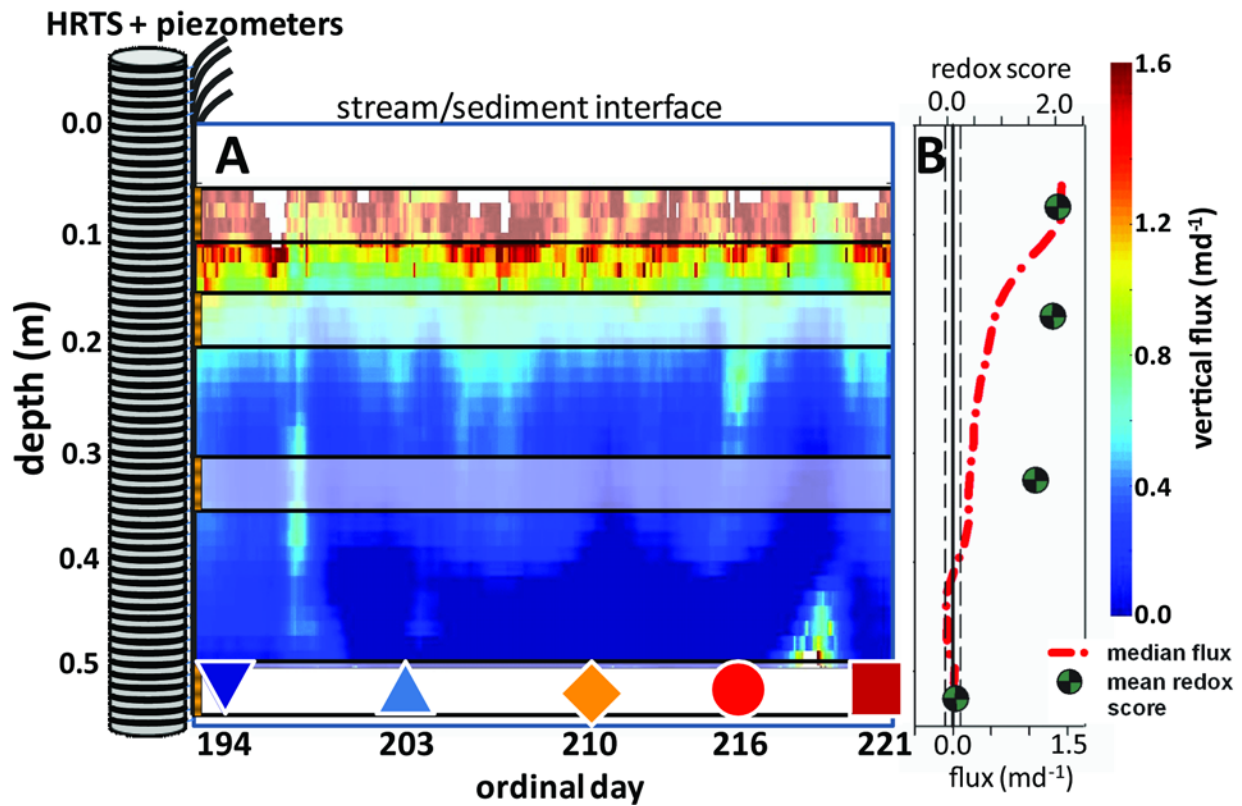
Figure 2. From left to right this figure shows the fiber-optic HRTS and adjacent piezometer nest, which are installed in the streambed and used to produce: A) a high-resolution map of vertical flux rates over time, shown here with corresponding pore water sampling screened intervals marked with transparent white bands and sampled on days 194, 203, 210, 216 and 221; and B) the median flux rate with depth over the six-week study period, shown here with the mean redox scores for hyporheic pore water collected from the piezometers at corresponding depths.
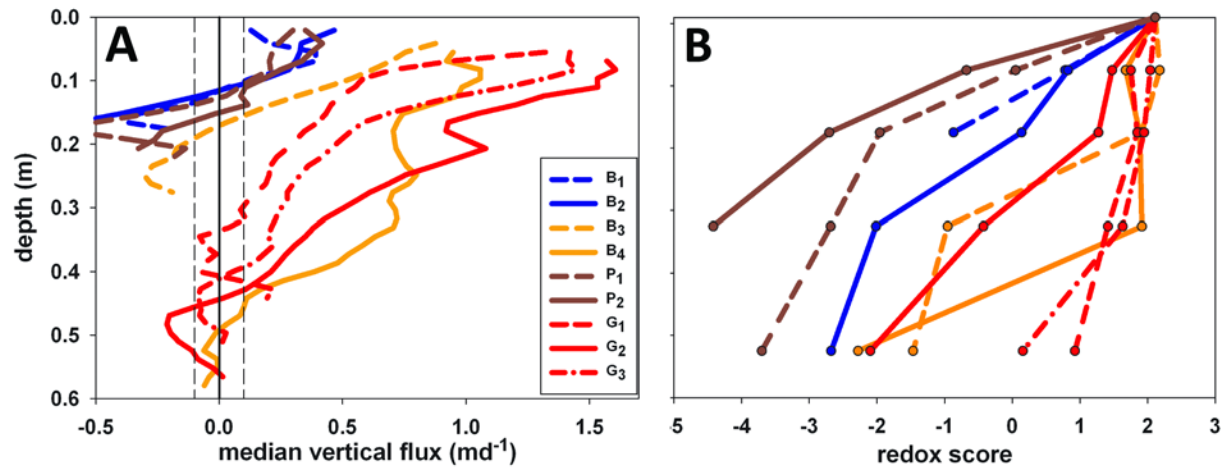
Figure 3. Panel A) Median vertical flux, and B) mean redox score by depth over the study period along each streambed profile. The vertical, black dashed lines in panel A show the range of flux values that are not significantly different from zero [Briggs *et al.*, 2012].
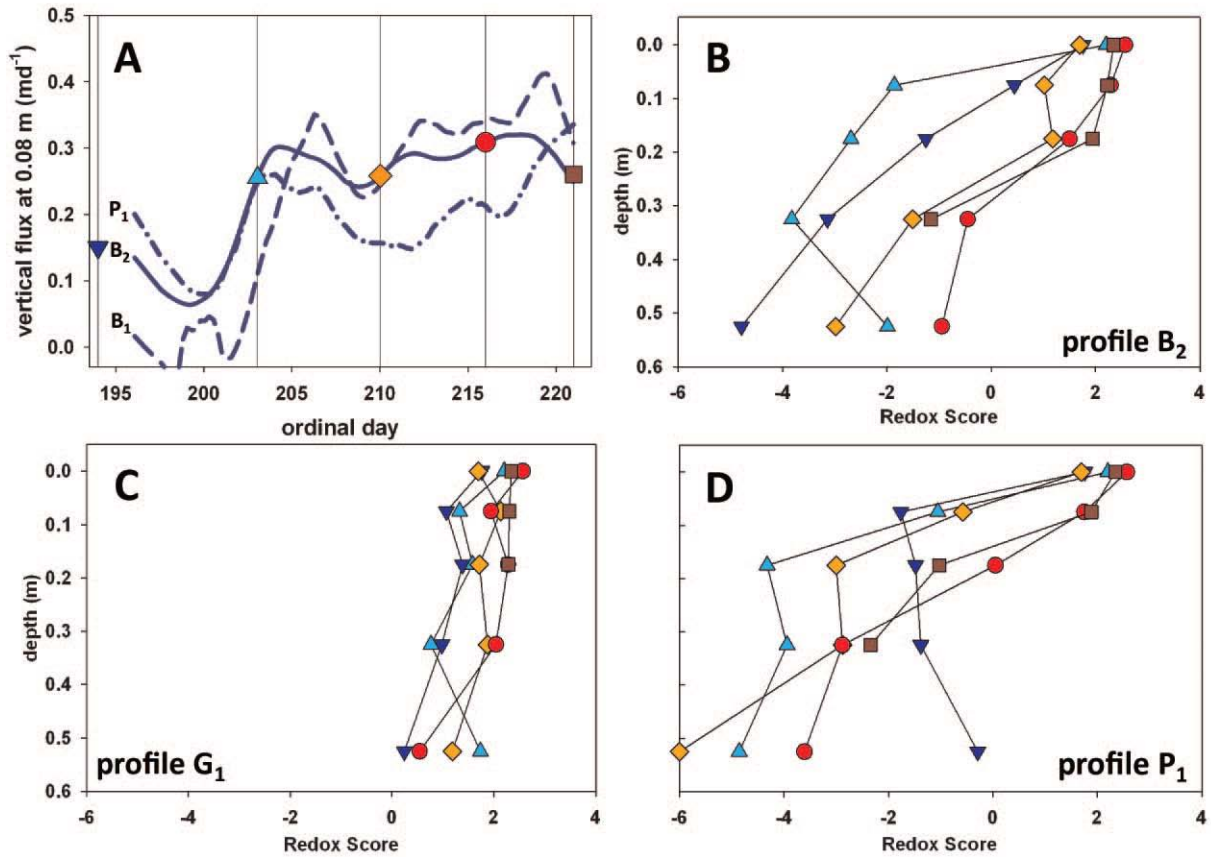
Figure 4. Panel A) Vertical flux through time, averaged over the 0.05 to 0.10 m depths at the profiles that showed significant increasing trends over the month (B_1, B_2, P_1), and a coincident drop in flux around ordinal day 200. Pore water chemistry was sampled on days shown by the geometric symbols and vertical black lines. Panels B, D) The broad "redox envelope" created by temporal variability in residence times at the low-flux B_2 and P_1 profiles; and C) The narrow envelope redox envelope generated by changes in residence time within the oxic range at the high-flux G_1 profile.
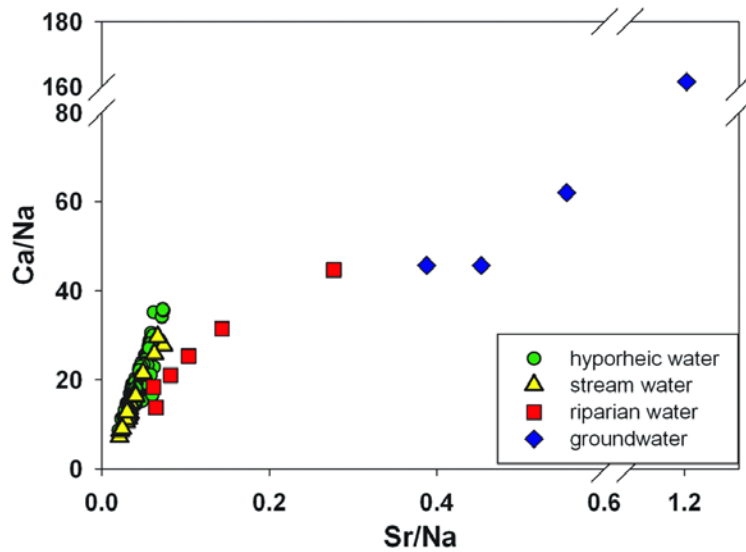
Figure 5. Spatial and temporal mixing relationships between the stream and streambed water for "conservative" species that had strong concentration differences between surface and groundwater. Variability in the streambed was generally in the range of surface water values. Water samples from the riparian wells appear to follow a different mixing line that trended toward the deeper groundwater.

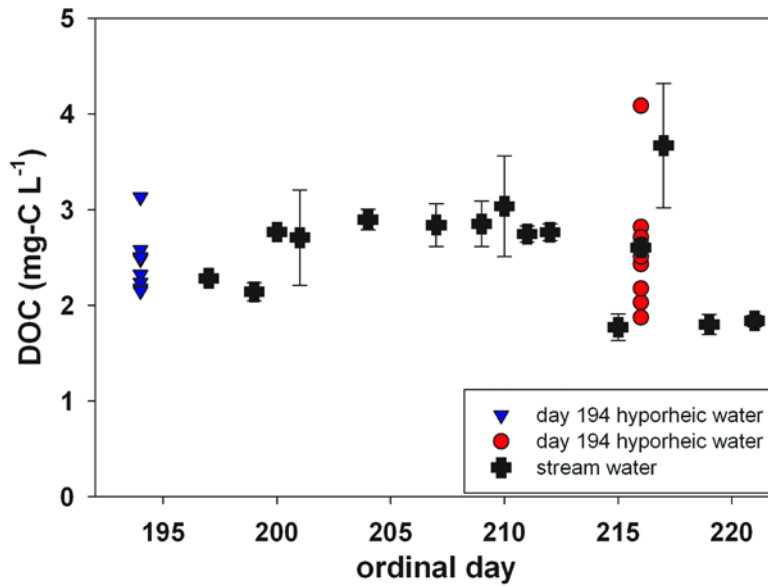Figure 6. Dissolved organic carbon (DOC) in the stream showed some temporal variability but no significant trend over the study period, error bars for the stream samples were determined through duplicate samples and several of these error ranges were smaller than the plotted symbol. DOC in the pore water at 0.08 m on days 194 and 216 was also variable with the highest values found at the pool locations.
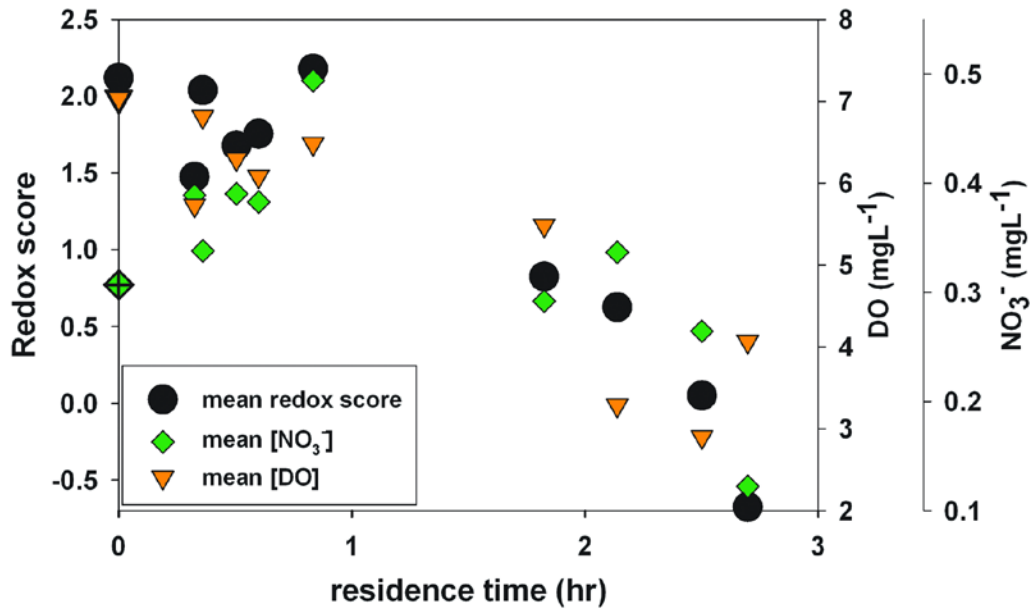
Figure 7. Relationship between mean residence time and the mean PCA score, [DO] and [NO$_3^-$] at 0.08 m depth at each profile and the stream (n=10). A quadratic polynomial was fit to the PCA data with an R^2 of 0.93. This empirical relationship was used to interpolate residence times for depths where the flowpath length was unknown (Table 4).
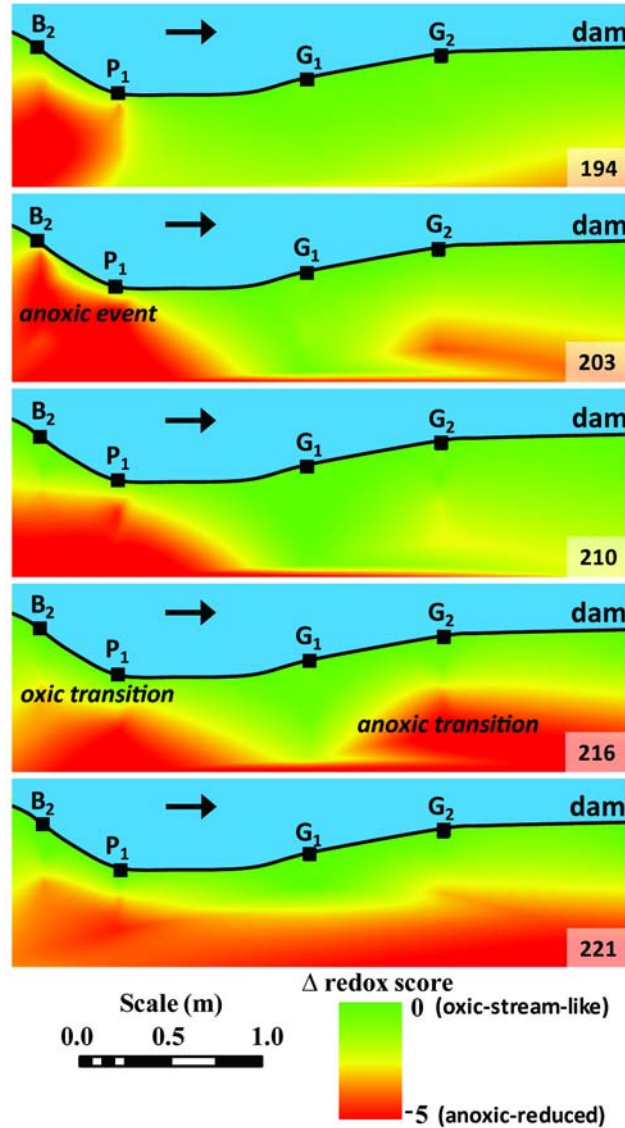
Figure 8. Change in hyporheic redox score from stream values above Dam #1 at each sampling event. Increasing shallow flux through time at B_2 and P_1 reduced residence times to create a shallow oxic zone; while closer to the dam decreasing deep flux/increasing residence times at G_1 and G_2 formed a zone of anoxia at depth. The low flux event at the upsteam locations prior to sampling on day 203 resulted in a "cold moment" of shallow biogeochemical cycling and increased anoxic conditions.

Figure 9. Rru:Raz ratio in the streambed sediments of varied morphology and flux condition.

Larger ratios indicate pore water has experienced greater aerobic respiration. All hyporheic

locations indicate reactive flowpaths, as ratios are higher than both the 0.17 input ratio (dotted

line), and the 0.18 net stream ratio after 1.4 km transport.
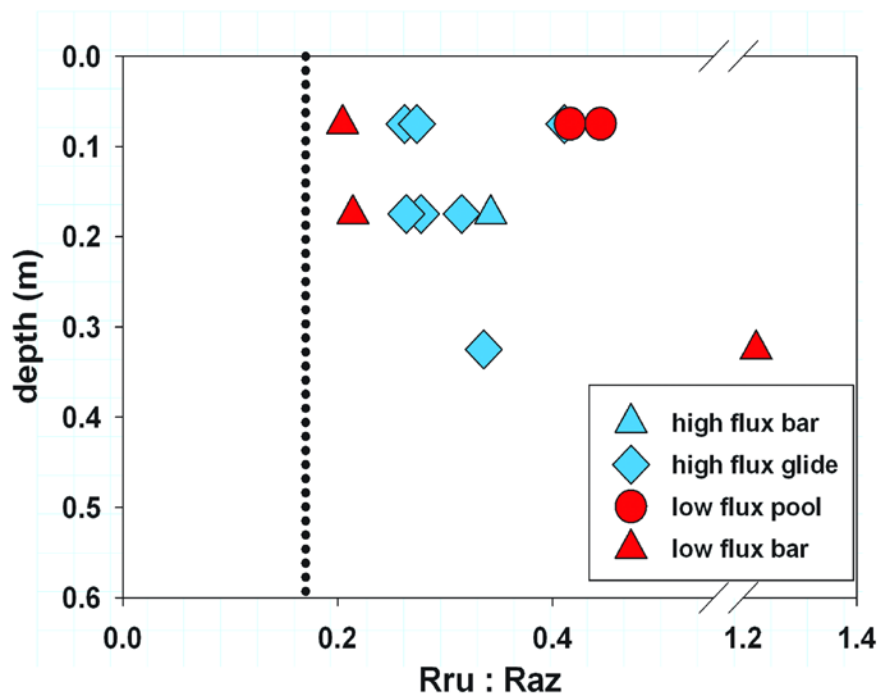
References

Anderson, M. P. (2005), Heat as a ground water tracer, *Ground Water, 43*(6), 951-968.

Anibas, C., J. H. Fleckenstein, N. Volze, K. Buis, R. Verhoeven, P. Meire, and O. Batelaan (2009), Transient or steady-state? Using vertical temperature profiles to quantify groundwater-surface water exchange, *Hydrol. Process, 23*(15), 2165-2177.

Argerich, A., E. Marti, F. Sabater, and M. Ribot (2011a), Temporal variation of hydrological exchange and hyporheic biogeochemistry in a headwater stream during autumn, *Journal of the North American Benthological Society, 30*(3), 635-652, doi: 10.1899/10-078.1.

Argerich, A., R. Haggerty, E. Marti, F. Sabater, and J. Zarnetske (2011b), Quantification of metabolically active transient storage (MATS) in two reaches with contrasting transient storage and ecosystem respiration, *J. Geophys. Res.-Biogeosci., 116*, doi: 10.1029/2010jg001379.

Baker, M. A., C. N. Dahm, and H. M. Valett (2000), Anoxia, anaerobic metabolism, and biogeochemistry of the stream-water-ground-water interface, in *Streams and Ground Waters*, edited by J. B. Jones and P. J. Mulholland, pp. 260-286, Academic Press, San Diego.

Battin, T. J., L. A. Kaplan, S. Findlay, C. S. Hopkinson, E. Marti, A. I. Packman, J. D. Newbold, and F. Sabater (2008), Biophysical controls on organic carbon fluxes in fluvial networks, *Nat. Geosci., 1*(2), 95-100, doi: 10.1038/ngeo101.

Bayani Cardenas, M., J. L. Wilson, and R. Haggerty (2008), Residence time of bedform-driven hyporheic exchange, *Advances in Water Resources, 31*(10), 1382-1386.

Boulton, A. J., S. Findlay, P. Marmonier, E. H. Stanley, and H. M. Valett (1998), The functional

significance of the hyporheic zone in streams and rivers, *Annual Review of Ecology and Systematics, 29*, 59-81.

Briggs, M. A., L. K. Lautz, and J. M. McKenzie (2012a), A comparison of fibre-optic distributed

temperature sensing to traditional methods of evaluating groundwater inflow to streams, *Hydrol. Process*., *26*, 1277-1290, doi: 10.1002/hyp.8200.

Briggs, M. A., L. K. Lautz, J. M. McKenzie, R. P. Gordon, and D. H. Hare (2012b), Using high-

resolution distributed temperature sensing to quantify spatial and temporal variability in vertical hyporheic flux, *Water Resources Research, 48*, doi: 10.1029/2011WR011227.

Brunke, M., and T. Gonser (1997), The ecological significance of exchange processes between

rivers and groundwater, *Freshwater Biology, 37*(1), 1-33.

Buffington, J. M., and D. Tonina (2009), Hyporheic exchange in mountain rivers II: Effects of

channel morphology on mechanics, scales, and rates of exchange, *Geography Compass, 3*(3), 1038-1062.

Cao, Z., P. Carling, and R. Oakey (2003), Flow reversal over a natural pool–riffle sequence: a

computational study, *Earth Surface Processes and Landforms, 28*(7), 689-705, doi: 10.1002/esp.466.

Cardenas, M. B., J. L. Wilson, and V. A. Zlotnik (2004), Impact of heterogeneity, bed forms, and

stream curvature on subchannel hyporheic exchange, *Water Resources Research, 40* W08307.

Carter, R.W., and J. Davidian (1968), *General procedure for gagging streams: U.S. Geological*

Survey Techniques of Water-Resources Investigations, book 3, chapt. A6, 13 p.

134

Champ, D. R., J. Gulens, and R. E. Jackson (1979), Oxidation–reduction sequences in ground water flow systems, *Canadian Journal of Earth Sciences, 16*(1), 12-23, doi: 10.1139/e79-002.

Christensen, T. H., P. Kjeldsen, P. L. Bjerg, D. L. Jensen, J. B. Christensen, A. Baun, H. J. Albrechtsen, and C. Heron (2001), Biogeochemistry of landfill leachate plumes, *Applied Geochemistry, 16*(7-8), 659-718.

Cirpka, O. A., M. N. Fienen, M. Hofer, E. Hoehn, A. Tessarini, R. Kipfer, and P. K. Kitanidis (2007), Analyzing bank filtration by deconvoluting time series of electric conductivity, *Ground Water, 45*(3), 318-328.

Claret, C., and A. J. Boulton (2009), Integrating hydraulic conductivity with biogeochemical gradients and microbial activity along river-groundwater exchange zones in a subtropical stream, *Hydrogeology Journal, 17*(1), 151-160, doi: 10.1007/s10040-008-0373-3.

Cloutier, V., R. Lefebvre, R. Therrien, and M. M. Savard (2008), Multivariate statistical analysis of geochemical data as indicative of the hydrogeochemical evolution of groundwater in a sedimentary rock aquifer system, *Journal of Hydrology, 353*, 294-313.

Conant, B. (2004), Delineating and quantifying ground water discharge zones using streambed temperatures, *Ground Water, 42*(2), 243-257.

Constantz, J. (1998), Interaction between stream temperature, streamflow, and groundwater exchanges in Alpine streams, *Water Resources Research, 34*(7), 1609-1615.

Constantz, J. (2008), Heat as a tracer to determine streambed water exchanges, *Water Resources Research, 44*, doi: 10.1029/2008wr006996.

Constantz, J., and C. L. Thomas (1996), The use of streambed temperature profiles to estimate the depth, duration, and rate of percolation beneath arroyos, *Water Resources Research, 32*(12), 3597-3602.

Constantz, J., C. L. Thomas, and G. Zellweger (1994), Influence of diurnal variations in stream temperature on streamflow loss and groundwater recharge, *Water Resources Research, 30*(12), 3253-3264.

Constantz, J., M. H. Cox, and G. W. Su (2003), Comparison of heat and bromide as ground water tracers near streams, *Ground Water, 41*(5), 647-656.

Dakin, J. P., D. J. Pratt, G. W. Bibby, and J. N. Ross (1985), Distributed optical fibre Raman temperature sensor using a semiconductor light source and detector, *Electronics Letters, 21*(13), 569-570.

Davis, J. C. (1986), *Statistics and data analysis in geology*, John Wiley & Sons Inc., New York.

Duff, J. H., and F. J. Triska (2000), Nitrogen biogeochemistry and surface-subsurface exchange in streams, in *Streams and Ground Waters*, edited by J. B. Jones and P. J. Mulholland, Academic Press, San Diego, California.

Effler, S. W., and K. Whitehead (1996), *Tributaries and Discharges. In: Limnological and Engineering Analysis of a Polluted Urban Lake: Prelude to Environmental Management of Onondaga Lake, New York*, Springer-Verlag, New York, NY.

Elliott, A. H., and N. H. Brooks (1997), Transfer of nonsorbing solutes to a streambed with bed forms: Theory, *Water Resources Research, 33*(1), 123-136.

Fanelli, R. M., and L. K. Lautz (2008), Patterns of water, heat and solute flux through the streambeds around small dams, *Ground Water, 46*(5), 671-687.

Fulford, J. M. (2001), Accuracy and consistency of water-current meters, *Journal of the American Water Resources Association, 37*(5), 1215-1224.

Gooseff, M. N., R. O. Hall, and J. L. Tank (2007), Relating transient storage to channel complexity in streams of varying land use in Jackson Hole, Wyoming, *Water Resources Research, 43*(1), doi: 10.1029/2005wr004626.

Gooseff, M. N., S. M. Wondzell, R. Haggerty, and J. Anderson (2003), Comparing transient storage modeling and residence time distribution (RTD) analysis in geomorphically varied reaches in the Lookout Creek basin, Oregon, USA, *Advances in Water Resources, 26*(9), 925-937.

Gooseff, M. N., J. K. Anderson, S. Wondzell, J. LaNier, and R. Haggerty (2006), A modeling study of hyporheic exchange pattern and the sequence, size, and spacing of stream bedforms in mountain stream networks, Oregon, USA (Retraction of vol 19, pg 2915, 2005), *Hydrol. Process, 20*(11), doi: 10.1002/Hyp.6350.

Gordon, R. P., L. K. Lautz, M. A. Briggs, and J. M. McKenzie (2012), Automated calculation of vertical pore-water flux from field temperature time series using the VFLUX method and computer program, *Journal of Hydrology*, doi: 10.1016/j.jhydrol.2011.11.053.

Goto, S., M. Yamano, and M. Kinoshita (2005), Thermal response of sediment with vertical fluid flow to periodic temperature variation at the surface, *Journal of Geophysical Research-Solid Earth, 110*, B01106, doi: 10.1029/2004JB003419.

Grattan, K. T. V., and T. Sun (2000), Fiber optic sensor technology: An overview, *Sensors and Actuators, A: Physical, 82*(1), 40-61.

Haggerty, R., S. M. Wondzell, and M. A. Johnson (2002), Power-law residence time distribution
in the hyporheic zone of a 2nd-order mountain stream, *Geophys. Res. Lett., 29*(13), 18-11
- 18-14.

Haggerty, R., E. Marti, A. Argerich, D. von Schiller, and N. B. Grimm (2009), Resazurin as a
"smart" tracer for quantifying metabolically active transient storage in stream ecosystems,
J. Geophys. Res.-Biogeosci., 114, doi: 10.1029/2008jg000942.

Harvey, J. W., and K. E. Bencala (1993), The effect of streambed topography on surface-
subsurface water exchange in mountain catchments, *Water Resources Research, 29*(1),
89-98.

Harvey, J. W., and B. J. Wagner (2000), Quantifying hydrologic interactions between streams
and their subsurface hyporheic zones, in *Streams and Ground Waters*, edited by J. B.
Jones and P. J. Mulholland, Academic Press, San Diego, CA.

Harvey, J. W., B. J. Wagner, and K. E. Bencala (1996), Evaluating the reliability of the stream
tracer approach to characterize stream-subsurface water exchange, *Water Resources
Research, 32*(8), 2441-2451.

Harvey, J. W., J. E. Saiers, and J. T. Newlin (2005), Solute transport and storage mechanisms in
wetlands of the Everglades, south Florida, *Water Resources Research, 41*(5), 1-14.

Hatch, C. E., A. T. Fisher, J. S. Revenaugh, J. Constantz, and C. Ruehl (2006), Quantifying
surface water-groundwater interactions using time series analysis of streambed thermal
records: Method development, *Water Resources Research, 42*(10), W10410, doi:
10.1029/2005WR004787.

Healy, R. W., and A. D. Ronan (1996), Documentation of computer program VS2DH for
simulation of energy transport in variably saturated porous media - modification of the

USG Geological Survey's computer program VS2DT, US Geological Survey Water-Resources Investigations Report 96-4230, 36 pp.

Hedin, L. O., J. C. von Fischer, N. E. Ostrom, B. P. Kennedy, M. G. Brown, and G. P. Robertson (1998), Thermodynamic constraints on nitrogen transformations and other biogeochemical processes at soil-stream interfaces, *Ecology, 79*(2), 684-703, doi: 10.1890/0012-9658(1998)079[0684:tconao]2.0.co;2.

Hester, E. T., and M. W. Doyle (2008), In-stream geomorphic structures as drivers of hyporheic exchange, *Water Resources Research, 44*, W03417.

Jensen, J. K., and P. Engesgaard (2011), Nonuniform Groundwater Discharge across a Streambed: Heat as a Tracer, *Vadose Zone Journal, 10*(1), 98-109, doi: 10.2136/vzj2010.0005.

Jin, L., D. I. Siegel, L. K. Lautz, and M. H. Otz (2009), Transient storage and downstream solute transport in nested stream reaches affected by beaver dams, *Hydrol Process, 23*(17), 2438-2449, doi: Doi 10.1002/Hyp.7359.

Jones, J. B., Jr., S. G. Fisher, and N. B. Grimm (1995), Nitrification in the Hyporheic Zone of a Desert Stream Ecosystem, *Journal of the North American Benthological Society, 14*(2), 249-258.

Kalbus, E., F. Reinstorf, and M. Schirmer (2006), Measuring methods for groundwater-surface water interactions: a review, *Hydrol. Earth Syst. Sc., 10*, 873-887.

Kasahara, T., and S. M. Wondzell (2003), Geomorphic controls on hyporheic exchange flow in mountain streams, *Water Resources Research, 39*(1), 1005, doi: 10.1029/2002WR001386.

Kasahara, T., and A. R. Hill (2006), Hyporheic exchange flows induced by contructed riffles and steps in lowland streams in sourthern Ontario, Canada, *Hydrol. Process, 20*, 4287-4305.

Kasnavia, T., D. Vu, and D. A. Sabatini (1999), Fluorescent dye and media properties affecting sorption and tracer selection, *Ground Water, 37*(3), 376-381.

Keery, J., A. Binley, N. Crook, and J. W. N. Smith (2007), Temporal and spatial variability of groundwater-surface water fluxes: Development and application of an analytical method using temperature time series, *Journal of Hydrology, 336*, 1-16.

Kilpatrick, F. A., and E. D. Cobb (1985), Measurement of discharge using tracers: U. S. Geological Survey Techniques of Water-Resources Investigations, Book 3, Chapter A16, edited, p. 52.

Kobayashi, D. (1985), Separation of the snowmelt hydrograph by stream temperatures, *Journal of Hydrology, 76*(1-2), 155-162.

Land, M., J. Ingri, P. S. Andersson, and B. Ohlander (2000), Ba/Sr, Ca/Sr and 87Sr/86Sr ratios in soil water and groundwater: implications for relative contributions to stream water discharge, *Applied Geochemistry, 15*(3), 311-325, doi: 10.1016/s0883-2927(99)00054-2.

Langmuir, C. H., J. R D Vocke, G. N. Hanson, and S. R. Hart (1978), A general mixing equation with applications in Icelandic basalts, *Earth and Planetary Science Letters, 37*, 380-392.

Lapham, W. W. (1989), Use of temperature profiles beneath streams to determine rates of vertical ground-water flow and vertical hydraulic conductivity. Water-Supply Paper 2337. Denver, Colorado: USGS.

Lautz, L. K. (2010), Impacts of non-ideal field conditions on vertical water velocity estimates from streambed temperature time series, *Water Resources Research, 46*, W01509.

Lautz, L. K., and D. I. Siegel (2006), Modeling surface and ground water mixing in the hyporheic zone using MODFLOW and MT3D, *Advances in Water Resources, 29*, 1618-1633.

Lautz, L. K., and R. M. Fanelli (2008), Seasonal Biogeochemical Hotspots in the Streambed around Restoration Structures, *Biogeochemistry, 91*(1), 85-104.

Lautz, L. K., D. I. Siegel, and R. L. Bauer (2006), Impact of debris dams on hyporheic interaction along a semi-arid stream, *Hydrol. Process, 20*(1), 183-196, doi: 10.1002/Hyp.5910.

Lautz, L. K., N. T. Kranes, and D. I. Siegel (2010), Heat tracing of heterogeneous hyporheic exchange adjacent to in-stream geomorphic features, *Hydrol. Process*, doi: 10.1002/hyp.7723.

Loheide, S. P., and S. M. Gorelick (2006), Quantifying stream-aquifer interactions through the analysis of remotely sensed thermographic profiles and in situ temperature histories, *Environmental science & technology, 40*(10), 3336-3341.

Lowry, C. S., J. F. Walker, R. J. Hunt, and M. P. Anderson (2007), Identifying spatial variability of groundwater discharge in a wetland stream using a distributed temperature sensor, *Water Resources Research, 43*(10), doi: 10.1029/2007wr006145.

Marzadri, A., D. Tonina, and A. Bellin (2011), A semianalytical three-dimensional process-based model for hyporheic nitrogen dynamics in gravel bed rivers, *Water Resources Research, 47*(11).

Matthews, D. A., and S. W. Effler (2003), Decreases in pollutant loading from residual soda ash production waste, *Water Air and Soil Pollution, 146*(1-4), 55-73.

McClain, M. E., et al. (2003), Biogeochemical hot spots and hot moments at the interface of terrestrial and aquatic ecosystems, *Ecosystems, 6*(4), 301-312, doi: 10.1007/S10021-003-0161-9.

Moffett, K. B., S. W. Tyler, T. Torgersen, M. Menon, J. S. Selker, and S. M. Gorelick (2008), Processes controlling the thermal regime of saltmarsh channel beds, *Environmental science & technology, 42*(3), 671-676, doi: 10.1021/Es071309m.

Morrice, J. A., C. N. Dahm, H. M. Valett, P. V. Unnikrishna, and M. E. Campana (2000), Terminal electron accepting processes in the alluvial sediments of a headwater stream, *Journal of the North American Benthological Society, 19*(4), 593-608.

Mortimer, C. H. (1941), The Exchange of Dissolved Substances Between Mud and Water in Lakes, *Journal of Ecology, 29*(2), 280-329.

Naiman, R. J., J. M. Melillo, and J. E. Hobbie (1986), Ecosystem Alteration of Boreal Forest Streams by Beaver (Castor Canadensis), *Ecology, 67*(5), 1254, doi: 10.2307/1938681.

Neilson, B., C. Hatch, H. Ban, and S. Tyler (2010), Solar radiative heating of fiber optic cables used to monitor temperatures in water, *Water Resources Research, 46*, doi: 10.1029/2009WRR008354.

Panno, S. V., K. C. Hackley, H. H. Hwang, S. E. Greenberg, I. G. Krapac, S. Landsberger, and D. J. O'Kelly (2006), Characterization and identification of Na-Cl sources om ground water, *Ground Water, 44*, 176-187.

Payn, R. A., M. N. Gooseff, B. L. McGlynn, K. E. Bencala, and S. M. Wondzell (2009), Channel water balance and exchange with subsurface flow along a mountain headwater stream in Montana, United States, *Water Resources Research, 45*, doi: 10.1029/2008wr007644.

Pidlisecky, A., and R. Knight (2011), The use of wavelet analysis to derive infiltration rates from time-lapse one-dimensional resisti vity records, *Vadose Zone Journal, 10*(2), 697-705.

Preisendorfer, R. W., F. W. Zwiers, and T. P. Barnett (1981), *Foundations of principal component selection rules*, 200 pp., SIO Rep., Scripps Institution of Oceanography.

Pretty, J. L., A. G. Hildrew, and M. Trimmer (2006), Nutrient dynamics in relation to surface-subsurface hydrological exchange in a groundwater fed chalk stream, *Journal of Hydrology, 330*(1-2), 84-100.

Rau, G., M. Andersen, A. McCallum, and R. Acworth (2010), Analytical methods that use natural heat as a tracer to quantify surface water–groundwater exchange, evaluated using field temperature records, *Hydrogeology Journal, 18*(5), 1093-1110, doi: 10.1007/s10040-010-0586-0.

Rau, G. C., M. S. Anderson, A. M. McCallum, and R. I. Acworth (2010), Analytical methods that use natural heat as a tracer to quantify surface water-groundwater exchange, evaluated using field temperature records, *Hydrogeology Journal, 18*, 1093-1110.

Robson, A., and C. Neal (1990), Hydrograph separation using chemical techniques: An application to catchments in Mid-Wales, *Journal of Hydrology, 116*(1-4), 345-363.

Rutherford, J. E., and H. B. N. Hynes (1987), Dissolved organic carbon in streams and groundwater, *Hydrobiologia, 154*(1), 33-48, doi: 10.1007/bf00026829.

Schmadel, N. M., B. T. Neilson, and D. K. Stevens (2010), Approaches to estimate uncertainty in longitudinal channel water balances, *Journal of Hydrology, 394*(3-4), 357-369.

Schmidt, C., M. Martienssen, and E. Kalbus (2011), Influence of water flux and redox conditions on chlorobenzene concentrations in a contaminated streambed, *Hydrol. Process, 25*(2), 234-245, doi: 10.1002/hyp.7839.

Selker, J. S., N. van de Giesen, M. Westhoff, W. Luxemburg, and M. B. Parlange (2006a), Fiber optics opens window on stream dynamics, *Geophys. Res. Lett., 33*(24), L24401, doi: 10.1029/2006gl027979.

Selker, J. S., L. Thevenaz, H. Huwald, A. Mallet, W. Luxemburg, N. V. de Giesen, M. Stejskal, J. Zeman, M. Westhoff, and M. B. Parlange (2006b), Distributed fiber-optic temperature sensing for hydrologic systems, *Water Resources Research, 42*(12), doi: 10.1029/2006wr005326.

Soupir, M. L., S. Mostaghimi, and C. Mitchem (2009), A Comparative Study of Stream-Gaging Techniques for Low-Flow Measurements in Two Virginia Tributaries, *Journal of the American Water Resources Association, 45*(1), 110-122, doi: 10.1111/J.1752-1688.2008.00264.X.

Stallman, R. W. (1965), Steady one-dimensional fluid flow in a semi-infinite porous medium with sinusoidal surface temperature, *Journal of Geophysical Research, 70*(12), 2821-2827.

Stewart, R. J., W. M. Wollheim, M. N. Gooseff, M. A. Briggs, J. M. Jacobs, B. J. Peterson, and C. S. Hopkinson (2011), Separation of river network–scale nitrogen removal among the main channel and two transient storage compartments, *Water Resources Research, 47*(1), W00J10, doi: 10.1029/2010wr009896.

Suárez, F., and S. W. Tyler (2011), Comments on "Evaluation of systems coupling vacuum membrane distillation and solar energy for seawater desalination", *Chemical Engineering Journal*.

Thoreau, H. D. (1854), *Walden; or, Life in the Woods*, Ticknor & Fields, Boston.

Triska, F. J., V. C. Kennedy, R. J. Avanzino, G. W. Zellweger, and K. E. Bencala (1989), Retention and transport of nutrients in a third-order stream in Northwestern California: hyporheic processes, *Ecology, 70*(6), 1893-1905.

Tyler, S. W., and J. S. Selker (2009), New user facility for environmental sensing, *Eos, 90*(50), 483.

Tyler, S. W., J. S. Selker, M. B. Hausner, C. E. Hatch, T. Torgersen, C. E. Thodal, and S. G. Schladow (2009), Environmental temperature sensing using Raman spectra DTS fiber-optic methods, *Water Resources Research, 45*, doi: 10.1029/2008wr007052.

Valett, H. M., J. A. Morrice, C. N. Dahm, and M. E. Campana (1996), Parent lithology, surface-groundwater exchange, and nitrate retention in headwater streams, *Limnol. Oceanogr., 41*(2), 333-345.

Vogt, T., P. Schneider, L. Hahn-Woernle, and O. A. Cirpka (2010), Estimation of seepage rates in a losing stream by means of fiber-optic high-resolution vertical temperature profiling, *Journal of Hydrology, 380*(1-2), 154-164.

Vroblesky, D. A., and F. H. Chapelle (1994), Temporal and Spatial Changes of Terminal Electron-Accepting Processes in a Petroleum Hydrocarbon-Contaminated Aquifer and the Significance for Contaminant Biodegradation, *Water Resources Research, 30*(5), 1561-1570, doi: 10.1029/94wr00067.

Ward, A. S., M. N. Gooseff, and K. Singha (2010), Imaging hyporheic zone solute transport using electrical resistivity, *Hydrol. Process, 24*(7), 948-953.

Weissmann, G. S., and G. E. Fogg (1999), Multi-scale alluvial fan heterogeneity modeled with transition probability geostatistics in a sequence stratigraphic framework, *Journal of Hydrology, 226*(1-2), 48-65.

Westhoff, M. C., H. H. G. Savenije, W. M. J. Luxemburg, G. S. Stelling, N. C. van de Giesen, J. S. Selker, L. Pfister, and S. Uhlenbrook (2007), A distributed stream temperature model using high resolution temperature observations, *Hydrol. Earth Syst. Sc., 11*(4), 1469-1480.

Whittemore, D. O. (2007), Fate and identification of oil-brine contamination in different hydrogeologic settings, *Applied Geochemistry, 22*(10), 2099-2114, doi: Doi 10.1016/J.Apgeochem.2007.04.002.

Wolman, M. G. (1954), A method of sampling coarse river-bed material, *Transactions of American Geophysical Union, 35*, 951-956.

Wondzell, S. M. (2011), The role of the hyporheic zone across stream networks, *Hydrol Process, 25*(22), 3525-3532, doi: 10.1002/hyp.8119.

Young, P. C., D. J. Pedregal, and W. Tych (1999), Dynamic Harmonic Regression, *Journal of Forcasting, 18*(6), 369-394.

Young, P. C., C. J. Taylor, W. Tych, and D. J. Pedregal (2010), The Captain Toolbox, edited, Centre for Research on Environmental Systems and Statistics, Lancaster, UK, www.es.lancs.ac.uk/cres/captain.

Zarnetske, J. P., R. Haggerty, S. M. Wondzell, and M. A. Baker (2011), Dynamics of nitrate production and removal as a function of residence time in the hyporheic zone, *J. Geophys. Res.-Biogeosci., 116*, doi: 10.1029/2010jg001356.

Zellweger, G. W. (1994), Testing and Comparison of 4 Ionic Tracers to Measure Stream-Flow Loss by Multiple Tracer Injection, *Hydrol. Process, 8*(2), 155-165.

Biographical Data

Name of Author: Martin Ashley Briggs
Place of Birth: Concord, Massachusetts USA
Date of Birth: March, 3, 1979

Graduate and Undergraduate Schools Attended:

Colorado School of Mines, Golden, Colorado USA
University of Massachusetts, Amherst, Massachusetts USA

Degrees Awarded:

Master of Science, 2009, Colorado School of Mines
Bachelor of Science, 2002, University of Massachusetts

Awards and Honors:

Syracuse University Graduate Fellowship, 2009-2011
NSF East Asia and Pacific Summer Institutes Fellowship, 2011
Invited talk, American Geophysical Union fall meeting, 2011
Best oral presentation: Novel Methods of Subsurface Characterization and Monitoring
    professional conference, 2011
Syracuse University Department of Earth Sciences Newton E. Chute Award, 2011
Syracuse University Department of Earth Sciences Graduate Student Publication award, 2010

Professional Experience:

Research Assistant, Department of Earth Sciences, Syracuse University, Syracuse, New York
    USA, Summer 2009 – present
Teaching Assistant, Department of Earth Sciences, Syracuse University, Syracuse, New York
    USA, Spring 2011
NSF East Asia and Pacific Summer Institutes Fellow, Fudan University, Shanghai, China,
    Summer 2011
Research Assistant, Colorado School of Mines, Golden, Colorado USA, Summer 2006 – Winter
    2009
Research Intern, University of California, Santa Cruz, CA USA, Summer 2005

Publications:

Briggs, M. A., L. K. Lautz, J. M. McKenzie, R. P. Gordon and D. K. Hare (2012b), Using high-resolution distributed temperature sensing to quantify spatial and temporal variability in vertical hyporheic flux, *Water Resources Research*, 48, doi:10.1029/2011WR011227.

Gordon, R. P., L. K. Lautz, M. A. Briggs, and J. M. McKenzie (2012), Automated calculation of vertical pore-water flux from field temperature time series using the VFLUX method and computer program, *Journal of Hydrology*, doi:10.1016/j.jhydrol.2011.11.053.

Briggs, M. A., L. K. Lautz and J. M. McKenzie (2012a), A comparison of Distributed Temperature Sensing to traditional methods of evaluating groundwater inflows to streams, *Hydrological Processes*, 25, doi:10.1002/hyp.8200.

Gooseff, M. N., D. A. Benson, M. A. Briggs, M. Weaver, W. Wollheim, B. Peterson and C.S. Hopkinson (2011), Residence time distributions in surface transient storage zones in streams: estimation via signal deconvolution, *Water Resources Research*, 47, W05509, doi:10.1029/2010WR009959.

Stewart, R. J., W. M. Wollheim, M. N. Gooseff, M. A. Briggs, J. M. Jacobs, B. J. Peterson and C. S. Hopkinson (2011), Separation of river scale nitrogen removal among main channel and two transient storage compartments, *Water Resources Research,* 47, W00J10, doi:10.1029/2010WR009896.

Briggs, M. A., M. N. Gooseff, B. J. Peterson, K. Morkeski, W. Wollheim and C. S. Hopkinson (2010), Surface and Hyporheic Transient Storage Dynamics Throughout A Coastal Stream Network, *Water Water Resources Research*, 46, W06516, doi:10.1029/2009WR008222.

Briggs, M. A., M. N. Gooseff, C. D. Arp and M. A. Baker (2009), A Method for estimating surface transient storage parameters for streams with concurrent hyporheic storage, *Water Resources Research*, 45, W00D27, doi:10.1029/2008WR006959.